Worcester Polytechnic Institute
Digital WPI

Doctoral Dissertations (All Dissertations, All Years)   Electronic Theses and Dissertations

2003-01-08

Design and Performance of a Localized Fiber Optic, Near-Infrared Spectroscopic Prototype Device for the Detection of the Metabolic Status of "Vulnerable Plaque": in-vitro Investigation of Human Carotid Plaque

Tania Nur Khan
Worcester Polytechnic Institute

Follow this and additional works at: https://digitalcommons.wpi.edu/etd-dissertations

Design and Performance of a Localized Fiber Optic, Near-Infrared Spectroscopic Prototype Device for the Detection of the Metabolic Status of "Vulnerable Plaque":

in-vitro Investigation of Human Carotid Plaque

by

Tania Nur Khan

A Dissertation

Submitted to the Faculty

of the

WORCESTER POLYTECHNIC INSTITUTE

AND

UNIVERSITY OF MASSACHUSETTS GRADUATE SCHOOL OF BIOMEDICAL SCIENCES

in partial fulfillment of the requirements for the

Degree of Doctor of Philosophy

in

Biomedical Engineering and Medical Physics

January 6, 2003

APPROVED:

_____
Babs R. Soller, PhD, Principal Advisor
University of Massachusetts

_____
Robert A. Peura, PhD, Co-Advisor
Worcester Polytechnic Institute

_____
Richard Tuft, PhD, Co-Advisor
University of Massachusetts

_____
Morteza Naghavi, M.D.
Texas Heart Institute, CVPR

_____
S. Ward Casscells, M.D.
University of Texas Health Science Center

_____
Christopher Sotak, PhD
WPI BME Head

_____
Anthony Carruthers, PhD
Dean, UMass GSBS

ABSTRACT

INTRODUCTION: The "vulnerable plaque" is defined as the "precursor lesion" that ultimately ends in acute coronary thrombi (clots) that create a heart attack. Macrophages and inflammatory cells, found preferentially in vulnerable plaque, sustain their activity in the plaque through anaerobic metabolism and lactate production. The ultimate goal is to assess anaerobic metabolism *in-vivo* by measuring tissue pH and lactate concentration in atherosclerotic plaques using optical spectroscopy. The proposed *in-vitro* optical probe design, experimental method, and spectroscopic data analysis methodology are established in this research.

METHODS: A fiber optic probe was designed and built based on both Monte Carlo simulations and bench testing with the goal to collect light from a small volume of tissue. A simulation of the depth penetration of the proposed probe was performed on normal and atherosclerotic aortic tissue, and the final probe was bench tested using normal aorta. A method was developed to preserve plaque metabolic status of tissue harvested from patients. Human atherosclerotic tissue obtained immediately after carotid endarterectomy was placed in Minimum Essential Medium (MEM) with non-essential amino acids supplement, bubbled with $75\%O_2/20\%N_2/5\%CO_2$ at 37°C. Tissue pH, pCO_2, pO_2 and temperature with (n=7) and without (n=2) the media preparation over time were reviewed to assess plaque viability and maintenance of physiological conditions. Additional plaques placed in media were used for development of chemometric methods to measure pH and lactate. Areas of each plaque were randomly chosen for analysis. Reflectance spectra were collected with a dispersive spectrometer (400-1100 nm) and a Fourier-transform near-infrared spectrometer (1100–2400 nm) using the fiber optic probe. Reference measurements for tissue pH and lactate were made with glass microelectrodes and micro-enzymatic assay, respectively. Partial least-squares (PLS) data analysis was used to develop multivariate calibration models on an initial set of 5-6 plaques relating the optical spectra to the reference tissue pH (n=20) or the lactate concentration (n=21) to assess data quality. The coefficient of multiple determination (R^2), the standard error of cross-validation (SECV), and the number of factors were used to assess the model performance. Additional points were collected from ~14 plaques and added to preliminary data. Pre-processing techniques were then used to see if preliminary data results could be improved by reducing different sources of variability with the introduction of more points.

RESULTS: Monte Carlo simulations and depth penetration tests with the final probe design showed light is collected from ~1 mm^3 volume of tissue using a 50 micron source-receiver separation. Tissue pH, pCO_2, pO_2 and temperature values demonstrated that the plaques were viable and stable in the media preparation for a maximum of 4 hours. Data from the first six plaques collected for lactate analysis showed that for seventeen points, a six-factor model produced adequate results (R^2=0.83 SECV=1.4 micromoles lactate/gram tissue). Data from the first five plaques collected for tissue pH analysis, showed for seventeen different points, a three-factor model produced adequate results (R^2=0.75 SECV=0.09 pH units). When additional points were added to either data set, model results were degraded.

CONCLUSIONS: The *in-vitro* optical probe design and experimental procedures was established and the feasibility of the optical method demonstrated with preliminary data. However, with the addition of more data points, different sources of tissue and spectral variability were observed to affect calibration. The gross pathology type and mismatched optical volume to reference measurement volume limited the tissue pH determination. The reference measurement precision, the spatial resolution of the reference lactate measurement, and unmodeled tissue variability (water and proteins) limited the lactate determination. Large variability in all optical measurements was observed. Additional *in-vitro* data collection would be required such that the variability due to the tissue is reduced and any spectrometer variability adequately compensated to be able to use the optical calibration *in-vivo*.

ACKNOWLEDGEMENTS

To my parents, Nurun Nahar, M.D. and Sukur G. Khan, Ph.D., for putting up with me for so long and being my first teachers.

To my brother, Shafi Khan and his wife Sheryl, for choosing the road that I so gratefully did not choose.

To Gabriel Alexander Khan, the Angel, welcome to this place, I'll show you everything.

To my cat, Harley G.M. Khan, always racing through my brain, when no one else could heal my pain, you are there!

To my Wendy, for being "Born to Run" anywhere in the U.S. and Canada.

To all the other Khans wandering somewhere around this crazy world, your thoughts and prayers have been so appreciated.

To my principal advisor and teacher, Babs R. Soller, Ph.D., I appreciate your patience; I know I've tested it many times and I probably will for life.

To ALL my teachers and coaches over my 22+ years of formal education—from Mrs. Cassin (kindergarten), Mrs. Brown to Mr. Costello (middle school), to Mrs. Walker and Mr. Bleistein and Mr. Martin and Mr. DePuglio and Mr. Gibbs and Ms. Z and Mr. Pflaummer, Mr. Cavanaugh, and of course, Delaware Hood (high school), to Dr. H.H. Winter, Dr. V. Haensel, Dr. J. van Egmond, Dr. N. Hellman, Dr. R.A. Lawrence, Dr. P. Westmoreland, and Dr. Stedman, Dr. Ragle, Mitch Kotler, and all the TA's who are by now hopefully Ph.D.'s (UMass Amherst), and to Dr. J. Miller, Dr. R.A. Peura, Dr. N. Cingo, Dr. S. Zhang, Dr. P. Idwasi, Dr. C. Hsi, Dr. R. Tuft, Dr. S. Litovsky, Dr. D. Engler, Dr. S.W. Casscells, Dr. J.T. Willerson, and Dr. M. Naghavi (WPI/UMMS/THI)—I will never forget what and how you taught me. I will never, ever, stop learning. And yes Jerry, I'm working on improving my time in the mile.

Special thanks to the doctors and researchers in the Vascular Surgery Department at UMass Memorial and everyone in the OR for dealing with a nutty graduate student.

To Markus Stratmann, for being my newest, kindest, and dearest friend, and helping me stay somewhat sane through the last leg of my doctorate. *Ich liebe dich.*

To Robin Marcel, Janice Favreau, Mitra Rajabi, Linda Jackman, Scott Jelley, Virginia Li, Erik North, Michelle Shin-Woo, Oren Froy, Ruth Brain, and the entire Waddell Lab; Charlotte, Tom, and Evan Nelson; Peter and Carol Jonietz; Kathy, Jeff, and Ryan Winston for just being there.

To all my former lovers and intimate strangers, thanks for letting me go, to do my life's work.

"The Rebirth, The Rededication and The Rising" – there's a special place in my heart & soul for G.H., J.L., P.M., J.J., R.O.; B.J., J.T., R.S., S.N., B.S., S.V., C.C., R.B., G.W.T., D.F., P.S., M.W., N.L., J.M., S.M., MLE, A.R., and E.S. and the countless that inspires y'all. Thank you.

And finally, to God, without God, none of this would be possible. I haven't even begun to show you how much I appreciate your love, mercy, and forgiveness. You ain't seen nothing yet!

It's really all about apples. Really.

TABLE OF CONTENTS

List of Figures

List of Tables

1. INTRODUCTION – PROBLEM IDENTIFICATION

Cardiovascular disease is the number one cause of death in the United States. Each year in the U.S., approximately 1.5 million people experience heart attacks, one of the many possible consequences of cardiovascular disease.   Approximately 250,000 are sudden cardiac deaths. Atherosclerosis, a form of cardiovascular disease, is an arterial disease primarily found in medium or large sized arteries, such as the aortic, carotid, coronary, and cerebral arteries. In the over forty age group, most sudden cardiac deaths are attributed to atherosclerotic cardiovascular disease. Due to the critical nature of sudden cardiac arrest, more than half of these individuals die before reaching the hospital. The direct and indirect cost of coronary heart disease is estimated at $111.8 billion dollars in the United States alone. [1] The World Heart Federation reports that atherosclerotic cardiovascular disease account for 6.3 million deaths per year world wide, and occurs in both developing and industrialized nations, with the poor being affected the most.

The prevention of heart attacks in genetically predisposed individuals is geared toward the modification of many environmental and lifestyle factors. Atherosclerotic disease is common in the middle-age population; however, the lesions (or plaques) may not manifest themselves on a typical angiogram, an invasive diagnostic test performed by physicians in a cardiac catheterization laboratory. Angiography involves injecting radio-opaque dyes through a catheter and viewing the dye distribution through the coronary vessels using x-ray fluoroscopy. Atherosclerotic disease is verified through the angioscopic identification of severely reduced lumen size or reduced intensity of the dye in the vessels. However, approximately a third of all sudden cardiac deaths occur in otherwise healthy individuals, with little to no risk factors, who did not have an angiogram performed. Current medical knowledge cannot predict those individuals that may be at risk due to this clinically silent, asymptomatic disease. This lack of information prevents the clinician from using more aggressive, prophylactic measures to prevent a first, and often fatal, heart attack. If this at-risk patient subtype could be identified, the at-risk or vulnerable atherosclerotic plaque(s) that would cause a fatal heart attack could be potentially reversed, or at the very least, the threat significantly reduced [2]. In the long run, this knowledge will improve the quality of life and productivity among the affected populations.

Several invasive and non-invasive technologies have been proposed. Some modalities are being implemented to address the problem of identification of the smaller atherosclerotic lesions by finding structural differences that the atherosclerotic process causes in the vessel walls [3-19]. The elusiveness lies in predicting those plaques that are prone to rupture and/or cause large clots to form, blocking the blood flow in the artery and causing severe damage to the heart muscle or tissue downstream. A more accurate method to diagnose the vulnerable atherosclerotic plaque(s) would be required to ensure that the individual would receive the most appropriate therapy. This method must be easily adapted into the cardiac catheterization laboratory or, if possible, be completely non-invasive. The information provided by the new diagnostic method should be clinically

acceptable and relevant to current research trends in atherosclerosis diagnosis and treatment in order to succeed in saving lives.

Optical spectroscopy, a minimally invasive technique that could be adapted into the cardiac catheterization laboratory, is such a technique that could meet this medical need. Chemical information and/or metabolism of the atherosclerotic plaques could potentially be studied *in-vivo* with optical spectroscopy. However, this method requires a calibration between the optical spectra and destructive reference chemical measurements with accepted techniques. The establishment of an *in-vitro* optical calibration is the first in a series of steps that would be required in bringing this technique to the clinic.

The precise mechanisms of atherosclerosis are unknown. It is a disease state under heavy research from several different fields including, among others, immunology, pathology, epidemiology, cardiology, pharmacology and hematology, all in an effort to improve the diagnosis, treatment, and outcomes. The challenge in providing this new metric or diagnostic tool is further complicated by not being able to fully appreciate how that information fits into the current understanding of the underlying mechanisms of atherosclerotic cardiovascular disease.

1.1.   Atherosclerotic Process

It has been well known since the 1950's that high blood cholesterol levels leads to deposit formation in the human arterial system. At the affected site(s), known as the plaque, the vessel wall will thicken and/or the vessel diameter will decrease, reducing the amount of blood that can pass through. This is known in layman's terms as "hardening of the arteries" or atherosclerosis, a process in which the artery's function is compromised. The decreased function over time can lead to the development of several types of cardiovascular disease states. For sudden death, it is believed that it should be possible to identify the specific atherosclerotic process(es) that create plaques that suddenly erode, erupt, or block a critical coronary artery, i.e. to identify the "vulnerable plaque". Lowering blood cholesterol alone has not been sufficient to prevent sudden cardiac death.

There are several important factors beyond cholesterol that have been implicated as part of the atherosclerotic process. It has been suggested by several researchers [20, 21] that atherosclerosis may be thought of as a chronic inflammatory response of the arterial wall, initiated by some injury to the lining of the vessel wall (also called the endothelium). How or why the chronic response sometimes forms a stable plaque versus an unstable, potentially life-threatening plaque is unknown [22]. The plausible injury could be either physical (e.g., high shear, turbulent blood flow due to a branching of arteries) or other chemical factors [23]. Similar to a wound healing response on the skin, the atherosclerotic process seems to initiate repair through recruiting blood components such as platelets and clotting factors and creating fibrous, necrotic scar tissue. Since the "wound" never seems to heal (or the source of injury isn't reduced), local and systemic signaling occurs to recruit inflammatory cells to attack the site(s).

Different molecular and cellular responses of the endothelium, smooth muscle cells, and/or extracellular matrix chemical influx/efflux, have been studied on their effects in alleviating vessel dysfunction with both positive and negative feedback cascades. Smooth muscle cells, present normally in the medial portion of the vessel wall, have been shown to migrate towards the luminal surface in some cases. Additional chemical factors have been identified, secreted into the extracellular matrix by either the infiltrating, activated inflammatory cells from the lumen or by the migrating smooth muscle cells from the medial portion of the vessel. New vessel development, or angiogenesis (a naturally occurring phenomenon throughout the body), can occur within the thickening diseased vessel wall, but, at the atherosclerotic site, these new vessels are erratically formed and are often "leaky", i.e. they do not hold the blood plasma components like a normal artery. These "leaky" vessels could contribute to blood clots (known as thrombi) inside the plaque and destabilize the plaque. Again, how or why this process may form the vulnerable plaque has not been elucidated.

1.2. The Unknown Diagnosis – Vulnerable Plaque

The "gold standard" in vulnerable plaque identification is histological classification. Current medical knowledge has not been able to explain all the observed vulnerable plaque characteristics such as fibrous cap erosions, ruptures, and clot inducing factors, as seen by microscopic examination of a heart's coronary arteries *post-mortem*. Histology is useful as a retrospective view of atherosclerotic disease, not as a diagnostic tool. The histology can significantly differ from coronary plaques, to carotid plaques, to aortic plaques. The individual plaques are very heterogeneous as to the cell types, amount of fatty deposits, and their make-up of structural components such as collagen, fibrin and elastin. Pathologists struggle with classification schemes and gradation of lesions that are not or were not angiographically apparent, as these are the typical culprits of sudden cardiac death. Current research is focusing on the chemical composition of the plaque to pinpoint the sources of vulnerability before they can cause an acute event [2, 24, 25].

A new metric or diagnostic tool must therefore be able to access the chemical information of the atherosclerotic plaque without losing sight of the importance of structural information in the living patient. First, the feasibility of the new metric must be shown *in-vitro,* and ultimately *in-vivo* with animal models. The technique should be accurate with respect to its own range of determination. The sensitivity and specificity of the new metric must ultimately be equal to or greater than the histological classification or another proven clinical method. However, only by looking at clinical outcomes over time for the affected populations, can one validate the final diagnostic accuracy of the new diagnostic tool.

1.3. Summary

The lack of an accurate technique to diagnose vulnerable plaque that is intuitive, clinically relevant, and inexpensive, presents a significant medical challenge. Vulnerable plaque diagnosis may require a novel, invasive approach that can deliver useful

information about the plaque to the physician. The active metabolism of the atherosclerotic plaques could potentially be studied *in-vivo* with optical spectroscopy and be used in the future as an indicator of vulnerability. Determining the feasibility of the optical method would require a better understanding of the atherosclerotic tissue energetics, tissue optics, and any factors that could affect the accuracy and range of an optical determination. In this research, feasibility is studied for a specific *in-vitro* optical probe design, experimental method, and spectroscopic data analysis methodology. The knowledge gained in this research is hoped to aid in the development of a clinical instrument for the detection of vulnerable plaque.

2. THE SPECIFIC AIMS OF THE RESEARCH

2.1. Project Statement

The intent of this research is to demonstrate the feasibility of using optical spectroscopy to accurately determine the metabolic status (tissue pH and lactate concentration) of living human atherosclerotic plaques. This goal is to be accomplished through the design of a small, fiber optic-based, reflectance-mode spectroscopic probe to collect continuous optical spectra (400-2400 nm) from an approximately 1-mm^3 volume of tissue. This probe will then be used in an *in-vitro* study in order to develop equations that calculate pH and lactate from these spectra. The *in-vitro* study is performed on freshly excised human carotid artery atherosclerotic plaques maintained for a prolonged period using tissue culture techniques. The spatial performance of the optical probe will be assessed by an actual measurement of the tissue depth interrogated. The optical spectra collected with this probe will be matched with the standard destructive reference measurements of tissue pH and lactate concentration of the living plaque. Multivariate mathematical models will be developed by analyzing the optical spectra for the most relevant factors that correlate with the individual reference measurements. These models will serve as a calibration of the optical system. Each calibration model will be tested for its capability to predict the desired parameter(s) from unknown optical spectra using accepted techniques for small sample sizes (N<100, e.g. cross-validation). Target acceptance criteria for model accuracy, predictive ability, and complexity are drawn to determine if feasibility has been met.

For the purposes of this research, the optically determined tissue pH and lactate calibration that provides the best accuracy and predictive ability after multivariate calibration will only be reviewed as to its possible correlation to the current destructive method of classifying atherosclerotic plaques (i.e. histology). At the conclusion of this phase of research, it is hoped that the model developed on *in-vitro* data can be translated to an appropriate *in-vivo* animal model for validation, with at the very most, minor additional destructive experimentation for improving model accuracy and prediction. It is not the intent of this research to definitively answer whether optically determined metabolic status based on tissue pH and/or tissue lactate is sensitive and/or specific enough to differentiate different atherosclerotic lesion types or identify vulnerability. Limitations will be discussed for the feasibility of using optical spectroscopy and for the long-term objective of making a clinical optical spectroscopy catheter that can predict plaques that are vulnerable to rupture. An additional contribution of this research is gaining a better understanding of the gross metabolic properties of atherosclerotic lesions, which could help future researchers develop better diagnostic and therapeutic agents to reduce the number of sudden cardiac deaths, and possibly aid in the prevention of heart attacks.

Short-term goals must first be achieved to realize the potential benefit to society. The following specific aims outline how these research goals will be met:

1) Design a reflectance-based optical fiber probe that uses visible to near-infrared light optimally to interrogate a small volume of tissue. The target of a 1 mm^3 tissue volume is based on the normal wall thickness of a coronary artery, the average thickness of atherosclerotic plaques with less than 70% blockage of the artery, and a plausible x-y plane of heterogeneity with respect to the atherosclerotic plaque.

   a) Perform Monte Carlo simulations of the probability of diffuse radial reflectance for several theoretical source-receiver separations as a function of depth. Optical properties of vessel wall and atherosclerotic lesions described in the literature are to be used. Infer possible source-receiver fiber separations that meet target volume based on the simulation depth penetration.
   b) Design and build fiber optic probe(s) using the simulation results as a starting point (*first design iteration*).
   c) Collect and analyze 400-2400 nm optical spectra using the fiber probe(s) and their different source-receiver separations on normal vessel walls. Estimate signal-to-noise ratio at different key wavelengths and implement design improvements (*second design iteration*).

2) Using the optimized custom-manufactured optical probe built after the second design iteration, estimate the depth penetration. Measure the depth penetration at key wavelengths by successively stacking thin sections of non-diseased tissue on to the end of optical probe and collecting the reflectance spectra. Compare to theoretical calculations and estimate resulting tissue volume over the wavelength region studied.

3) Identify major interferents to the optical spectra and reference measurements. Determine which may prove to be significant to the calibration accuracy. Propose or develop methodology to reduce their effects. Show that the stability of metabolic parameters over the time course of data collection can be achieved using tissue culture techniques. The stability is required to mimic *in-vivo* situations and decrease time-correlated effects on the measurements.

4) Using the optimized fiber optic probe, collect and analyze a large calibration set of human carotid endarterectomy specimens (~100 data points) while maintaining physiological state *in-vitro*.
   a) Perform multivariate calibration using wavelength selection and/or signal conditioning for optical tissue pH and tissue lactate determinations.
   b) Compare the optically-predicted values from the multivariate calibration to the reference measurements using calibration metrics of correlation coefficient (R^2), standard error of cross-validation (SECV), and the number of factors needed to describe the correlation for model accuracy. Review acceptance criteria and make recommendations.

2.2. General Requirements

Table 2.2.1 summarizes the general performance requirements for this feasibility study. There is no consensus as to what the exact requirements are to find the vulnerable plaque

based on metabolic status. However, to ensure the applicability of the methods and apparatus described within, performance specifications must be outlined, and it must be shown that the apparatus meets these specifications. The expected range of measurement and estimated accuracy required for each parameter is needed. Frequency of measurements (time dependence issues), and experimental stability also need to be addressed. The experiments are conducted in a controlled environment, so it is important to understand how the multivariate calibration model will respond to the presence of other unmodeled inputs such as experimental conditions or compounds. The maximum number of factors allowed is based on the current multivariate calibration literature for small data sets [26]. The performance of the final optical prototype shall be discussed in terms of the feasibility to optically determine the metabolic status of atherosclerotic plaques.

Table 2.2.1: General Performance Requirements

Specification	Tissue pH	Tissue Lactate Concentration [micromoles lactate / gram tissue]	*in-vitro* Temperature (°C)
in-vitro Experimental Stability	< 0.03 change/hr	-	<0.4°C change/hr
Optical Calibration Range	6.80 – 7.60	2 – 20	32.0 – 38.0
Optical Calibration Coefficient of Multiple Determination (R^2) / Estimated Accuracy (SECV)	≥0.75 / 0.08 pH units	≥0.75 / 1.0 umoles/ gram tissue	-
Maximum # of Factors in Optical Calibration Model [26]	5 to 6 independent samples per factor	5 to 6 independent samples per factor	-

In review, the optical spectroscopy techniques described here are investigated to determine feasibility and the potential use in identifying the metabolic status of atherosclerotic plaques in a cardiac catheterization setting. In 1997, an estimated 2 million inpatient cardiac catheterizations were performed [1]. Technological improvements in other modalities for vulnerable plaque detection such as intravascular ultrasound (IVUS) and magnetic resonance coronary catheters are still on the horizon. Optical fiber technology is currently used in different intravascular applications, and can be rapidly adapted to include spectroscopic techniques. The interventional cardiologist's interest drives the industry to produce sterile, disposable coronary catheters within the $200-400 price range. An accurate spectroscopic optical catheter system for determining the metabolic status of atherosclerotic plaque should meet this need. The research here aims to establish feasibility of a spectroscopic-based catheter for vulnerable plaque identification. As the optical method gains acceptance, so will the interest to outfit cardiac catheterization labs with new, inexpensive technology, in order to improve the health and well being of patients.

3. HYPOTHESES AND RESEARCH METHODS

3.1. Hypotheses

The long-term objective is to develop an optical spectroscopy catheter system to determine the metabolic status of atherosclerotic vessels without the need for exogenous dyes, ionizing radiation or a high capital medical unit setting. To date, there have not been any reports of using this technique to determine metabolic parameters such as the tissue pH or lactate concentration of atherosclerotic plaques. The feasibility of using optical spectroscopy to accurately determine metabolic derangements (namely, tissue pH and lactate concentration) in living human atherosclerotic lesions is under investigation. The overall hypothesis is that reflectance-mode optical spectroscopy, using visible to near infrared light energy, can be used *in-vitro* to develop calibration equations that provide an optical determination of the atherosclerotic tissue pH and lactate concentration. The performance of the optical probe will be reviewed in light of the calibration accuracy that can be achieved.

Three specific hypotheses will be tested in this research:

1) A small fiber optic prototype (< 3 mm optical working diameter) can make optical measurements *in-vitro* for the assessment of metabolically active plaque in a defined region of tissue (< $1mm^3$ volume). Both theoretical and practical considerations are allowed for in the design and implementation.

2) The *in-vitro* experimental factors, identified *a priori* as the tissue temperature, experiment time, and the gross constituent information of the plaque (i.e. gross pathology), can be assessed to their importance in affecting the optical calibration. It is hypothesized that the acceptance criteria for *in-vitro* experimental stability as defined in Section 2.2 can be met.

3) Mathematical models can be developed which relate the corresponding optical spectra to the individual metabolic parameters (pH and lactate), measured with accepted reference methods, in the presence of inherent pathological variability. By collecting the optical spectra in a controlled, stable *in-vitro* environment and by using partial least-squares (PLS) multivariate calibration, accurate determinations can be achieved for the individual metabolic parameters of plaque tissue pH and plaque lactate concentration. The correlation coefficient of the determination and standard error of cross-validation will be used to determine calibration performance. The number of factors will be used to determine the appropriateness (e.g., overfit/underfit) of the optical calibration.

3.2. Research Methods

Methods and apparatus based on reflectance-mode spectroscopy of visible and near-infrared light were chosen to solve the main research problem (Chapter 1) for the following reasons:

- Standard medical-grade optical fibers can provide inexpensive, remote, vascular access to the atherosclerotic lesion or known diseased areas. Optical spectroscopy can provide specific biochemical information, unlike intravascular ultrasound (IVUS), or magnetic resonance (MR) catheters that currently provide only structural information.

- The potential for Catheterization Laboratory research and clinical use is enormous.

- Preliminary results in Dr. Soller's laboratory show tissue pH can be feasibly determined by optical reflectance spectroscopy in several different tissue beds. [27-29] Other researchers have used optical methods to determine lactate and other metabolites in cell culture [30], and blood plasma [31].

- No other researchers have reported results on using this method for determining the metabolic status of atherosclerotic lesions. This is a novel approach based on the idea that vulnerable plaques are more metabolically active than the stable plaque or background vessel wall. This research will contribute significantly to the existing knowledge in the field of vulnerable plaque research.

Optical spectroscopy is one of many techniques available for non-destructive analysis of tissues. However, it is relatively inexpensive compared to other modalities such as NMR, B-mode ultrasound, and nuclear (x-ray) radiography. Optical spectroscopy has been proposed by several researchers (Lodder [12], Muller [32], Feld [33], Jaross [34], Wang [35]) to characterize the properties of vulnerable atherosclerotic plaques, such as thin cap and large lipid core. However, in this previous body of work they were not able to resolve the issue of the inherent tissue heterogeneity with respect to these histological variables and their optical measurement. The apparent mismatch is identified as a key reason why the optical methods accuracy is less than desired.

There is also considerable metabolic heterogeneity in human atherosclerotic lesions [25], [36]. It is precisely because of the structural and metabolic heterogeneities observed that an accurate optical tissue pH or lactate determination can only be made in the atherosclerotic plaque when the light is collected from a known volume of tissue, and the reference measurements are equally well resolved. Therefore, the primary requirement for the reflectance-mode optical probe design in this research is to have a well-defined region of interrogation, such that the optical measurement is matched to the reference measurement, within the limits of the size of a typical intravascular catheter. This is achieved by examining both the theoretical and experimental depth penetration for different source-receiver separations. This distance between the source light optical fibers, interacting with the tissue, and the light receiving optical fibers is critical to the ultimate performance of the prototype. First, Monte Carlo simulations are performed, using optical property data of the vessel wall and atherosclerotic plaque available in the literature. The resulting output of the probabilities of diffuse reflectance as a function of radius, and the probabilities of absorption as a function of depth are interpreted. The simulations aid in the practical design of the probe by providing a starting point for the testing of different source-receiver separations. Since optical property data is available only at certain wavelengths, some extrapolation is necessary. A final depth penetration test shall confirm the design.

The experimental optical setup will include the building and testing of source-receiver separations of 50 and 500 um, different fiber sizes, with and without an optical window. The probe(s) signal-to-noise ratios on a specified spectrometer are analyzed to aid in decision-making of optical components and configurations. The depth penetration of the optimal configuration is measured at several key wavelengths and assessed to see if the target volume criterion has been met.

The potentially confounding and unmodeled experimental variables are identified *a priori*. These variables are the *in-vitro* tissue temperature, the experiment time, and the gross pathology of the atherosclerotic plaque. The thickness and the co-registration of optical spectra to the reference measurements are documented. The existence of other systematic errors that affect the optical determination or the multivariate calibration model development, if any, shall be evaluated. Large-scale *in-vitro* experimentation on freshly excised human carotid plaques are conducted in oxygenated tissue culture media with temperature control. The stability of this methodology is validated over time by using a pCO_2, pO_2, and tissue pH multi-parameter sensor for several different plaques. The maximum data collection time is fixed at four (4) hours to ensure tissue stability for all plaque types and thickness.

The optical calibration model development process will begin with a multivariate data analysis technique called partial least squares regression. It is the technique known to work for tissue pH in other applications in Dr. Soller's lab [29]. Different wavelength regions for the tissue pH and lactate determination will be used and selection criteria developed based on model improvements. The calibration model statistics will be reviewed and standard calibration set acceptance criteria (such as the F-ratio for outlier detection and minimum PRESS for optimal number of factors) will be used.

Figure 3.2.1 shows a flowchart for this research approach. The major components are the optical design, the *in-vitro* carotid plaque experiments, and finally the multivariate calibration model development. The design and experiment process is usually iterative, however, for the purposes of this study, only the performance through the second iteration was evaluated.

The optical design process involved several steps, including:
- Definition of optical probe requirements;
- Theoretical considerations of tissue optical properties;
- Monte Carlo simulations and interpretation;
- Building and testing several optical probes;
- Depth penetration assessment

Preliminary experimentation with intermediate design optical probes provided insight into the methodology and execution of the *in-vitro* experiments for the desired optical determinations. Once the optical probe has been designed and built to address as many of the issues as possible, the large-scale *in-vitro* testing program will provide the data for the optical calibration models. Preliminary data analysis will be performed after

approximately 20 points to assess data quality. Factors that may influence the results will be documented. Additional data collection and points will be added to see if model results may be improved. The calibration model development is a complex, statistically based empirical process involving, but not limited to, data compression, factor analysis, and outlier selection. The performance of the final optical prototype will be evaluated using standard metrics in the multivariate calibration literature. The feasibility of the optical determination of plaque tissue pH and lactate concentration in the context of any unmodeled variables will be assessed. Finally, the applicability of the prototype's performance towards detection of the vulnerable plaque via metabolic status and recommendations for future modifications to either the optical design or calibration method will be addressed.

```
                        ┌──────────────────────┐
                        │    Previous Work      │
                        │    Considerations     │
                        └──────────┬───────────┘
              ┌────────────────────┼────────────────────┐
              ▼                    │                    ▼
    ┌──────────────────┐          │          ┌──────────────────┐
    │   Experimental    │          │          │   Theoretical     │
    │   Probe(s) Tests  │          │          │   Calculations    │
    └────────┬─────────┘          │          └─────────┬────────┘
             └──────────────────► ⊗ ◄──────────────────┘
                                   │
                                   ▼
                        ┌──────────────────────┐
                        │  Optical Probe and    │
                        │  Experimental Setup   │
                        │      Validation       │
                        └──────────┬───────────┘
                                   ▼
                        ┌──────────────────────┐
                        │  in-vitro experiments │
                        │     n≈100 points      │
                        │ Preliminary analysis  │
                        │      at n≈20 pts      │
                        └──────────┬───────────┘
                                   ▼
                        ┌──────────────────────┐
                        │ Determination of      │
                        │ significance of major │
                        │ experimental factors  │
                        │ on the desired        │
                        │ measurements          │
                        └──────────┬───────────┘
                                   ▼
                        ┌──────────────────────┐
                        │ Development of a      │
                        │ calibration model for │
                        │ plaque tissue pH and  │
                        │ lactate concentration │
                        └──────────┬───────────┘
                                   ▼
                        ┌──────────────────────┐
                        │ Assess if Acceptance  │
                        │ Criteria are met,     │
                        │ make recommendations  │
                        └──────────────────────┘
```

Figure 3.2.1: Flowchart for research approach.

4. BACKGROUND

This research endeavors to establish the feasibility of the determination of metabolic status in atherosclerotic plaque by using optical spectroscopy. Specifically, the plaque tissue pH and tissue lactate concentration are used as the primary indicators of metabolic status. The key concepts for the research performed are discussed in this chapter. It is expected that the reader will grasp the nature and complexity of the proposed research aims, and how each concept is important to the outcome of the studies reported. The following sections outline the basis for the research methodology:

1) Vasculature – structure, function, and mechanisms of disease;
2) Natural history of atherosclerosis and the concept of the vulnerable plaque;
3) Available technology;
4) Reflectance spectroscopy and tissue optics;
5) Multivariate calibration methods;
6) Absorbance characteristics of the vessel wall and atherosclerotic plaques; and
7) Experimental factors

The vasculature and concept of the vulnerable plaque is thoroughly reviewed to gain understanding of changes that can affect vessel wall structure and metabolism. Next, the current technology to diagnose cardiovascular disease and vulnerable plaque are reviewed. Basic optical terminology and tissue optics are described to appreciate the complexity of the optical probe design requirements. Multivariate calibration methods and their necessity are introduced. Finally, the absorbance characteristics and the experimental factors associated with making optical measurements in living atherosclerotic plaques are presented. Challenges in establishing the metabolic status independent of optical or pathophysiological interferents is briefly discussed as it relates to the overall research goals.

4.1. Vasculature – Structure, Function, and Mechanisms of Disease

The structure and function of the different types of arteries found in the cardiovascular system play a major role in maintaining systemic balance and health. In this section, the normal cardiovascular system is described in the context of arterial structure and function. Possible mechanisms of atherosclerotic disease are briefly discussed with clinical correlation. Finally, the importance of environmental and genetic factors that imply that atherosclerotic cardiovascular disease is a world epidemic that requires more accurate diagnostic methods is discussed.

4.1.1. The Cardiovascular System

The arteries and veins form a comprehensive network to maintain homeostasis by carrying blood throughout the human body. The purpose of the cardiovascular system is to deliver blood to the various organs and tissue beds such that the following basic, life-supporting functions are adequately maintained: gas exchange, nutrient exchange, blood flow/pressure and circulation, and systemic hormones exchange. A schematic view of the human cardiovascular system is depicted in Figure 4.1.1. The heart (H) functions as the

pump that drives oxygenated blood through the arteries (A) to the head and body and deoxygenated blood returns to the lungs via the veins (V) for gas exchange. Ventricular contraction of the heart (or systole) propels the blood through the aorta, which in turn, through muscular recoil, gives the appropriate pressure head such that blood can reach the lower part of the body and steady blood flow is achieved in capillary beds. Ventricular relaxation (or diastole) both allows the heart to refill to its oxygenated (left ventricle) and deoxygenated (right ventricle) blood capacity as well as letting blood flow into the coronary tree. The heart itself has its own network of arteries, the coronary system, which branches directly from the aorta and experiences flow only in diastole [37].

Figure 4.1.1: Overview of Cardiovascular System
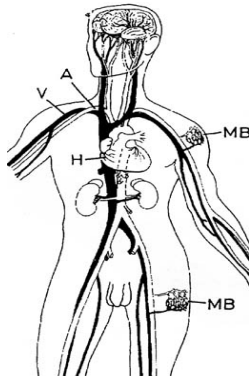
The main components of human cardiovasculature: H - heart, A - arteries, V - veins, MB – microvascular beds.

Arteries are divided into three basic types: 1) large or elastic, 2) medium-sized or muscular, and 3) small (< 2mm in diameter). All arteries -- the aorta, to the coronary, carotid, femoral, and brachial arteries -- to the smaller arterioles -- are composed of three distinct layers, the intima, media, and adventitia (Figure 4.1.2).

Figure 4.1.2: Schematic representation of the principal structural components of a medium-sized artery. [38]
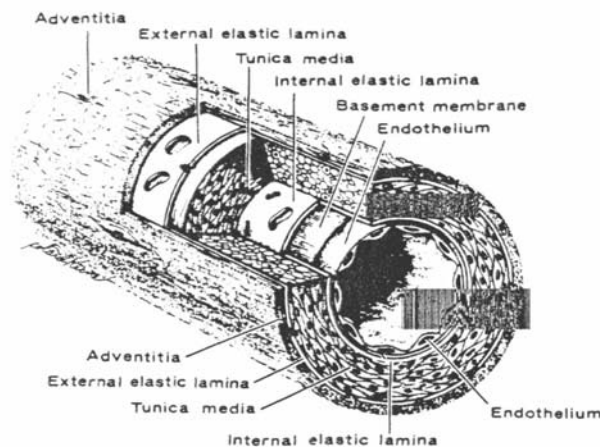
The intimal layer is characterized by a single cell layer of endothelial cells, which line the interior of the vessel wall (the endothelium). It is in direct contact with the blood and

blood components. The endothelium lines the entire cardiovascular system and facilitates the above basic functions. Smooth muscle cells (SMCs) and varying levels of Type III collagen and elastin (for vessel tone) characterize the medial layer. SMCs contain actin and myosin, providing vasoconstriction and dilation functions in response to physiological or pharmacological stimuli as well as motility, produce collagen, and are capable of secreting growth factors. The adventitia, the outermost layer, is characterized by additional collagen (Type I) and elastin, and smooth muscle cells and may contain vasa vasorum (lit. vessels of the vessels, e.g., aorta has small arterioles that feed the outer half to two-thirds of the medial layer). Connective tissue and nerve fibers are also found in the adventitia. The size and cellular components of each layer establishes the vessel's functional capability. The relative sizes and musculature of both the macrovessels and microvessels are shown in Figure 4.1.3.

Figure 4.1.3: Relative sizes and cellular components of blood vessels. [37]
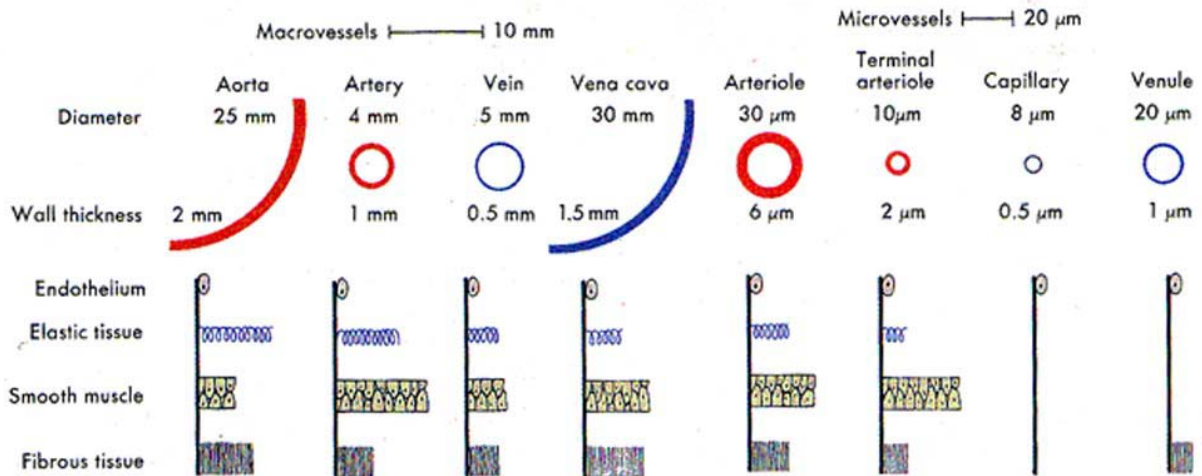
Elastic arteries (i.e., the aorta, common carotid and pulmonary arteries, and the beginning of the major branches) convert large pressure changes in pulsatile blood flow into a steady continuous stream. These arteries have a high proportion of elastic fibers in the medial layer; the walls appear yellow due to the abundance of elastic tissue. Smooth muscle indirectly regulates the recoil of the artery, and Type I collagen in the adventitia prevents further distention. The vasa vasorum supply blood only to the outermost layers (adventitia and outermost media layers). As a result, the walls are under relatively low oxygen tension in normal elastic arteries. Certain elastic arteries contain functional specialization. For example, at the carotid sinus (where the common carotid artery bifurcates into the external carotid and internal carotid arteries) there are baroreceptors and chemoreceptors that have additional functions and can affect systemic blood pressure and respiratory factors (for example, based on pH, partial pressure of oxygen in the blood). The carotid sinus is also innervated and has reflex-like activity to increasing blood pressure and chemical stimuli independent of the brain's neurohormonal sympathetic drive.

Muscular arteries (i.e., the brachial, femoral, radial, popliteal, renal, and coronary arteries and their branches) adjust the blood distribution from the heart to the major areas of the body. These arteries have a higher proportion of smooth muscle and less elastic tissue in the medial layer than elastic arteries. The adventitia, in comparison, is less structured; it is oriented longitudinally which allows for continuous changes in diameter. Structure varies considerably depending on the internal and external forces to which a particular muscular artery is subjected.

In addition to the different pressures and chemical stimuli that any single vessel may experience, structural changes also occur in the macrovasculature with age. From birth to approximately 25 years of age, the elastic arteries first have the histological appearance of a muscular artery (esp. the aorta) and then the wall thickens as there is an increased amount of elastic layers developing as the individual grows. Throughout adulthood, all arteries undergo normal, controlled, remodeling for various physiological and developmental reasons. In muscular arteries, the media thickens with increasing smooth muscle content but not as rapidly or to the same extent as the elastic arteries. From middle age and above, more connective tissue forms in the vessel wall (collagen, elastin, and proteoglycans). This causes the walls of the largest arteries to become less compliant or stiffer to changes in blood flow. The intimal layer however, thickens from birth on. The thickness varies along different parts of the arteries; in certain areas where tensile stresses are high, or flow is turbulent, the intima has a normal adaptive thickening response (esp. carotid bifurcation, coronary arteries). It is difficult to differentiate between development, early regression, or atherosclerosis in the intimal layer. In a sense, each artery has its own "aging pattern". The coronary vessels seem to "age" at a younger age than other vessels. [20] Therefore, the relation between structure and function is further complicated by developmental factors.

4.1.2.   Pathological Basis

Atherosclerosis affects primarily the large and medium-sized arteries (> 2mm in diameter) [22]. It is the underlying cause of most cardiovascular diseases. Clinically, it may manifest itself as luminal narrowing of the artery (stenosis), myocardial infarction (heart attack), cerebral infarction (stroke), claudications and aneurysms, among other less obvious effects [1]. However, the exact mechanisms of atherosclerosis are not well understood. At present, histological identification of the diseased vessel wall after surgical excision or *post-mortem* is the only way atherosclerotic lesions can be investigated and classified. Based on these histological studies of varying ages and disease states, the most accepted theory for atherosclerotic initiation and progression is called the "response to injury" theory, i.e., atherosclerosis may be thought of as a chronic inflammatory response of the arterial wall initiated by endothelial dysfunction [22, 23]. The atherosclerotic vessel wall may be ischemic (lack of oxygen), and the molecular and cellular responses of the endothelium and smooth muscle cells are activated [39, 40]. The importance of the endothelium and its contribution to metabolic stress is discussed.

The endothelium acts as a semi-permeable barrier between the blood and tissue. It has significant implications in the mechanism and progression of many diseases. The main functions of the endothelium are:

- Control the transfer of small and large moieties into the vessel wall
- Maintain a non-thrombogenic (not clot prone) interface by regulating, in part, platelet adherence
- Control vascular tone and blood flow
- Metabolize hormones
- Regulate immune and inflammatory cell reactions through receptor-mediated interactions
- Modify lipoproteins in the artery wall
- Regulate the growth of smooth muscle cells

The response of the endothelium is defined by what kinds of properties are induced (see Figure 4.1.4) [22]. In general, endothelial dysfunction refers to potentially reversible, functional changes that occur due to the local environment. Endothelial stimulation is a transient functional change that occurs within minutes, is reversible, and does not result in any new protein synthesis. These changes can be caused by either short-lived, vaso-active substances in the blood or temporary mechanical stress. Endothelial activation, however, requires hours or days to occur and results in changes in gene expression and protein synthesis. It is this activation that is thought to contribute to the progression of many vascular diseases [22].

Figure 4.1.4: Endothelial activation and induced properties.
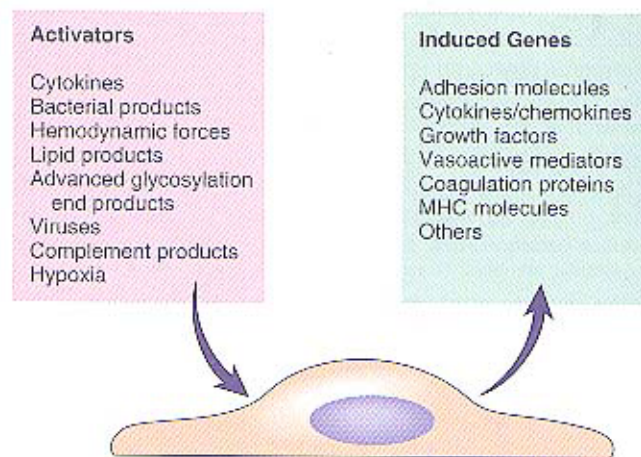
Several activators found in the blood can cause long term endothelial dysfunction or activation. Gene expression or protein synthesis occurs as a result of endothelial activation. MHC – major histocompatibility complex. Partial list.

The normal and inflammatory responses of the endothelium both culminate in the retention of lipoproteins in the arterial wall. Plaques occur as a result of chronic oxidative stress (initially, lipid oxidation) in the arterial wall, and other factors beyond cholesterol deposition, especially in sites that are predisposed to thickening due to normal vessel function or location in the body. This oxidative stress is thought to in turn stimulate more inflammatory responses from the endothelium and smooth muscle activation/migration into the intima [39, 40]. This process can lead to cell death (necrosis and/or apoptosis), where cell lipids and debris accumulate deep in the vessel wall. These deposits are

responsible for vessel dysfunction and when disrupted, lead to acute blockage of the artery.

However, it has not been possible to predict which plaque deposits will cause clinical events. It has become a research imperative to develop blood tests, instruments, and/or drug therapy protocols that will allow clinicians to understand atherosclerosis better, effectively manage patients, and ultimately reduce acute events that impair life and increase the cost of care. It should be possible to develop an intravascular device based on the living, physiological effects of atherosclerosis on the vessel wall to identify vulnerable plaque. Such a device should be able to elucidate silent lesions that will cause death if not diagnosed and treated, be minimally invasive, and cost-effective in order to save lives. The clinician, armed with such a device, will be able decrease cardiovascular disease morbidity in their community.

4.1.3.   *Cardiovascular Disease – Risk Factors*

There are several environmental risk factors for cardiovascular disease (or CVD; includes coronary heart disease among several other disease states). Some are uncontrollable, such as increasing age, male gender, family history, and genetic abnormalities. Some are potentially controllable, such as hyperlipidemia, hypertension, cigarette smoking, and diabetes. The American Heart Association's 2002 Heart and Stroke Statistical Update lists the five major risk factors for cardiovascular disease physicians consider in diagnosis and treatment [1]:

- Smoking
- High blood cholesterol and other lipids
- Physical inactivity
- Overweight and obesity
- Diabetes mellitus

Disease progression can be slowed down, and even reversed in some cases for gross lesions with drug therapy (e.g., statins such as LIPITOR®, ZOCOR®). The removal of risk factors such as smoking is very important. Surgery, drugs, and lifestyle changes prolong and improve the quality of life in most cases. However, when the disease is asymptomatic, which is the norm rather than the exception, it can only be silently managed. No one knows when or to whom a heart attack will occur. Symptoms may go on for days before the individual realizes he/she is having a heart attack. Detecting these high-risk or "vulnerable" atherosclerotic lesions (lesions that suddenly rupture or block the flow of blood) before the acute event ever occurs has become a global scientific imperative.

4.2.   Natural History of Atherosclerosis: Concept of the Vulnerable Plaque

Dr. James Muller first introduced the concept of "vulnerable" atherosclerotic lesions in 1992 [41, 42]. Since then considerable debate has occurred as to whether this lesion

exists, or can even be defined with current technology. In this section, the vulnerable plaque concept is reviewed. The medical necessity to understand atherosclerosis in-vivo drives much of the current research efforts to develop diagnostic instruments. Finally, the justification for looking at the metabolic status of atherosclerotic vessels through spectroscopy is discussed, as well as its potential benefit to the field of vulnerable plaque research.

The current scientific consensus from Virmani *et al* [25] defines vulnerable plaques as "precursor lesions" that ultimately end in acute coronary thrombi (clots) that create a heart attack. These plaques are further classified as ruptured, eroded, or calcified nodules. The most common of these are the ruptured plaque. Its precursor, the thin-cap fibroatheroma (TCFA), is defined as a plaque with less than a 650 micron thick fibrous cap. The identification of these vulnerable plaque(s) in the asymptomatic population may be better resolved by knowing the chemical composition instead of or in addition to the structural size [25].

The atherosclerotic process in the arterial walls starts at an early age where some initial injury is presumed to cause endothelial dysfunction. Embryonic studies show that there is a difference between vasculature at birth versus young children. Fatty deposits or streaks characterize early lesions in teens. By young adulthood, the fatty deposits become more pronounced and frequent the more disruptive parts of artery walls, areas of high shear such as bifurcations and large vessel divergence. Diet, lifestyle, and genetic predisposition are some of the factors that may account for the different pathology in young adults. As the population gets older, disease progression continues as inflammatory responses, ischemic injury and/or tissue repair mechanisms affect the vessel wall and loses it ability to function properly. Calcification and necrosis occur as these fatty deposits make the intimal layer and/or medial layer dysfunctional [22]. Structural changes accompany the dysfunction, resulting in both luminal narrowing (stenosis) and wall thickening. However, it has been shown that having less than 50% stenosis of a vessel does not completely remove the risk of having a heart attack [23].
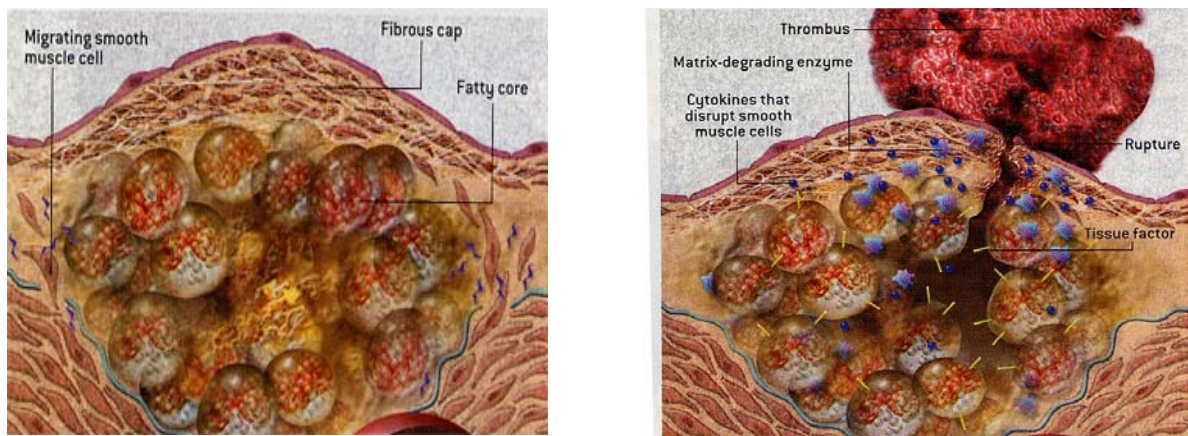
Figure 4.2.1: Plaque progression (left) and rupture (right). Plaque progression from stable plaque with a thick fibrous cap and fatty core, active cells in the core create changes that lead to rupture. Rupture is indicated by breakage of the fibrous cap and release of core materials into the bloodstream A blood clot or thrombus can form at this site, further limiting the blood flow in the lumen or causing acute blockage.

The plaque itself may have asymptomatic or symptomatic consequences. Asymptomatic consequences imply that the disease progression continues undetected and untreated, creating a possibly inferior cardiovascular system that would be unable to respond properly to further traumatic injury. Symptomatic consequences are clinically apparent when a proper medical history is taken. Symptoms range from angina (chest pain, both stable and unstable), clots, stenosis, reduced blood flow, heart attack, ischemic heart disease, and in the case of cerebral vasculature, transient ischemic attacks and stroke. The symptomatic consequences of atherosclerosis also create an inferior cardiovascular system, but at least it is detectable and treatable through differential diagnosis, lifestyle modifications, and FDA-approved drug or surgical technologies.

Up until recently, post-mortem studies have provided all the information regarding atherosclerotic plaque composition. Plaques may contain stabilizing fibrous caps (collagen, fibrin) that encompass the milieu of inflammatory cells (most notably monocyte-derived macrophages), fat, regions of calcification, necrosis, or even neovascularization (uncontrolled angiogenesis) within the diseased vessel wall. However, histological identification of the atherosclerotic plaque is an imperfect gold standard. Plaque histology, not only being very technique dependent, is a fairly qualitative measure of plaque composition and is subjective from pathologist to pathologist. It also is not a proactive diagnostic tool. Supplemental biochemical data of blood components have show strong correlations between circulating total blood cholesterol, high-density lipoproteins (HDL), low-density lipoproteins (LDL), and triglyceride levels and the lipid deposition seen histologically in the arterial wall. Blood markers of inflammation may also indicate the presence of vulnerable atherosclerotic lesions.

It is understandable then why much research in the area of identifying the chemical composition of plaques has focused on lipid accumulation of cholesterols or calcification [32, 34, 43, 44] However, a large lipid core alone is not significantly correlated with sudden plaque rupture or thrombosis (i.e. the vulnerable plaque). Since inflammatory responses are correlated with the incidence of plaque rupture, research has shifted in finding suitable markers for inflammation. Several molecular or immunological markers have been proposed (metallomatrix proteases, antibody staining, IL-6, etc.). Since inflammation characteristically produces heat, metabolic parameters--such as temperature [45], tissue pH [36], and metabolic by-products of inflammatory cells [46] have also been suggested as inflammatory markers, on a thermodynamic or tissue energetics basis.

Activated macrophages, an inflammatory cell type, play an important role in the plaque's susceptibility to rupture. In a large histological survey, plaques that had a high degree of activated macrophages, indicating an inflammatory response to plaque disruption, were more often responsible for an acute coronary syndrome versus lesions responsible for stable angina (14% versus 3% of plaque tissue occupied by macrophages) [21]. Cell density and temperature may also be indicators of the inflammatory response [45]. Macrophages, whose duty is to repair and remove fibrous tissues, infiltrate the cap region and affect the thickness, strength, and collagen content of a developing plaque. Plaque rupture would release the lipid core contents, which may cause an acute blockage

downstream (see Figure 4.2.1). Macrophages are working typically under conditions of low oxygen tension and metabolize glucose as their main source of energy. Anaerobic metabolism occurs due to lack of oxygen delivery, as the intimal layer gets most of its oxygen through simple diffusion from the blood. Lactate, a product of anaerobic metabolism, has been found in atherosclerotic plaques [47-49]. It also has been demonstrated that plaques with large lipid cores and low calcifications are associated with lower pH [36, 50]. A higher lactate or hydrogen ion concentration may indicate higher macrophage activity and acidic conditions, and therefore, be potentially associated with an increasing risk of rupture or vulnerability.

Early studies of atherosclerosis in the 1950's attempted to assess various enzymatic activities in the vessel wall of normal and atherosclerotic human vessels. The enzyme lactate dehydrogenase (LDH) catalyzes the reversible reaction of lactate to pyruvate by means of hydrogen transfer to and from NAD:

$$\text{L-lactate} + \text{NAD}^+ \overset{\text{LDH}}{\Longleftrightarrow} \text{pyruvate} + \text{NADH} + \text{H}^+$$
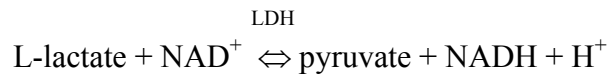
In alkaline conditions and at high lactate and NAD concentrations, the reaction proceeds left to right and pyruvate returns to the Krebs cycle. Kirk *et al* demonstrated using LDH activity that lactic acid production predominates in human aortic tissue and high glycolysis occurs both under aerobic and anaerobic conditions. It was proposed that lactic acid production arose from "originally neutral compounds", causing low pH of the tissue, which in turn may be important in preventing insoluble calcium deposits in the wall [51]. Zemplenyi et al used a microenzymatic method to quantify lactate in atherosclerotic plaques in rabbits [48] [49]and in rats [47]. A significant difference in lactate levels was demonstrated between normal and experimental atherosclerotic White New Zealand rabbit aortas (278 and 474 nmole/100 μg DNA mean values, normal and atherosclerotic respectively) [48].   The biochemical pathway for lactate production and anaerobic metabolism is summarized below:

Glucose aerobic oxidation: [52]

$$\text{Glucose} + 2\text{NAD}^+ + 2\text{ADP} + 2\text{P}_i \rightarrow 2\text{NADH} + 2\text{pyruvate} + 2\text{ATP} + 2\text{H}_2\text{0} + 4\text{H}^+$$

Anaerobic glycolysis: NADH free energy of oxidation is dissipated as heat, regenerate NAD$^+$

$$\text{Pyruvate} + \text{NADH} \rightarrow \text{L-lactate} + \text{NAD}^+$$
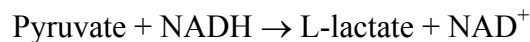
Overall anaerobic process:

$$\text{Glucose} + 2\text{ADP} + 2\text{P}_i \rightarrow 2\text{lactate} + 2\text{ATP} + 2\text{H}_2\text{0} + 2\text{H}^+$$

A more recent study of acidity in atherosclerotic lesions showed that the pH in lipid cores were significantly lower than the pH in calcified and thrombosed areas of 35 human carotid endarterectomized atherosclerotic plaques [50]. Similar results in atherosclerotic Watanabe rabbits, which exhibit more lipid cores in the aortic lesions formed, showed pH

was lower in the plaque than in the normal vessel wall. Inflammation and macrophage cell density was considered by collaborating investigators to be a source of temperature heterogeneity in plaques [45]. These studies indicate that pH and temperature may play an indicative role in plaque vulnerability.

4.3.   Available Technology

Presently, there is no FDA-approved monitoring technique or instrument that meets the requirements of a cost-effective, clinically acceptable, and useful instrument to assess plaque vulnerability. A comprehensive exam by a cardiologist or family physician must be performed in order to determine diagnosis, prophylaxis, and/or treatment. No one device can be used alone, especially without knowledge of family history and lifestyle. Blood tests for cholesterol, HDL/LDL ratio, and triglycerides can be predictive of cardiovascular disease in general. A new blood test for C-reactive protein (relative measure of inflammation) is being integrated into clinical practice as a predictor of acute myocardial infarction. [53, 54]Current clinical practice for coronary artery disease diagnosis uses either x-ray angiography or trans-esophageal echocardiography (TEE), which provide the clinician with degree of stenosis and approximate lumen size based on flow of contrast media or echogeneicity. There are several methods under research to locate gross lesions and stenoses, however, none predicts plaque vulnerability adequately.

Table 4.3.1 summarizes the advantages and disadvantages of both optical and non-optical techniques currently in the research stage for vulnerable plaque detection. The optical techniques—angioscopy [15], optical coherence tomography (OCT) [9], and photonic spectroscopy (including Raman [24, 33, 55-57], fluorescence [58-60], and near infrared [12, 32, 34])--are of great interest as they have the potential to provide both chemical and structural information at relatively low cost and are fairly intuitive. Raman spectroscopy initially was developed as an adjunct to histology, a destructive micro-analytical technique that was intended to remove the subjective nature of the standard H&E staining. Now, fiber optic Raman spectroscopy is being developed, using laser and graded-index fiber technologies reducing the inherent dispersion of the Raman scattered signal in standard optical grade materials. Fiber optic Raman spectroscopy has been used to quantify cholesterol and structural components in a small set of human coronary plaques [44]. Fluorescence spectroscopy can be used, however, it requires injection of a contrast agent (such as Antrin®, a hematoporphyrin derivative) that will have preferential uptake in the plaque. Some endogenous fluorophores exist in the lipid core of atherosclerotic plaque that may adversely affect the signal from the contrast agent as well. The fluorphore contrast agent is used to gain signal-to-noise and improve the consistency of this technique. Plaques that have neovascularization or intra-plaque hemorrhage have improved detection with fluorescence spectroscopy in animal models and in *in-vitro* human plaque studies [60, 61]. Near infrared spectroscopy techniques have historically looked at cholesterol deposits, oxidized LDL, or other morphological-related chemical species such as collagen [12, 34, 62, 63].   This research focuses on using near infrared spectroscopy to assess the metabolism of the atherosclerotic plaque, rather than a relatively static chemical species such as lipid content. All the optical

techniques are still in research phase and have yet to show whether the new metric will be an accurate predictor of vulnerability.

Out of the non-optical techniques, the issues of cost and ease of use currently make them restricted to large medical centers or research facilities. Intravascular ultrasound (IVUS) is being used more frequently outside of the U.S., however, its lack of specificity to chemical constituents is the main reason for poor predictability of vulnerability. Recent MRI research developments show biochemical profiles may be possible in small regions. Technical challenges such as small slice sizes and motion artifact currently preclude its use as a rapid in-vivo analyzer for vessels that are not superficial. Nuclear medicine techniques such as scintigraphy are also plagued with poor resolution and require more radioactive injections over and above the concurrent fluoroscope use in the Catheterization Lab [21].

Spectroscopic measurement of metabolic derangements such as tissue pH or lactate, in combination with one of the localization techniques, such as angioscopy, would be superior to cholesterol concentration determinations alone. Such an optically based, spectroscopic measurement would indicate macrophage activity and acidic plaque, as well as the influence of hypoxic cells on their way to necrosis or apoptosis. A catheter-based fiber optic, near infrared spectroscopy system is ultimately envisioned to assess the metabolic status of atherosclerotic plaques. Cardiac catheterization offers minimally invasive access to coronary arteries and can be used to evaluate multiple sites in one session.

Near infrared spectral data contain a wealth of chemical information that, if extracted properly, could provide a robust chemical assessment of vulnerability. The spectroscopic measurement can potentially be coupled with other clinical correlations to provide additional information about the plaque(s) and guide the clinician in preventing thrombosis and heart attacks. The ultimate design concept of an *in-vivo* spectroscopic catheter would be to adapt a Fogarty-type balloon angioscope to include near infrared spectroscopic transmitting/receiving fibers. Spectroscopic examination could potentially identify the extent of metabolic derangement in the arterial wall. Metabolic status of the diseased vessels and clinical presentation could be combined to construct a vulnerability score from a longitudinal clinical trial [36].

Table 4.3.1: Advantages and disadvantages of techniques for vulnerable plaque detection [2].

INVASIVE TECHNIQUES	Advantages	Disadvantages	Projected Use
Intravascular Ultrasound (IVUS)	Morphology of vessel wall/plaque not just the lumen or surface; echogenic density for fibrous cap	Echolucent areas cannot be distinguished as to composition; spatial resolution can not distinguish cap thickness with accuracy; calcium deposits cause "shadow" effect, such that deeper into the plaque can not be imaged; can not identify inflammation	In clinical testing stage; with additional B-mode specialized algorithms may be able to obtain more information towards identifying vulnerable plaque (elastography, tissue Doppler, shear stress imaging)
Intravascular Thermography	Sensitive thermistor technology; powerful clinical correlations to outcome; inflammatory response theory	Requires proximal occluding balloon; inflammation versus blood flow confounders; may not provide information about eroded but not inflamed plaques	Use in conjunction with IVUS; in animal testing stage
Intravascular and Transesophageal MRI	High resolution images and lack of ionizing radiation or exogenous compounds	Long acquisition times; cost; need in Catheterization Lab for other cardiovascular testing; patient ineligibility (metal implants, pacemakers)	In research phase; combine with thermometry
Angioscopy	Intuitive, simple to use	Visualizes only surface of vessel wall plaque; requires proximal occluding balloon; limited spatial resolution with imaging fibers	In clinical testing stage in Japan [21]; as technology improves and catheters can go down to 1-3 Fr without perceived operator loss of information; new algorithms in research stage for automated colorimetric detection
Optical Coherence Tomography (OCT)	Excellent spatial resolution for plaque surface and cap fissuring; anatomic imaging	May require proximal occluding balloon or saline flush (index matching); long acquisition times; cost; limited penetration (<200 um); no composition info	In research phase
Photonic Spectroscopy A. Raman B. Near Infrared Diffuse Reflectance C. Fluorescence / Exogenous Tracers	Can potentially measure both morphological and physiological data for vulnerable plaque detection	May require proximal occlusion; size of fibers competitive with angioscopy	In research phase; use in conjunction with IVUS or angioscopy
NON-INVASIVE TECHNIQUES			
Magnetic Resonance Imaging (MRI) A. Contrast Media – Gadolinium, SPIO, others	High resolution images (slice to slice); additional flow information	Long acquisition times; ineligibility of patients with metal prosthetics; cost; currently unable to provide in-plane resolution less than 300 microns	Algorithm development in research phase; current clinical instruments must be upgraded to perform cardiac imaging; Possibly combine with NMR spectroscopy for increased accuracy (magnet size issue)
Electron Beam Computed Tomography (EBCT)	Detects advanced atherosclerosis based on calcium content (Calcium Score)	Have not shown predictability for vulnerable plaque sub-types	IN USE: Calcium Score; new algorithms being developed for 3D images
Multi-Slice / Helical CT	High resolution (comparable to MRI), provides increased accuracy in Calcium Score; simultaneous recording of ECG	Ionizing radiation; may not characterize the vulnerable plaque sub-type well; cost	Unknown
Nuclear Imaging	Provides metabolic information when using tracers; allows serial monitoring of progression and regression	Ionizing radiation; limited spatial resolution; cost	In animal testing stage
OTHER			
Blood Tests and Serum Markers	Simple test; lowest cost	Need supplemental patient data; history	IN USE: C-reactive protein (CRP), other markers in research stage
Endothelial Function Test - Non-invasive ultrasound test of brachial artery	Simple test; low cost	Lack of specificity	IN USE

4.4. Reflectance Spectroscopy and Tissue Optics

The optical measurements of choice in this research are the pH and lactate concentration of plaque tissue. Using diffuse reflectance near-infrared spectroscopy, these metabolic parameters will be determined optically, based in part on the expected optical properties and the spectra of normal versus atherosclerotic tissues. Human atherosclerotic plaques are investigated using both Fourier-transform near infrared spectroscopy (FT-NIR) and visible/near-infrared (NIR) spectroscopy, spanning the wavelength region of approximately 400 to 2400 nm, using a custom designed fiber optic probe. By collecting a large wavelength range, the spectral data collection is maximally efficient for the number of specimens expected. The plaque's metabolic data (tissue pH, temperature, and lactate concentration) are measured at the same location as the optical spectra.

One important factor in the design of a spectroscopic, fiber optic, catheter-based sensor that can determine concentration of specific molecules (and/or chemical shifts) is to understand the differences between the optical measurement volume and the reference measurement volume. The underlying principles of reflectance spectroscopy, photon migration in tissue, fiber optics, and system signal-to-noise all play an important role in the design and performance of the prototype device. In this section, these concepts are reviewed.

4.4.1. Reflectance Spectroscopy

Spectroscopy – the study of energy interaction with matter – is useful in several applications to identify good products from bad products, purity of component, etc. There are four basic interactions involved: 1) reflectance, 2) absorbance, 3) scattering, and 4) transmission. These basic interactions on a homogeneous medium are depicted in Figure 4.4.1. The refractive index of the external and internal medium is represented by n_1 and n_2 respectively. If $n_1 = n_2$, then the reflection off the incident surface (termed specular reflection) is negligible.

Figure 4.4.1: Energy interaction (incident light) with homogeneous medium.
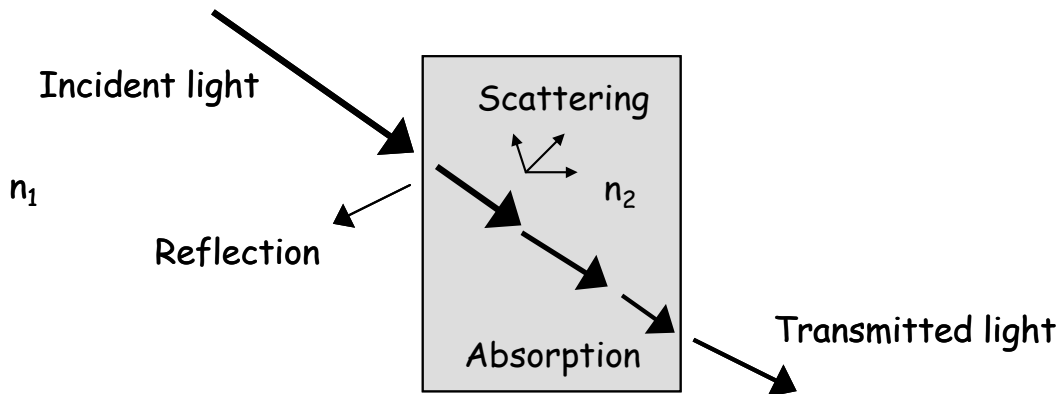
In classical absorption spectrophotometry, one is interested in how much light at a certain wavelength or energy is absorbed by a homogenous (i.e., isotropically scattering)

medium in a fixed pathlength (for example, in a 1-cm cuvette). Since absorption and scattering are two different events, the scattering effect can be ignored only in an isotropically scattering medium. Absorbance of the light is calculated by using Beer's Law. Beer's Law states that the absorbance at a certain wavelength is proportional to the thickness of the sample (i.e., the pathlength the light travels from the incident position to the transmission position). The proportionality constant is a characteristic parameter of the pure absorbing species. The analogous equation, the Lambert Law, states that the amount of light transmitted through a homogenous medium is proportional to the number of molecules of absorbing species in solution. The Beer-Lambert Law combines the two equations under the assumption that the **probability** of absorption is unaffected by the absorbing species concentration (i.e., it can be considered a molecular process that only involves the number of the absorbing species molecules traversed in a fixed depth per fixed unit cross sectional area of light; the **probability** remains the same whether there is 5 moles per liter (molarity, M) or 1 mole per liter of the absorbing species of interest. The probability is affected only by wavelength in an isotropic, homogeneous medium. The derivation is as follows:

Beer's Law:

k_l Probability that light at a given wavelength will be absorbed per unit length of matter [cm^{-1}]

δ Infinitesimally small distance, [cm]

$k_l \cdot \delta$	Probability of absorption in some small distance, δ
$1 - k_l \cdot \delta$	Probability of not being absorbed in δ
$(1 - k_l \cdot \delta)^2 \ldots (1 - k_l \cdot \delta)^n$	Probability of not being absorbed for increasing increments of distance δ, 2 ….n

Let $l = n \cdot \delta$ and take limit as $n \to \infty$, making substitutions

$$\lim_{n \to \infty} \left(1 - \frac{k_l \cdot l}{n}\right)^n = e^{-k_l \cdot l}$$

Note bene: $\displaystyle\lim_{n \to \infty} \left(1 + \frac{1}{n}\right)^n = e$

∴   Probability that light will not be absorbed in total distance, l is $e^{-k_l \cdot l}$

Lambert's Law:

I_i Incident light (intensity or irradiance units)

I_o Transmitted light (same units as transmitted light)

$$\frac{I_o}{I_i}$$

Fraction of light *transmitted*, equivalently

$$I_o = I_i \cdot e^{-k_l \cdot l}$$

Transmission (light not absorbed)

Molecular process of light absorption (single absorbing species in solution):

N Number of molecules of absorbing species in solution
ρ Molecular density [kg/cm^3]
m Molecular mass [kg]
$\dfrac{l \cdot \rho}{m}$ Number of molecules traversed in depth l per unit cross section [cm^{-2}]

Let $k_N = \dfrac{k_l \cdot m}{\rho \cdot l}$ Define k_N as the molecular absorption coefficient, assumed to be unaffected by concentration, [cm^{-1}]

$\therefore$ $$\frac{I_o}{I_i} = e^{-k_N \cdot N}$$

Beer-Lambert Law:

N_A Avagadro's Number, [6.02x10^{23} molecules/mole]
ε Extinction coefficient of the absorbing species [L/(mole · cm)], function of wavelength
c Molar concentration of the absorbing species, [mole/L]
l Pathlength, [cm]
λ Wavelength
A Absorbance, function of wavelength, arbitrary units

$$N = \frac{N_A \cdot c \cdot l}{1000}$$ *(by definition)*

$$\alpha = \frac{k_N \cdot N_A}{1000}$$ Molar absorption coefficient

$$\frac{I_o}{I_i} = e^{-\alpha \cdot c \cdot l} \text{ and } \varepsilon = \frac{\alpha}{2.303}$$

$$\frac{I_o}{I_i} = 10^{-\alpha \cdot c \cdot l} \text{ or } \log\left(\frac{I_i}{I_o}\right) = \varepsilon \cdot c \cdot l$$

Since ε is a function of wavelength, λ, the absorbance, A, as a function of wavelength is defined in a homogeneous medium:

$$A(\lambda) = \log\left(\frac{I_i(\lambda)}{I_o(\lambda)}\right) = \varepsilon(\lambda) \cdot c \cdot l$$

In reflectance spectroscopy, one measures the amount of light reflected back by the sample medium at its incidence interface. The source and receiving cross-sectional geometry becomes important, as scattering and absorption losses are separate events that need to be understood and optimized for a particular application. Conventionally, this requires a measurement of a reference material of known intensity to obtain the relative absorbance of the sample. In the ideal case (homogenous, isotropic medium), what is not absorbed (A) or transmitted (T) must be reflected (R) and all incident light is conserved. However, it may not be possible to measure all the transmitted light due to a large sample thickness, source or receiving hardware limitations, or other design constraints. In this research, it would not be feasible to measure the light transmitted through the vessel wall and the desired intravascular catheter requires that reflectance-mode spectroscopy be used. The anisotropic nature of tissue scattering affects how much light will be reflected back to the receiving geometry after any absorption events have occurred. This diffuse reflectance may contain both specular and higher-order reflectance interactions with the sample, depending on the relative indices of refraction at the interface (n_1 and n_2, for an air-sample interface $n_{1,\,air}=1$, n_2 may be a function of wavelength for tissues).

$I_{incidence}(\lambda)$ Incidence intensity, fixed *source* geometry, constant or known

$I_{reflectance}(\lambda)$ Measured reflected intensity, fixed *receiving* geometry

$$\frac{I_{reflectance}(\lambda),\,reference}{I_{incidence}(\lambda)}$$

Fraction of light reflected by the reference material

$$\frac{I_{reflectance}(\lambda),\,sample}{I_{incidence}(\lambda)}$$

Fraction of light reflected by the sample

$$\frac{\dfrac{I_{reflectance}(\lambda),\,reference}{I_{incidence}(\lambda)}}{\dfrac{I_{reflectance}(\lambda),\,sample}{I_{incidence}(\lambda)}} = \frac{I_{reflectance}(\lambda),\,reference}{I_{reflectance}(\lambda),\,sample}$$

$$\log\left[\frac{I_{reflectance}(\lambda),\,reference}{I_{reflectance}(\lambda),\,sample}\right] = A(\lambda),\,sample$$

The logarithm of the inverse of the measured sample diffuse reflectance, R, (log $(1/R)$) at incident wavelength(s) is defined as the absorbance, A, of the sample at that wavelength when the incident intensity is known and normalized (for example, using a blank in a cuvette-based, monochromatic spectrophotometer). A *univariate* calibration curve is typically constructed from knowing absorbance versus concentration over a specified range. The concentration of the desired analyte can be deduced from this curve. The more complicated the sample, the more the desired analyte becomes buried in the measured diffuse reflectance, making it difficult to derive a univariate calibration curve. Tissue samples are notorious for being complicated; they have many different absorbing species, scattering components, and possible physiological or other unknown effects on the desired analyte or signal needed for calibration. The design of a reflectance-mode fiber optic probe for the determination of metabolically active analytes in an inhomogeneous, anisotropic tissue bed is therefore inherently complex. In this research, the optical design must be aided not only by the practical considerations of reflectance-mode spectroscopy but also the theoretical optical properties and how light might travel (photon migration) in the atherosclerotic vessel wall.

4.4.2.   System Considerations

Near infrared spectroscopic measurement of tissue pH, developed in Dr. Soller's laboratory, can provide a minimally invasive assessment of tissue ischemia in the myocardium [28]. Improvements in the accuracy and reliability of this method for myocardial pH were required. The initial feasibility study performed in the canine myocardium used an approximately 6 mm diameter NIR reflectance fiber-optic probe (Remspec, Inc. Sturbridge MA) to illuminate and collect light in the 575-1100 nm region. The studies with this probe show that reflected light was collected down through a 5 mm thick layer of myocardium. Electrochemical tissue pH measurements (1.2 mm diameter, Microelectrodes, MA) were collected simultaneously with NIR spectra and multivariate calibration models were developed.

One factor affecting the accuracy of these models is the depth-dependent tissue pH levels that exist in the normal [64] and ischemic heart. It has been shown that tissue pH declines more in the endocardium than in the epicardium during coronary occlusion [65]. Impaired metabolic response and the duration of ischemia are more severe in the endocardium as evidenced by pH electrodes placed 8-10 mm in the left ventricular anterior wall (subendocardial) than 2-3 mm below the surface (subepicardial) after repeat occlusions. In this earlier work, reference pH electrodes were placed 5 mm into tissue, at the boundary between the epicardium and endocardium. Similarly, light was collected from both layers, merging the different pH values from the separate layers of tissue. An accurate optical pH measurement can only be made in the heart when light is collected from a known volume of tissue. Analyzing photon migration in the tissues and optimizing the probe geometry to localize the collected light from a smaller region can provide better calibration and ultimately improve performance.

An additional constraint is imposed on the optimal probe size for the vulnerable plaque research. As it is intended to be intravascular, the working optical area should be less than 2 mm in diameter or 6 French (the French scale, unit of measurement typically used to for catheters, is defined as 1 French $\approx 1/3$ mm). For this geometry, the realizable source-receiver separation is on the order of 1-2 mean free path of most biological tissues. This makes the diffusion approximation of photon transport invalid. The Monte Carlo Method is recognized as an appropriate, statistically based model for light transport for a small geometry. Monte Carlo simulations provide a "random" walk assessment of the migration of photons at a specific wavelength in a complex absorbing and scattering medium, defined by its optical absorption and scattering coefficients, and the tissue anisotropy factor. The results of diffuse reflectance as a function of radius, and the absorption as a function of depth are interpreted in terms of probabilities. Monte Carlo simulations of source-receiver separations for optimization of other optical spectroscopy methods [66] and tissue optical property measurements [67] have shown that there exists an optimal separation such that the pathlength dependence on scattering is minimized for the specified tissue layers.

Khan *et al* [68] have shown that in a Monte Carlo simulation of both purely scattering (Intralipid), and absorbing and scattering medium, the simulated diffuse reflectance as a function of radial distance can be obtained. The minimization of scattering was demonstrated and the localization of the light entering and exiting the tissue was shown to be less than 1 mm^3 from simulated data for a two-fiber system in a myocardial tissue pH application. The simulations for normal and atherosclerotic vessel wall also provide further evidence that the optimal source-receiver separation can be achieved given the design constraints for the vulnerable plaque.

4.5. Multivariate Calibration Methods

Spectroscopic determination of one chemical component in a complex, scattering and absorbing mixture such as the vessel wall or other tissue beds can be achieved by the use of multivariate calibration. Using a spectral calibration set, a model is generated to correlate the tissue spectra to the reference measurements. In this manner, the model is trained to recognize features that are highly correlated with the reference measurement. Partial least-squares (PLS) data analysis is an extensively used mathematical technique in the analysis of spectroscopic data [69, 70]. It extracts information from the spectra that is most correlated to the reference measurement of interest by decomposing the data into loading vectors (spectral B, chemical v) and scores (T), the linear combination of which represent the original spectrum (see Figure 4.5.1). Some residual error always exists. Inclusion of too much of this residual error may cause overfit of the data, and necessitates that the calibration process be closely monitored. Mean centering is typically used to eliminate the need to fit to a nonzero intercept in the calibration model and it decreases the complexity of the model by one factor (i.e., degrees of freedom reduced in the number of linear combinations needed) [71]. The optimum number of factors (and the subsequent loading vectors that describe the model) used in the final calibration equation is determined by how well the model predicts the concentration from an independent, unknown spectrum. Acceptable models should contain a low number of factors, with at

most 5 to 6 points per factor used [26]. Qualitative assessment of the loading vectors should provide some insight of the absorbance of the specific chemical species being calibrated, otherwise the loading vector contribution could be coincidental and noise-related [70].

The optimal number of factors for each calibration will be calculated using the leave-one-point-out (or cross-validation) procedure, calculating the Predicted Residual Sum of Squares (PRESS) for each factor, and using a F-test (alpha level of 0.25) to identify the smallest number of factors where the PRESS minimized [71]. Cross validation methodology is used to assess the ability to predict the *nth* reference concentration of one specimen in the calibration set based on the spectral decomposition of all the other calibration spectral pairs. This is performed successively for each spectrum in the calibration set until all spectra have been predicted based on *n-1* calibration spectra. The R^2 and standard error of cross-validation (SECV) are calculated from the actual versus predicted values. These parameters provide a measure of the accuracy and predictive ability of the calibration equation.

The calibration set should span the variability expected in the entire population in order to be robust. Therefore, a significant number of atherosclerotic areas must be studied to span the variability expected in lesion types. The variance in the data set should be related to the desired reference measurements; however, other chemical compositions and instrumental noise affect the spectra and ultimately, the optical determinations. Different pre-processing algorithms can be used to remove some of the variability unrelated to the reference measurements (e.g., baseline correction or multiplicative signal correction) in the wavelength region of interest. The information content in the final calibration model ultimately should be related to real physical or chemical absorption changes in the atherosclerotic plaques that are indicative of the desired reference determination of either tissue pH or lactate concentration.
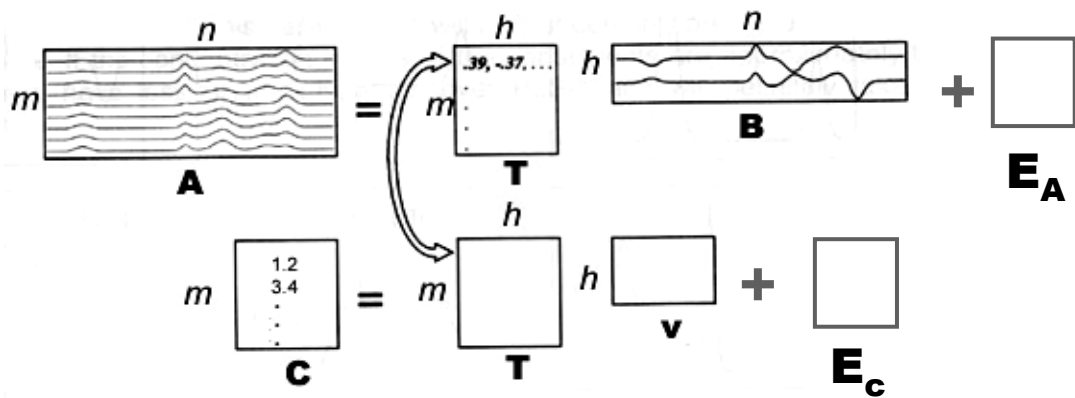
Figure 4.5.1: Partial least-squares illustrated. PLS regression technique is effective in establishing relationships between spectral changes and reference values. Using multivariate regression (white arrow), it is a non-iterative, factor analysis based decomposition of the spectra data (A) using reference values denoted as C. T are the scores, B and v are the loading vectors, E is the residual matrix of either the spectra E_a or the concentration (reference values) E_c.

4.6. The Near-IR Characteristics of Vessel Wall and Atherosclerotic Plaques

In this section, the visible and near-infrared characteristic absorption spectra of the vessel wall available in the literature are briefly reviewed in terms of the major absorbing components. The multiple components and overlapping peaks in normal and diseased vessels support the hypothesis that a multivariate, multi-wavelength approach may be required to deconvolve spectra into factors that are relevant for the optically determined plaque tissue pH and lactate concentration in atherosclerotic plaques.

Cholesterol and its esters have significant absorbance peaks in the NIR. Plaque spectra collected by Jaross *et al* [34] are shown in Figure 4.6.1(d). They reported cholesterol absorption peaks at 1750 nm. These spectra from 1000 to 2500 nm show the two water bands (~1450 and ~1950 nm) in the region as well. The effects of other absorbers (Figure 4.6.1 (a)) in the atherosclerotic vessel wall on the optical determination of tissue pH and lactate are assumed to be minimal, based on their pure component spectra in the wavelength region of interest, and their relative importance to the expected predictability towards metabolic status.
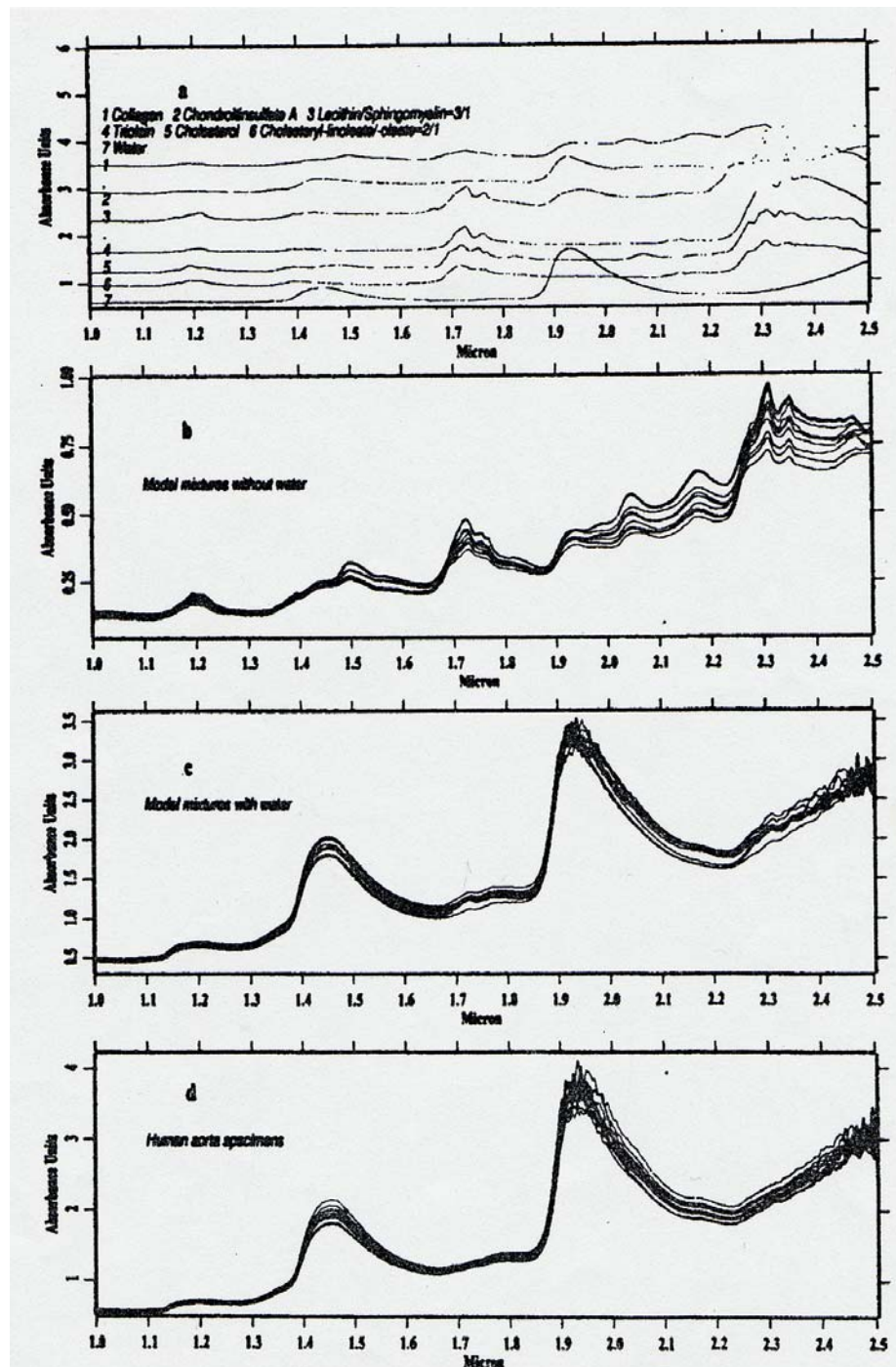
Figure 4.6.1 From Jaross *et al* a) NIR spectra of several pure compounds of an arterial intima. From bottom to top: Water, cholesteryl-linoleate/oleate 2/1, cholesterol, triolein, lecithin/sphingomyelin 3/1, chondrosulfonate A, collagen. These compounds were identified by Jaross *et al* as important components of arterial intima.(b) NIR spectra of the model mixtures without water; (c) NIR spectra of the model mixtures with water; (d) NIR spectra of aortic specimens. (1 Micron=Wavelength 1000 nm).

Lactic acid ($C_3H_6O_3$) is a metabolic by-product of anaerobic glycolysis, and healthy levels are found in blood, exercising muscles, sweat, and tears [31]. The two peaks at ~2250 and ~2295 nm are important in the optical determination for lactate concentration in the atherosclerotic plaque (lactic acid solution spectra, Figure 4.6.2).
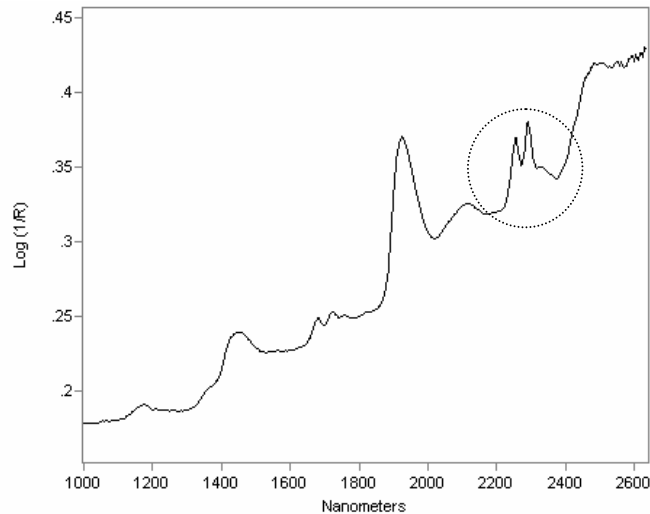
Figure 4.6.2: Lactic acid (70% solution in water, CAS#50-21-5), FOSS NIRSystems commercial spectrometer, resolution = 7 nm [72]. Water peaks at 1450 and 1950 nm, the two characteristic lactate peaks at 2250 and 2295 nm are circled.
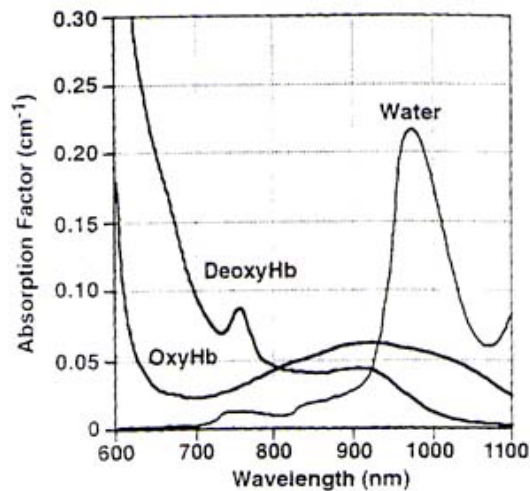
Figure 4.6.3: : Major biological absorbers in the visible to near infrared spectrum of *de novo* tissue.

Keijzer *et al* [73] measured the absorption coefficients in the intima, media, and adventitia of human aorta. Between 400-600 nm, hemoglobin absorption is observed in the vessel wall. The absorption coefficients increase toward 200-400 nm due to protein

absorption, and again past 1300 nm, due to water absorption. In the 600-1300 nm region, tissue absorption is the lowest; the major absorbers include hemoglobin, both oxygenated and deoxygenated states, and water (Figure 4.6.3) [74]. These constituents, due to pH-induced changes in hemoglobin spectra, contribute to the optical determination of tissue pH.

4.7. Experimental Factors

In this section, an introduction of the known experimental factors that affect optical tissue spectra is made. Background information on the *in-vitro* temperature, the overall experiment time, and the gross pathology of atherosclerotic plaques is presented as to the impact these variables may have on the accuracy of the optical determinations.

4.7.1. Temperature

Temperature is known to affect optical spectra. Water and hemoglobin have significant peak shifts with temperature; however, the effect is over a large temperature range 25-40°C [75]. The less the temperature is allowed to fluctuate the less likely the shift will be apparent. The *in-vitro* media temperature is set to ~37°C for the final set of experiments. This also helps mimic *in-vivo* conditions for optical spectroscopy, where tissues and cells are constantly bathed in oxygenated, nutrient-rich blood or interstitial fluids at a nominal human body temperature of 37°C. It must be noted however, that the plaque tissue, due to inflammatory response, may have real, physiological fluctuations in temperature [45]. Measured tissue pH and temperature for different plaque types showed clustering of the range over which these metabolic parameters may change. (Figure 4.7.1.). Therefore, the accuracy of the optical determinations must be reviewed with respect to the measured tissue temperature.
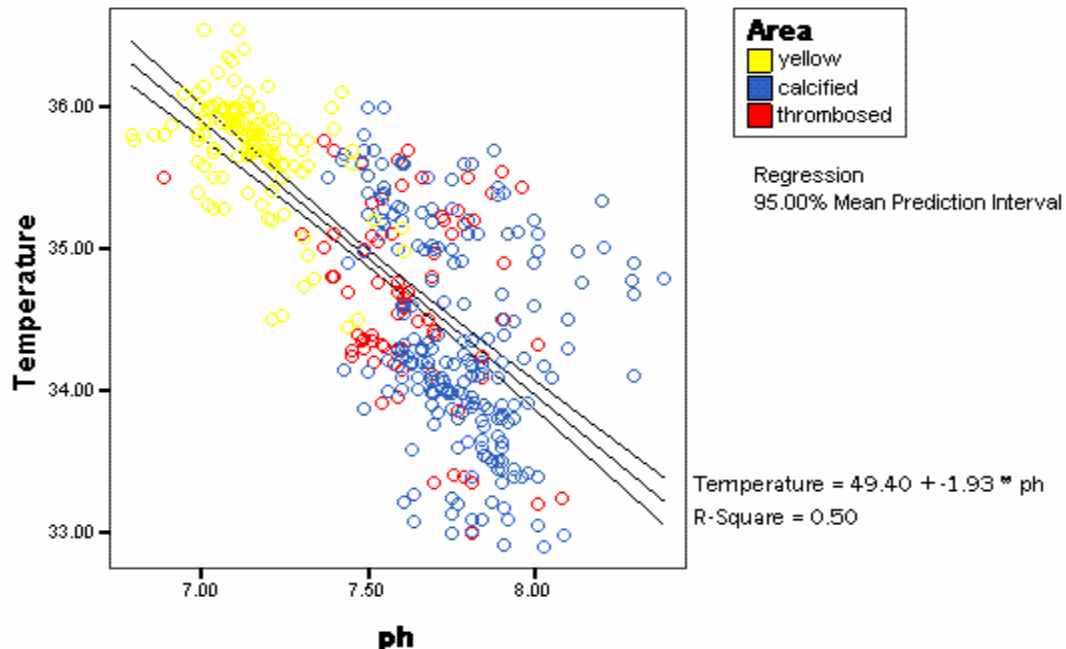
Figure 4.7.1: Tissue pH and temperature measurements in grossly pathological different areas of plaque. Yellow- lipid laden, Blue-calcified, and Red-thrombosed. Tissue pH and temperature are inversely correlated.

4.7.2.   Experiment Time Course

Inadvertent time correlation of spectra has been shown to be a significant challenge in chemometric methods and multivariate calibration [76]. The complexity of physiological events and their time course, mostly unknown in atherosclerotic plaques, makes the collection of tissue spectra dependent on the rate of change of the metabolic and physical parameters. To remove the time correlation effect as much as possible, the metabolic parameters that are measured should remain stable as possible from their starting points as the plaque tissue is removed from the body into the *in-vitro* environment. The optical spectra should be taken as quickly as possible, and the reference measurements should be taken immediately after (simultaneous measurement is not possible in this case due to the destructive nature of the reference measurements). The stability of the plaque tissue was validated in an optically transparent, oxygenated physiological nutrient media at 37°C (Chapter 6). The effect that the duration of the experiment has on the multivariate calibration will be reviewed and shown to be minimal.

4.7.3.   Gross Pathology

It has been demonstrated there exists a correlation between the gross pathology and the tissue pH and temperature of the atherosclerotic plaque *ex-vivo*. [36]. There is considerable histological evidence of structural heterogeneity [21, 23, 25]. Moreno *et al* have also demonstrated that it is possible to make an optical determination of the pathology [32]. In making an optical determination of plaque tissue pH or lactate, it is unknown how the unmodeled variable of the gross pathology may affect the accuracy. Whether the accuracy of the reference measurement of lactate concentration is dependent on the gross pathology is unknown [77], primarily due to the technological hurdles in refining the biochemical assay resolution. The following characteristics are qualitatively assessed for each plaque:

- Yellow or lipid-laden area (glistening yellow or "fibrofatty")
- Calcified (hard, white, rough, rocky, "crunchy")
- Thrombosed (reddish/reddish brown, bloody, "raspberries")

A value of 1 is marked for the most prominent feature of the measured location, the others are marked 0. In this manner, each point measured will be scored. The effect that the gross pathology has on the optical determination will be reviewed.

4.8.   Summary

Presently, there is no monitoring technique that meets the major requirements of a cost-effective, clinically acceptable, and useful instrument to assess atherosclerotic plaque vulnerability. Spectroscopic measurement of tissue pH using multivariate calibration techniques is a feasible method for assessing metabolic status of tissue. With advances and understanding of interferents, both experimental and physiological, one can monitor tissue pH and/or lactate concentrations in various tissue beds. The application for atherosclerotic vessel walls is the main focus of this research.

5. OPTICAL DESIGN

5.1. Rationale

Optical spectroscopy is one of the few available non-destructive techniques for *in vivo* determination of tissue pH and lactate. Atherosclerotic plaques have various levels of inflammation, calcification, fibrosis/necrosis, and neovascularization as demonstrated by histological record [25]. They are considered structurally heterogeneous. It has also been demonstrated that metabolic heterogeneity exists. Significant tissue pH heterogeneity has been shown in both human carotid endarterectomized atherosclerotic plaques and Watanabe heritable hyperlipidemic (WHHL) rabbit aortas as compared to control non-atherosclerotic vessels [36]. Lactate concentrations, however, may be more homogenous, as it is not as well resolved or compartmentalized in the interstitial space [77]. Due to this known heterogeneity, an accurate optical tissue pH or lactate determination can only be made in the atherosclerotic plaque when the light is collected from a small volume of tissue.

The objective of the design process is to produce a probe that has the appropriate spatial resolution for accurate optical measurements in plaque. Photon migration simulation and analysis, using various tissue optical property data, combined with the appropriate modification of the probe geometry to optimize the collected light from a smaller volume, can provide better calibration spectra and, ultimately improve performance. In this section, the theoretical and practical optical data used to design such a probe that can achieve light collection from a localized volume of atherosclerotic tissue are reviewed and discussed.

5.2. Monte Carlo Simulations Setup

Monte Carlo simulations provide a "random" walk assessment of the migration of photons at a specific wavelength in a complex absorbing and scattering medium. A random number generation for each photon determines the event (i.e., reflection, absorption, scattering, or transmission) that will occur in a probabilistic fashion, given the optical properties of the medium. This process is repeated and each photon is followed until it leaves the defined grid geometry (by a reflection, transmission, or scattering event) or the photon is absorbed. All photons are conserved. The medium is defined by its optical absorption and scattering coefficients (μ_a (1/cm) and μ_s (1/cm) respectively, at a specific wavelength), and the tissue anisotropy factor, g. (direction of scattering, g=0 is defined as isotropic scattering). The outputs of the simulation are the probability of diffuse reflectance as a function of radius, and the probability of absorption as a function of depth. This is done for a number of wavelengths in the region of interest where optical property data is available. The simulations aid in the practical design of the probe by providing a starting point for the testing of different source-receiver separations.

All Monte Carlo simulations were performed with the ANSI Standard C code provided by Wang and Jacques on the Internet [78, 79]. A cylindrically symmetric geometry is

assumed with a point source at radius r=0. A matched refractive index between the probe-tissue interface ($n_1=n_2$, i.e. direct probe-to-tissue contact or an appropriate fluid index matching) and an anisotropy factor of 0.9, which simulates the typical anisotropic scattering properties of tissue [80], were used. The diffuse reflectance and absorption per area as a function of depth are normalized by the number of incident photons, N, to obtain probability per unit volume. The number of events or light interactions to follow was set to 10,000. To investigate possible source-receiver separations, simulations were performed with changes in absorption and scattering coefficients as a function of wavelength taken into account. Four separate simulations were performed:

- Scattering only
- De-oxygenated hemoglobin and scattering
- Normal aorta at specific wavelengths
- Atherosclerotic aorta at specific wavelengths

First, purely scattering models of Intralipid were performed using the measured scattering coefficients (500 – 900 nm) provided by van Staveren *et al* [81] and absorption coefficients from Flock *et al* [82] These values are valid for actual Intralipid-10% concentrations between ~ 4 and 17 volume percent. The optical properties of Intralipid are approximate, due to real variation in scatterer size and preparations. Intralipid is also known to have some absorption at the longer wavelengths (>900 nm) due to water. The absorption (μ_a) and the scattering (μ_s) coefficients input to the code were between 5.5×10^{-3} to 0.06 cm^{-1} and ~206 to 846 cm^{-1} respectively. The standard deviation across the simulated wavelengths was used as a measure of the wavelength dependence of scattering for each radial distance. To estimate the effective penetration depth (i.e., reflected photons return from a depth z, as a function of source-receiver separation), the absorption probability as a function of depth was calculated for each wavelength. The penetration depth was estimated by identifying the depth, z, to which at least 90% of the total absorption probability had occurred.

Second, absorption and scattering models were performed using absorption coefficients for a 2 mM deoxy-hemoglobin tissue concentration (hemoglobin (Hb) protein without oxygen attached, Fe^{2+} conformation) with the same scattering coefficients used from the Intralipid simulations. Tabulated molar extinction coefficient values [83] of deoxy-Hb were converted to absorption coefficients by 2.303*(molar concentration). A 2 mM concentration is approximately 13 g/dl, which is physiologically relevant for blood-containing tissue. The absorption coefficients input to the code were between 3.5 and 246
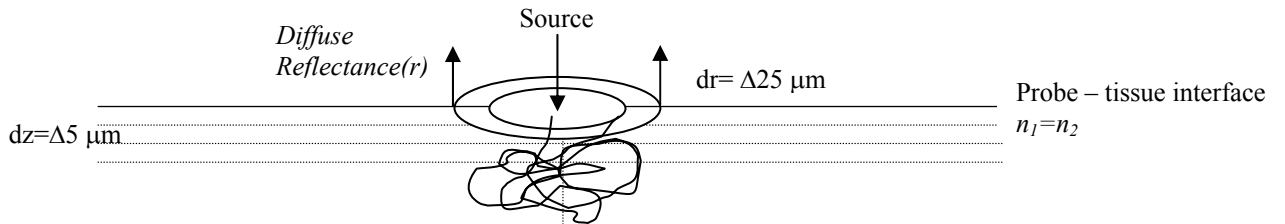
Figure 5.2.1: Monte Carlo grid geometry for all simulations. Symmetry in the x-y plane at the probe-tissue interface was assumed. The grid size was 25 microns x 5 microns (radius x depth).

cm^{-1} for the deoxy-Hb models between 500 – 900 nm. The absorption probability as a function of depth was calculated for each wavelength. The penetration depth was estimated by identifying the depth, z, to which at least 90% of the total absorption probability had occurred.

The last two simulations used optical property data collected at three different wavelengths for normal aorta, and five different wavelengths for atherosclerotic aorta [84-86]. The radial resolution, or x-y plane, of the simulation was set to 0.025 mm (25 microns). The depth resolution, or z-plane, was set to 5 microns (approximately the typical histology resolution). The grid was set to follow photons to a 1.5 mm radius (3 mm diameter) and a 1.5 mm depth away from the source (Figure 5.2.1). Absorption and scattering coefficients used for all simulations are summarized in Table 5.2.1.   The diffuse reflectance as a function of source-receiver separation (radial distance away from source) and the effective penetration depth were calculated.

Table 5.2.1: Absorption and scattering coefficients used for Monte Carlo simulations.

Simulation	μ_a (1/cm)	μ_s (1/cm)	Wavelength (nm)	Reference
Scattering only	$5.5 \times 10^{-3} - 0.06$	206 - 846	500 – 900 (50 nm increments)	[82] [81]
De-oxy Hb + scattering	3.5 – 256	206 –846	500 – 900 (50 nm increments)	[83] [81]
Normal Aorta	6.856 0.88 0.508	148.7 86.21 42.85	514 633 1064	[85]
Atherosclerotic Plaque	54 10.98 1.076 10.0 0.9	8.0 290.6 142.9 8 33.54	470 514 633 1050 1064	[84] [85] [85] [84] [85]

5.3.   Experimental Optical Setup

The optimal probe geometry that can be achieved given the practical considerations of designing a probe for intravascular use, and the additional requirement that the light be collected from a small, well-defined region of the heterogeneous plaque tissue, were investigated simultaneously. All probes that were studied were of the reflectance-mode design. By exploiting the combinations of the key variables that affect the optical signal in both the commercial probe that was available (FOSS NirSystems, MD) and the custom-manufactured optical probes (i.e., fiber size and types, optical attenuation, collection efficiencies, etc.) an optimal set of materials and design geometry was realized. All optical tests were performed on a FOSS NirSystems 6500 scanning spectrophotometer with 32-bit ADC and a fiber optic adapter. A Si detector covers the wavelength region 400-1100 nm; a PbSe detector covers the wavelength region 1100-2500 nm. Both detectors are uncooled (room temperature ~ 19-27°C). The source is a 75 W tungsten-halogen lamp that is filtered using a monochromator, and the wavelength calibration is factory set. The spectrometer has a set 2 nm wavelength resolution across both regions. Signal-to-noise ratio (SNR) as a function of wavelength was evaluated for

each probe. The tissue penetration test (Section 5.3.3) was performed only on the probe that eventually demonstrated an adequate SNR and had a working optical area small enough for the practical measurement in plaque.

5.3.1.   Source-receiver optics test probes characteristics

Source-receiver fiber separation is assumed to be the critical factor in determining performance based on Monte Carlo theory. However, in practicality, other variables may exist. Seven different probes were tested that had varied fiber size/type, fiber number, collection interface, collection geometry, and source-receiver fiber separation. The working optical diameter is determined by fiber number (size), collection interface, and the nominal separation. Table 5.3.1 summarizes each optical probe's characteristics. Each probe was evaluated as to its contribution in improving optical signal collection and adhering to design constraints.

5.3.2.   Signal-to-Noise Ratio (SNR) testing

For each probe (except probe #8), fibrofatty plaque tissue at 37°C was used to collect representative absorbance spectra. All absorbance spectra were collected at 60 scans for the full range (400-2500 nm) by ratioing to a Spectralon 50% reflectance standard (or $I_{reflectance}(\lambda),reference_o$) collected earlier on the same day. Since single-beam spectra (raw counts per wavelength) could not be collected with the spectrometer software, the tissue absorbance spectrum and a "noise" absorbance spectrum, i.e., an absorbance spectrum of the Spectralon 50% reflectance standard, were both measured. The "noise" spectrum was collected independently to assess the effect of the spectrometer change without the added tissue variation before ($I_{reflectance}(\lambda),reference_1$) and after ($I_{reflectance}(\lambda),reference_2$) a tissue spectrum was taken. The tissue absorbance spectrum was measured on an representative area of plaque as:

$$\log\left[\frac{I_{reflectance}(\lambda),reference_o}{I_{reflectance}(\lambda),tissue}\right] = A(\lambda),tissue$$

The "noise" spectrum as defined above was measured as:

$$\log\left[\frac{I_{reflectance}(\lambda),reference_o}{I_{reflectance}(\lambda),reference_{1,2}}\right] = A(\lambda),"noise"$$

The "signal-to-noise ratio" or SNR, for the purposes of this study, was calculated using a 4 nm bandwidth, as the average absorbance of the tissue over the average absorbance of the "noise" (spectrometer changes in measuring the reflectance standard):

$$SNR = \frac{<A(\lambda \pm 2nm),tissue>}{<A(\lambda \pm 2nm),"noise">}$$

In other words, the signal-to-noise ratio was calculated as the ratio of the average absorbance collected from a representative piece of tissue to the average absorbance collected from the same reference material used to make the absorbance calculation at different time points. The center wavelengths chosen, λ, are those where a maximal SNR is desired for atherosclerotic plaque optical collection, that is, where the important absorbers are found (e.g., hemoglobin, water, lipids, lactate). The average is done using a 4 nm bandwidth (center wavelength, $\lambda \pm 2$ nm). The average absorbance was chosen instead of the standard deviation to ensure the SNR values were not inadvertently inflated due to the non-standard methodology. By using relative SNR values, different probe configurations can be compared.

In addition, the average detector voltage readings for each wavelength region were collected for all seven probes. Performance factor multipliers for each wavelength range (visible and NIR) were derived with respect to a significant numerical improvement over the first design probe (Probe #2) and was calculated as such:

Factor Multiplier = (Receiver Area Improvement, if any) x (Relative Voltage Improvement) x (Optical Window Improvement, if any)

These performance factors were assessed for the first seven probes' characteristics outlined in Table 5.3.1 (a schematic illustration of the probe iteration and evolution is shown in Figure 5.3.1). The factor multipliers assisted in the decision to identify and incorporate those probe characteristics that would be best in combination for the ultimate performance of a final probe design, based on the absorbance signal collection on representative spectrometer(s). The actual SNR and average voltage readings were measured for probe #8 on a fresh fibrofatty plaque tissue.

Large OD
Probe

360 degree
illumination w/ optical
window

Forward illumination
No optical window

Final probe
W/ optical window
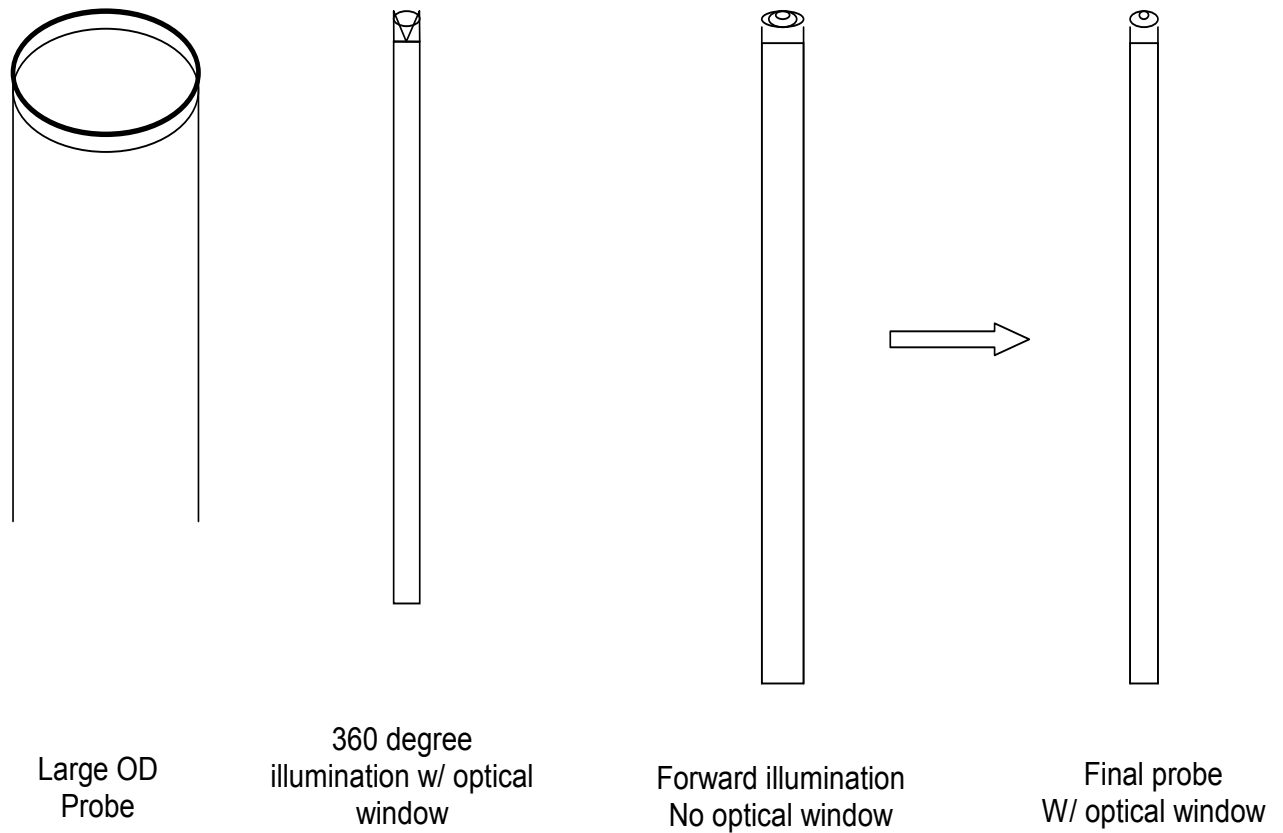
Figure 5.3.1: A schematic illustration of different probe configurations as described in Table 5.3.1. From left to right: Probe 1 with optical window, Probe 3 - 360° side-illumination and collection 3 French catheter prototype, Probe 2 without optical window, and Probe 8, forward viewing with mounted quartz optical window.

Table 5.3.1: Optics test probes described as part of the optical design process. For all fibers NA=0.22.

Probe ID (Manufacturer, description)	Fiber Core Diameter/Type	Fiber Number	Collection Interface	Collection Geometry	Source-Receiver Fiber Separation	Working Optical Diameter
1 (FOSS commercial probe, large outer diameter)	200 micron extended transmission to 2400 nm (low OH)	Source: 210 Receiver: 210	7 mm thick sapphire optical window; flat optical surface	Forward-viewing	1 mm	25 mm (2.5 cm)
2 (Multimode (NJ), first custom design iteration)	200 micron (source, low OH); 100 micron (receiver), limited transmission above 1400 nm (low OH)	Source: 7 Receiver: 37	Flat optical surface	Forward-viewing	0.5 mm (500 microns)	5 mm (0.5 cm)
3 (Remspec (MA), 360° catheter prototype)	100 micron fibers, extended transmission to 1700 nm	Source: 26 Receiver: 13	0.5 mm thick quartz optical window; radial optical interface	Side-viewing (360°)	0.05 mm (50 microns)	1.2 mm (0.12 cm)
4 (FOSS commercial probe, optical window sheath removed)	200 micron extended transmission to 2400 nm (low OH)	Source: 210 Receiver: 210	Flat optical surface	Forward-viewing	1 mm	25 mm (2.5 cm)
5 (same probe as in 2, but with custom optical window tested)	200 micron (source, low OH); 100 micron (receiver), limited transmission above 1400 nm (low OH)	Source: 7 Receiver: 37	1.75 mm thick quartz optical window (transmission to ~2500 nm); Flat optical surface	Forward-viewing	0.5 mm (500 microns)	5 mm (0.5 cm)
6 (same probe as in 2, but with custom optical window tested)	200 micron (source, low OH); 100 micron (receiver), limited transmission above 1400 nm (low OH)	Source: 7 Receiver: 37	0.5 mm thick sapphire optical window (transmission to 5500 nm); Flat optical surface	Forward-viewing	0.5 mm (500 microns)	6.35 mm (0.635 cm)
7 (same probe as in 2, but with custom optical window tested)	200 micron (source, low OH); 100 micron (receiver), limited transmission above 1400 nm (low OH)	Source: 7 Receiver: 37	1 mm thick sapphire optical window (transmission to 5500 nm); Flat optical surface	Forward-viewing	0.5 mm (500 microns)	5 mm (0.5 cm)
8 (Remspec, forward-viewing mounted optical window)	200 micron, extended transmission to 2400 nm	Source: 7 Receiver: 13	0.5 mm thick quartz optical window (transmission to ~2500 nm); Flat optical surface	Forward-viewing	0.05 mm (50 microns)	2.0 mm (0.2 cm)

5.3.3. *Tissue depth penetration testing*

The measurement and calculation of depth penetration was adapted from Jaross *et al* [34]. All spectra were collected on the FOSS NirSystems spectrometer using a combination probe (probes #5 and 8) trifurcated with two concentric rings of receiver fiber optics containing the two source-receiver separations (the 50 micron and 500 micron configurations) at the common end or probe-tissue interface. First, reference spectra (50% Spectrolan, Labsphere, NH) were measured for each configuration. A 50-micron piece of tissue from frozen section, O.C.T. embedded (Sakura Finetek, CA), fresh cow aorta (cut longitudinal into vessel wall using a microtome, first slice is the luminal side of vessel) was used. Tissue-Tek® O.C.T. Compound is an optically clear embedding substance routinely used for optical microscopy of fresh-frozen tissue sections. It is made of less than 10% each of polyvinyl alcohol and polyethylene glycol (and other water-based non-reactive substances). The tissue slice was first washed with DI water three times (to remove the water-soluble embedding compound), and then stacked on the face of the probe (see Figure 5.3.2).

Next, absorbance spectra were taken with both configurations using the appropriate reference signal. After one absorbance spectrum was taken with tissue only, another spectrum was taken, using the 50% reference standard as the backing for the diffuse tissue reflectance (that is, the reference was placed on top of the tissue and another spectrum taken with the tissue plus the reference). The reference was then removed, and another 50-micron piece was stacked on top of the previous one. Care was taken to remove wrinkles, and excess water, if any, was gently squeezed out with Kim wipes. This procedure was repeated; two spectra for each configuration and thickness, up to a total of 1.0 mm thickness, were collected. The difference spectrum was taken, i.e. the absorbance signal from the tissue only minus the absorbance signal from the tissue plus reference. For each of the wavelengths used in the SNR calculation, the average difference spectra
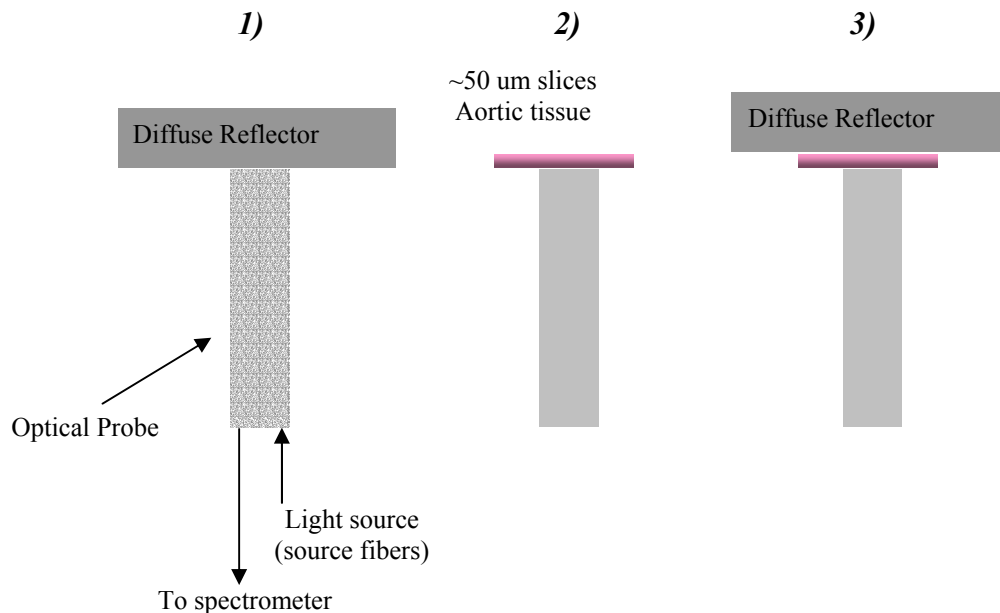
Figure 5.3.2: Depth penetration test method. 1) Reference spectra collected for each optical configuration. 2) Absorbance spectra collected with n-th slice of 50 micron tissue. 3) Second absorbance spectrum collected with n-th slice plus diffuse reflector. Both absorption and scattering attenuate tissue signal.

(4 nm bandwidth) for each tissue thickness was calculated. The percent difference (or attenuation) was calculated using the 50 um tissue signal as zero attenuation. When the percent difference is over 90%, this was considered to be the penetration depth for that wavelength.

5.4. Monte Carlo Simulations Analysis

Intralipid Simulations

Table 5.4.1 shows that the relative diffuse reflectance profiles have a weak wavelength dependency for source-receiver separations less than 0.75 mm. For source-receiver separations between 0.45 and 0.75 mm, scattering effects, as measured by the standard deviation from the nominal 500 nm wavelength, was minimized. At a 750 nm wavelength, the Intralipid simulation showed that the total absorbed fraction of incident photons was 6.4%. Ninety percent of the 6.4% total absorbance probability occurs up to the depth of ~ 1.2 cm (i.e., the other 10% of the 6.4% total absorbance occurs greater than a depth of 1.2 cm or 12 mm). Therefore, the effective penetration depth at 750 nm is 1.2 cm. Further decomposition of the data into its radial (r) and depth (z) components showed that the probability of absorption increases, then decreases, at a depth of 0.75 mm as the radial distance away from the source increases (i.e. the source-receiver separation increases).

Table 5.4.1: Minimization of scattering as measured by the reduction of standard deviation from 500 nm of the diffuse reflectance profiles as a function of source-receiver separation. Scattering is minimized with a source-receiver separation of 0.65 mm [68].

Source-Receiver Separation (mm)	Standard Deviation Of Diffuse Reflectance from 500 nm (λ)
0.25	0.235
0.35	0.199
0.45	0.133
0.65	0.114
0.75	0.139
1.05	0.331
1.75	0.641

De-oxy Hb Simulations

Deoxy-Hb simulations at λ=750 nm showed that the total absorbed fraction of incident photons was 72.5%. Deoxy-Hb has a strong absorbance at 760 nm. The probability of absorption at 750 nm in the deoxy-Hb simulation is therefore naturally much higher than the purely scattering model. In the deoxy-Hb models, all of the absorption occurs by a depth of 3 mm, and 90% of the total absorption occurs by a depth of 0.75 mm (Figure 5.4.1a). Therefore, the effective penetration depth at 750 nm for de-oxy Hb is approximately 0.75 mm. Similar trends, as in the Intralipid-only models, occurred for increasing source-detector spacing when the deoxy-Hb data was decomposed into its radial and depth components (Figure 5.4.1b).
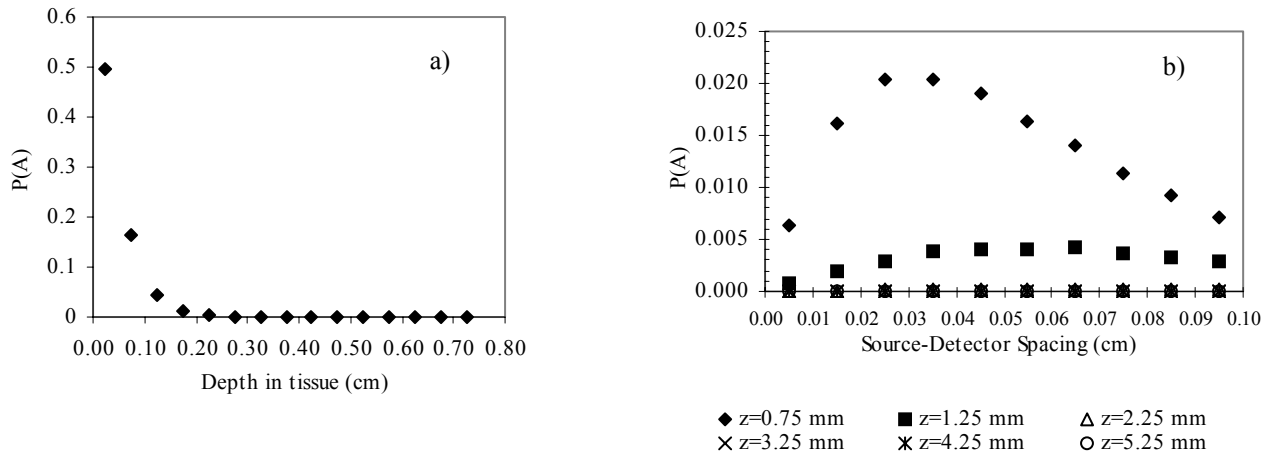
Figure 5.4.1: 2mM deoxy-Hb in Intralipid scatterer at λ = 750 nm. P(A), probability of absorption a) versus depth; represents 72.5% total absorption at 750 nm b) spatial decomposition of probabilities as a function of depth in a) as the distance away from source increases, e.g. source-receiver separation. Source is at (r,z)=(0,0).

Normal and Atherosclerotic Aorta Simulations

The diffuse reflectance $(1/cm^2)$ as a function of the source-receiver separation and wavelength for the normal and atherosclerotic aorta simulations are shown in Figure 5.4.2 a) and b), respectively. Diffuse reflectance drops off fairly quickly as the source-receiver
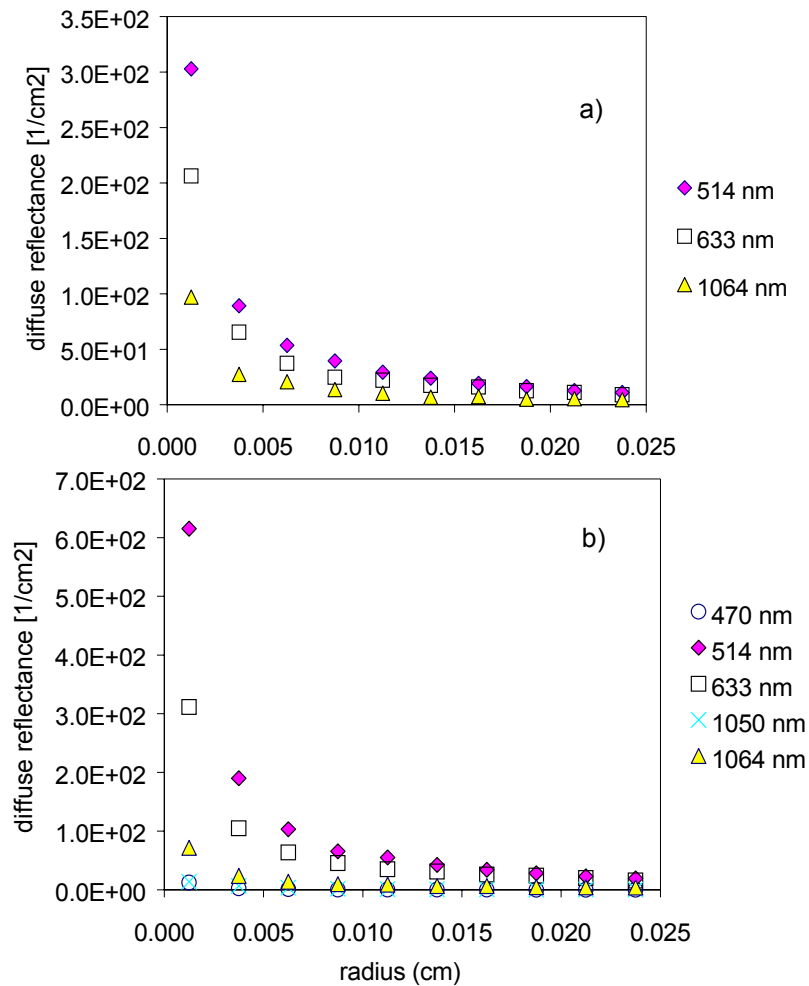
Figure 5.4.2: Diffuse reflectance $(1/cm^2)$ as a function of radius (cm), or source-receiver separation, for five different wavelengths. a) Normal aorta. b) Atherosclerotic aorta. Diffuse reflectance drops off fairly quickly as the source-receiver distance is increased). The probability of diffuse reflectance is actually higher at small source-receiver separations (<0.005 cm or 50 microns) for the atherosclerotic aorta at 514 nm.

46

distance is increased in both cases. The probability of diffuse reflectance is actually higher at small source-receiver separations (<0.005 cm or 50 microns) for the atherosclerotic aorta at 514 nm.

The depth penetration in the simulated normal and atherosclerotic aorta as a function of wavelength, as calculated as the depth where 90% of the total absorption probability occurs, is summarized in Table 5.4.2 for a 50 micron source-receiver separation. The atherosclerotic aorta consistently showed less penetration depth versus the normal aorta at the same wavelength for all other source-receiver separations.

Table 5.4.2: Estimated penetration depth for a 50 micron source-receiver separation based on Monte Carlo simulations of normal and atherosclerotic aorta optical property data.

Wavelength (nm)	Normal Aorta (microns)	Atherosclerotic Aorta (microns)
470	--	417.5
514	1063	722
633	1338	1197
1050	1333	1187
1064	--	927

5.5. Optical Probe Analysis

Signal-to-Noise Ratios (SNR)

The relative signal-to-noise ratios at 420, 550, 760, 970, 1450, 1750, and 2250 nm with respect to probe #2 (first design iteration) are shown in Figure 5.5.1. The relative N-fold improvements in noise alone over the first design iteration probe is shown in Figure 5.5.2.
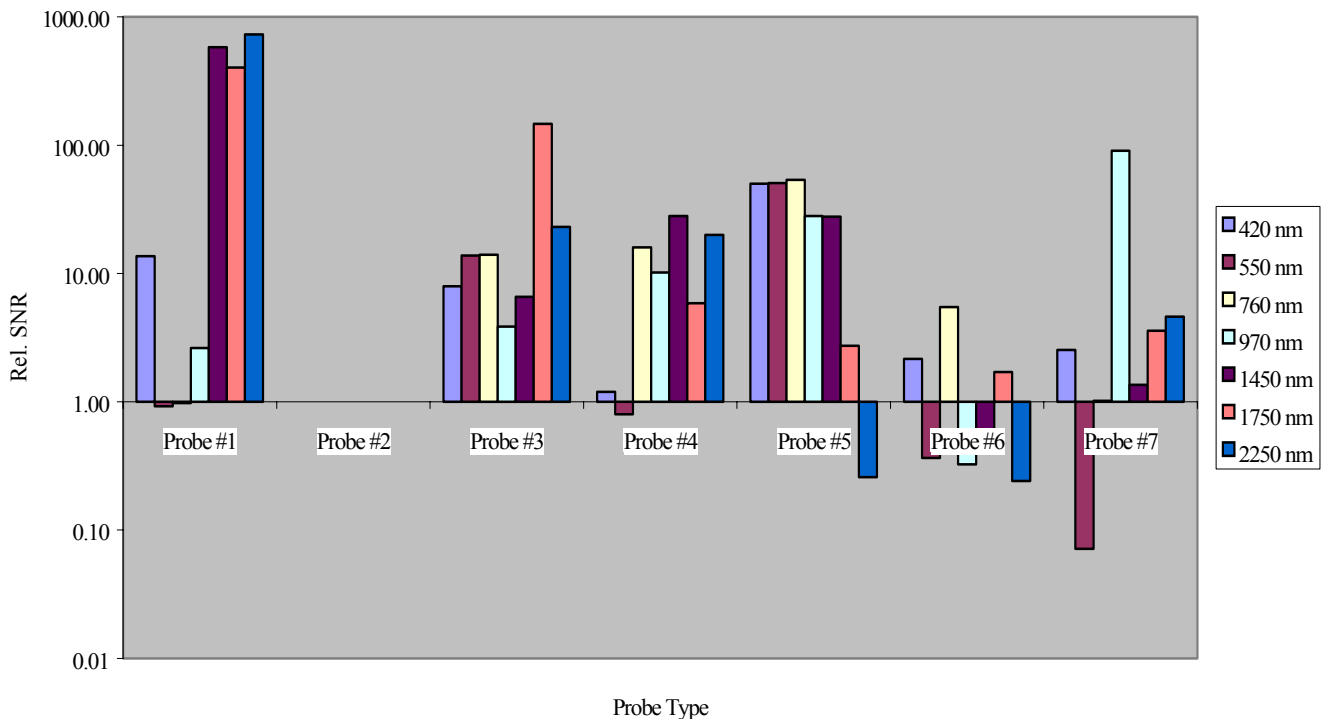
Figure 5.5.1: Relative SNR compared to Probe #2 (first design iteration probe): Log Scale. For specific wavelengths. From left to right, probes #1 to #7 as described in Table 5.3.1.

47
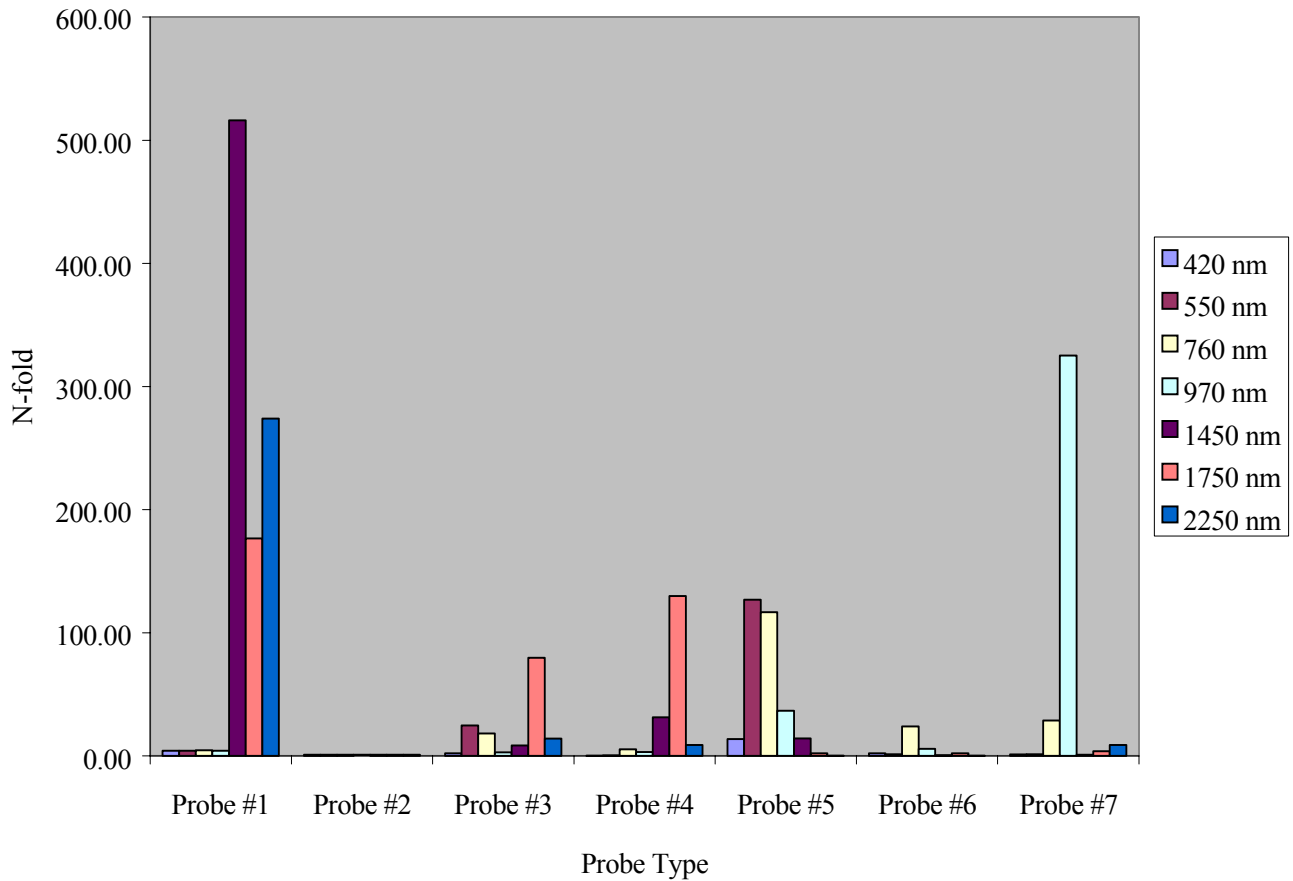
Figure 5.5.2: Relative N-fold improvement in noise (reduction) with respect to probe #2 (first design iteration probe) for specific wavelengths. From left to right, probes #1 to #7 as described in Table 5.3.1.

The average detector voltage reading in millivolts (visible, Si; NIR, PbSe) and the performance factor multipliers with respect to probe #2 are tabulated in Table 5.5.1.

Table 5.5.1: Performance factor multipliers with respect to first design iteration probe (probe #2).

Probe ID	Relative Receiver Area Improvement	Average Voltage Reading (mV)		Relative Voltage Improvement (500 um separation)		Optical Window Improvement (for same probe)
		Visible	NIR	Visible	NIR	
1	23	2.39	323.2	122	71.5	90
2	1	0.01963	4.519	1	1	--
3	(0.3513)	0.04138	12.50	2.1	2.8	--
4	23	0.02998	3.573	1.5	(0.79)	--
5	1	0.03363	7.638	1.7	1.7	1.7
6	1				1.4	1.9
7	1	0.0223	5.45	1.1	1.2	1.2

The second design iteration probe, requiring a 50-micron separation (probe #8), had an estimated relative receiver area improvement factor of 4 over probe #3, the only other probe tested with a 50-micron separation (that is, thirteen 200 micron fibers versus

thirteen 100 micron fibers), a relative voltage improvement in the NIR of 1.4, and a estimated optical window improvement in the NIR of 1.9, based on the results with respect to the first design iteration probe (probe #2). The actual SNR and average voltage readings were measured for probe #8 on fresh fibrofatty plaque tissue. The actual SNR, relative SNR, average voltage readings for the visible and NIR detectors, and the relative voltage improvement over the first design iteration probe are summarized in Table 5.5.2. Figure 5.5.3 is identical to Figure 5.5.1, with the data for probe #8 added.

Table 5.5.2: Analysis for probe #8, 50 um separation.

Wavelength (nm)	Actual SNR	Relative SNR (w/ respect to probe #2)	Average Voltage Reading (mV)	Relative Voltage Improvement (w/ respect to probe #2)
420	1742	92	0.2345 (visible)	12x
550	3528.5	30.7		
760	1101	9.1		
970	4187	18.95		
1450	299	12.5	87.3 (NIR)	19x
1750	740.5	370		
2250	142	71		
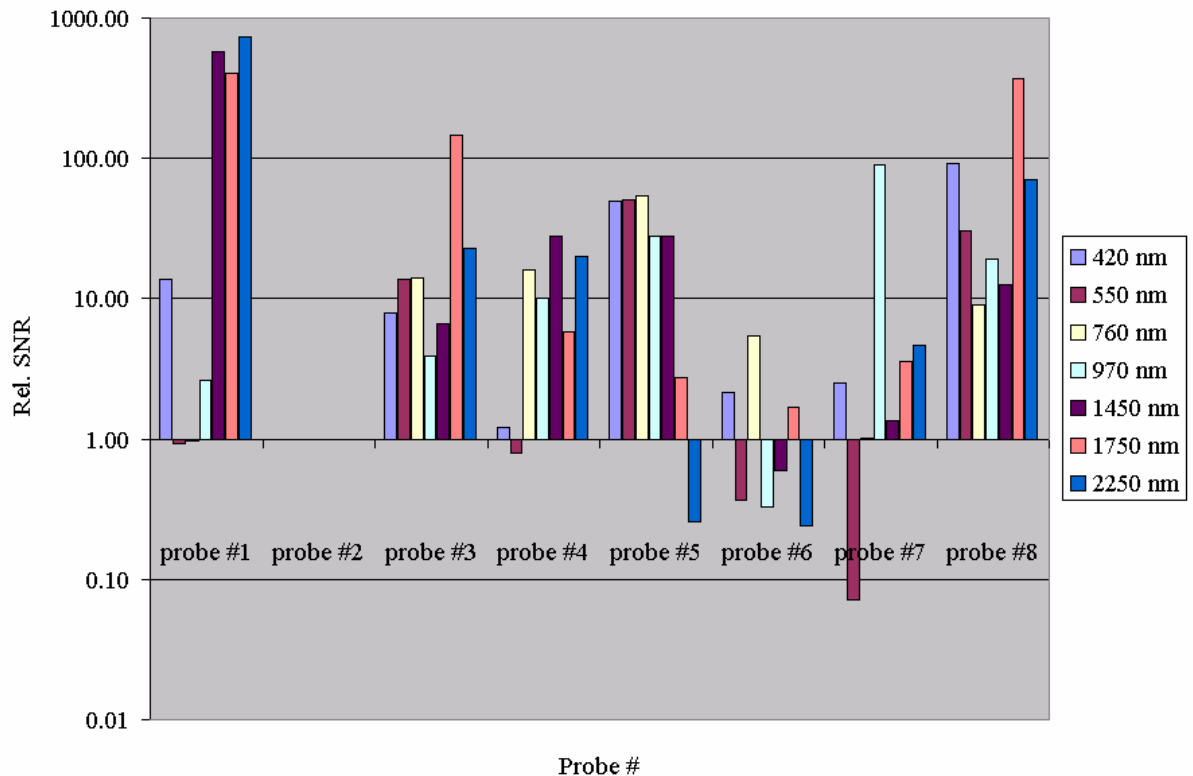
Figure 5.5.3: Relative SNR log scale with respect to Probe #2 (first design iteration). Results of Probe #8 added. Probe #8 has adequate signal-to-noise and it is appropriately sized for the research applications.

49

Tissue Depth Penetration Testing

The results for the tissue penetration tests using O.C.T. embedded frozen section, 50-micron pieces of normal aortic tissue (as described in Section 5.3.3) are shown in Figure 5.5.4 for the 50 and 500 micron source-receiver separations. The 50 micron separation (black bars) showed deeper light penetration at λ=2250 nm, which is the wavelength where lactate absorbance would occur. At least a 300 micron depth penetration is achieved for all other wavelengths with either separation, which is useful information for the optical tissue pH determination.
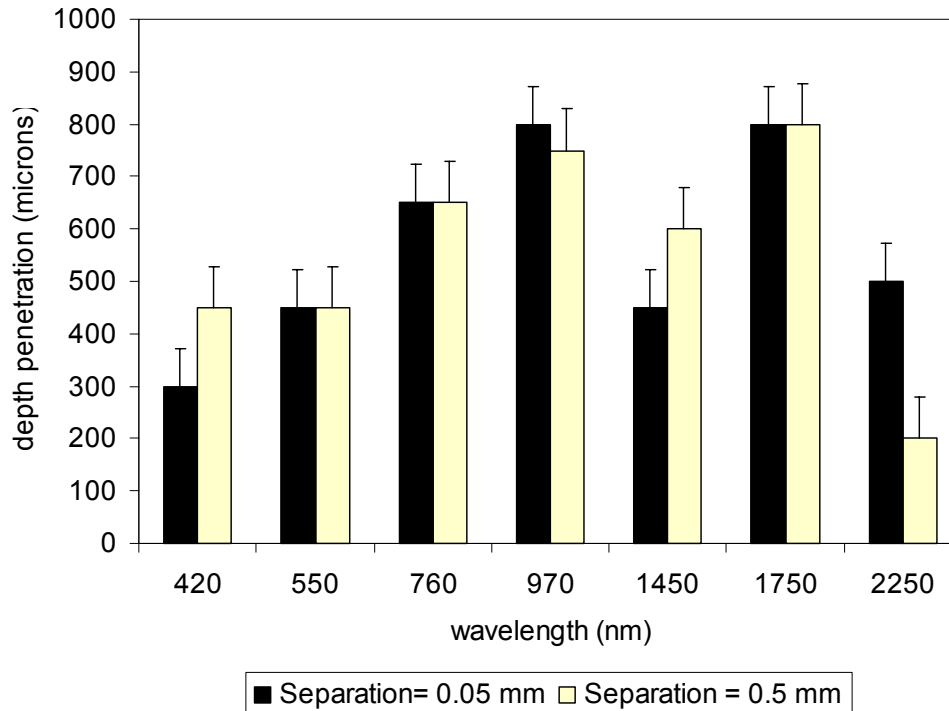
Figure 5.5.4: Measured tissue penetration depth (in microns) as a function of wavelength and source-receiver separation (0.05 mm = 50 microns).

5.6. Discussion

The Intralipid simulations demonstrated that minimization of the wavelength dependence of scattering was possible for source-receiver separations between 0.45 and 0.75 mm. However, the probability of absorption of a 2 mM deoxy-Hb containing tissue is high between 500-900 nm, therefore the amount of light returning to receiving interface is low over the same range of source-receiver separations due to added absorber. By minimizing the scattering for spectroscopic measurement, it is expected that the contribution in absorbance due to small changes in the optical spectra will be improved when interrogating a small volume. However, it must be realized that the benefit of high backscattering geometry provided by small source-receiver separations is offset by the

information loss of principal absorbers. Measuring small changes in absorbance may require two different separations—one to account for scattering, and one to collect a large variation in reflectance to be sensitive to the main absorbers.

From the Intralipid and de-oxy Hb simulations, it was concluded that the tissue depth interrogated by a source-detector separation of 0.75 mm is approximately 1.25 mm in a one-component absorbing medium between 500-900 nm. For source-receiver separations less than 0.75 mm, the penetration depth should be smaller as the probability of absorption increases. The propagation was modeled as forward directed (anisotropy factor, g=0.9), therefore this depth may appropriately be taken as the most likely deepest layer of tissue from which photons could scatter back to the detecting layer. For comparison, diffusion theory predicts a penetration depth (defined as $\delta=1/(3\mu_a(\mu_a+\mu_s(1-g)))^{1/2}$) of 0.04 to 0.64 mm for the optical properties simulated. Ninety percent of the absorption occurs by a depth of 0.75 mm; after that the probability is reduced significantly such that the probability of absorption, (P(A)), at 1.25 mm is ½ that of the P(A) at 0.75 mm. Stated another way, the probability of photons visiting a depth of 1.25 mm and returning back to the detecting layer is severely reduced. This "detection" limit (spherical volume $\pi d^3/6$, d=1.25 mm) corresponds to interrogating ~1 mm^3 tissue volume for a 0.75 mm source-detector spacing. The limitation in this simulation was that only the highest absorbing species was modeled and any effects of concentration and scattering were considered static.

Additional simulation data using normal and atherosclerotic aorta absorption and scattering coefficients provided more relevant depth penetration for the assessment of spatial resolution versus the source-receiver separation for this research. The atherosclerotic aorta consistently showed less penetration depth versus the normal aorta at the same wavelength for all source-receiver separations (Table 5.5.2, shown for the 50 micron separation). The diffuse reflectance provided an additional piece of information for the optimal source-receiver separation (Figure 5.4.2). The amount of diffuse reflectance is actually higher at small source-receiver separations (<0.005 cm or 50 microns) for the atherosclerotic aorta at 514 nm. At 1064 nm, however, the normal aorta has a higher diffuse reflectance probability per cm^2 less than <0.005 cm source-receiver separation, and falls off less sharply than the atherosclerotic data. Greater than 0.03 cm (or 300 microns radius), both diffuse reflectance probabilities across all wavelengths are very low, in contrast to the Intralipid and de-oxy Hb simulations. It can be concluded that the source-receiver separation must be much smaller than anticipated (in comparison to the first design iteration based on the Intralipid and de-oxy Hb simulations). The penetration depth is smaller, as expected for a smaller source-receiver separation. There should be adequate signal however based on the relative magnitudes of the diffuse reflectance probabilities for separations ~ 0.005 cm (50 microns). The optical property data for normal and atherosclerotic aorta were primarily different in the scattering coefficient. The amount of scattering seems significantly higher in the atherosclerotic aorta, possibly creating more events for the light to backscatter towards the receiving plane, resulting in a higher diffuse reflectance probability at small source-receiver separations.

The simulations shown above are for a point source. However, optical fibers have finite diameter (e.g., a standard medical-grade, multimode glass fiber has 200/225 um core and cladding diameter, respectively), small numerical aperture, and dispersion, thus, the realistic source is not a point source. Data convolution to a finite Gaussian beam may be more precise, but the results are equivalent to point source simulations due to the geometric symmetry assumption in the small volume under study. The accuracy of the probability (per cm^3 or cm^2) value is proportional to the square root of the number of incident photons, N. Although larger values of N may improve the statistical error, it will not affect the trends, i.e., the photons will follow the same most likely paths for a given set of optical properties. It was therefore assumed that the trends observed could be used to help estimate the spatial resolution of the first optical design (Probe 2), even in the absence of optical property data being available for several key wavelengths, such as for λ=2250 and 2295 nm, the wavelengths where lactate absorbance occurs. The theoretical observations are augmented and complimentary data obtained through bench tests performed at the wavelengths used for the simulations and additional wavelengths important for the optical determinations.

The probe(s) signal-to-noise ratios measured on the same spectrometer were analyzed to aid in decision-making for the optimal optical components and configurations. The two factors that improved the signal the most were the fiber size and type, and the use of an optical window. The only factor that reduced the noise was the use of an optical window. This may imply that there is slightly better optical matching between the optical fibers and tissue when an optical window is used. The incorporation of both the larger 200 um core, ultra-low OH fibers, and a borosilicate or quartz optical window material in the second iteration design (Probe #8), showed significant improvements in both the visible and near-infrared regions for the same source-receiver separation (compared to Probe #3). The added benefit of a simpler forward-facing optical probe (Probe #8) should make the spectra collection on the plaque tissue easier to identify and reproduce than the 360° optical probe (Probe #3).

The measured depth penetration for two different source-receiver separations (50 and 500 microns) showed that at the key wavelengths (550, 760, and 1750 nm, absorption peaks of oxy-Hb, deoxy-Hb, and cholesterols, respectively) the respective depth penetrations did not change. However, there were differences at 470, 970, 1450 and 2250 nm. There was more penetration for the 50 micron separation at 970 nm (water absorption peak) and at 2250 nm (a trough between two large water peaks at 2000 and 2500 nm).

For the optical determination of plaque lactate concentration, the depth penetration at 2250 nm is important; this wavelength is in the region where tissue lactate would absorb. The estimated penetration depth based on these experimental observations at 2250 nm was 500 microns, for the 50 micron source-receiver separation, and only 200 microns for the 500 micron separation. Therefore, it was concluded that the 50 micron separation should be incorporated in the final design. The actual working optical diameter of the second design iteration probe (probe #8) is ~2.5 mm, which is less than the 4 mm diameter of the tissue lactate punch biopsy (interface resolution). The biopsy procedure requires that the entire thickness of the plaque is collected at the point being measured.

The depth resolution of the optical measurement will be finer than the reference measurement in most cases, but the interface resolution is acceptable. The spatial resolution may still affect the calibration accuracy of the lactate determination.

For the optical determination of plaque tissue pH, the visible wavelengths are considered important. At 760 nm, both the 50 and 500 micron separation experiments demonstrated a penetration depth of ~650 microns. The micro-pH electrodes are approximately spherical or "tear-drop" in their contact area, and require to be placed at least a depth of 750 microns to obtain accurate readings. The depth resolution of the optical measurement is finer than the reference measurement. However, the probe-tissue interface (area) for a 50 micron separation will still be greater than the micro-electrode diameter (~2.5 mm versus 0.75 mm). Considerable care must be taken to register the site where the optical spectrum is taken on the tissue. The interface resolution may affect the calibration accuracy of the tissue pH determination.

5.7.   Summary

Based on the theoretical simulations and the depth penetration testing, it was concluded that by:

- Using a source-receiver separation of 50 microns, adequate depth resolution could be achieved in plaque in both the visible and near-infrared;
- Increasing the collection fiber core diameter size to 200 microns with improved transmission out to 2400 nm, higher signal-to-noise ratio is achieved by improving the fiber collection area by 4 times and collection efficiency; and
- Using a 0.5 mm thick quartz optical window fused on the common end, with forward-viewing optics, the signal-to-noise ratio would be further improved across all wavelengths

This probe as built would have adequate resolution for accurate optical determinations in atherosclerotic plaque in a controlled environment with careful registration of the optical and reference measurements. It was expected that at least a ~6-fold improvement in the visible region (or an actual voltage of 0.24 mV vs. 0.04 mV) and ~10-fold improvement in the NIR region (or an actual voltage of 130 mV vs. 13 mV) would be realized for the source-receiver separation of 50 microns as compared to the first design iteration probe (Probe #2). The measured improvements were higher, (12-fold improvement in the visible and ~19-fold improvement in the NIR). The practical considerations in the optical design process were able to improve the signal-to-noise ratio, maintain the necessary source-receiver separation, and collect light from a small (<1 mm^3) region of tissue, based on both the experimental and theoretical depth penetration results.

6. METHODS

Methodology to collect metabolic data from freshly excised carotid tissue is first described in this research. In order to obtain ~100 data points for the optical calibrations, verification that the laboratory setup could reproducibly maintain the status of the previously assumed living, metabolically active plaques had to be made first (Section 6.1). Next, the *in-vitro* optical spectra collection is described using two different spectrometers and the proposed optical probe design built as specified in Section 5. Description of the methodology used to collect reference data that co-registered with the optical measurements is presented along with the tissue pH measurement and the lactate concentration assay method. Lastly, the calibration model development strategy is presented in Section 6.4. Preliminary analysis was done on ~20 points for each optical calibration to assess data quality. Additional points were added to the initial calibration model results after the data collection program was completed, and the data analyzed in the aggregate was compared to the preliminary results.

6.1.   Laboratory Setup and Validation

In this section, the laboratory setup is described. The method to maintain the ~30 living human plaque tissues studied after surgical removal at near *in-vivo*, physiologic conditions during the optical and reference data collection is presented. Tissue culture techniques and biological atmosphere gas were used to preserve the plaque tissue. Physiological parameters were monitored in an initial set of nine plaques (no optical measurements) to validate this method. The total experiment duration allowable was determined through this process by observing the degradation over time in physiological parameters of the plaque tissue.

A schematic of the laboratory setup is shown in Figure 6.1.1. The bath temperature was maintained at 37°C using a heating pad. The entire bath apparatus was enclosed in a 37°C humidified incubator. Biological atmosphere gas was bubbled in through a tube placed under the liquid surface (tissue culture media). The fiber optic probe, electrodes, thermistor(s), optical reflectance standard, and balance were configured as shown in diagram. A gridded ceramic plate (not shown) was used to attach the plaque tissue in a fixed location with respect to the micromanipulator such that co-registration of the exact location from which the optical spectra were collected to the gross pathology and reference measurements could be made (see Section 6.3 Reference Measurements).
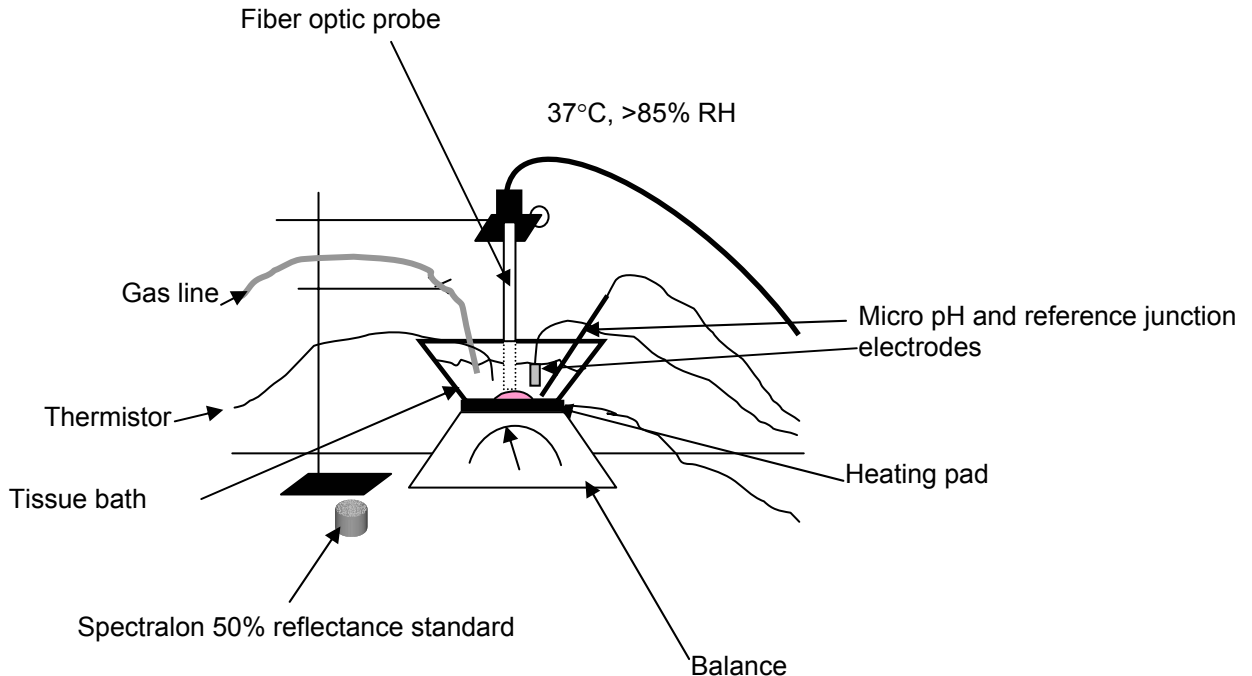
Figure 6.1.1: Laboratory Setup. The tissue bath was maintained at 37°C using a heating pad. The fiber optic probe is shown mounted on a x-y-z micromanipulator. The gas line from the biological atmosphere tank is placed under the liquid surface to provide oxygenation and mixing to the tissue culture media. The balance is used to reproducibly maintain a constant pressure when the fiber optic probe is pressed down on to the tissue fixed to a gridded, ceramic plate on the bottom of the tissue bath (not shown). A 100 mg deflection is used for all optical measurements. The thermistor, micro-pH and reference junction electrodes are placed in the liquid media. The entire bath apparatus, Spectralon standard, and ancillary equipment are enclosed in a humidified, 37°C

An initial set of nine plaques was used to validate the tissue bath preparation. Fresh carotid plaque tissue was collected from UMass Memorial Healthcare University Campus Vascular Surgery operations over a period of three months (IRB approval Docket#10041). The plaque was immediately placed in a tissue culture medium (Minimum Essential Medium, Invitrogen, MD, pH 7.4, 5.6 mM glucose, 26.2 mM sodium bicarbonate, non-essential amino acids supplement) in a 37°C heated porcelain bath, bubbled with a $75\%O_2/20\%N_2/5\%CO_2$ gas mixture (n=7). This particular MEM was chosen because it was the only available prepared sterile liquid media with high glucose concentration that did not contain phenol red, a colored dye that is used to indicate gross pH changes. The media bath was equilibrated with the gas mixture for a half hour prior to tissue addition. Plaque tissue that was not placed in the bath (only in the 37°C humidified air of the incubator) served as controls (n=2). Tissue pH, pCO_2, and pO_2 measurements were taken continuously by placing a 0.5 mm diameter by 25 mm long multi-parameter sensor (Diametrics Medical, MN) within the thickness of the plaque tissue in all nine plaques (Figure 6.1.2, control plaque photograph). The location chosen was based only on the ability to place the sensor safely within the tissue. The sensor readings were observed for stability during the experiments. The media pH, pCO_2, and pO_2 values were discretely measured with a blood-gas analyzer every ~30 minutes

(Model IL428, Instrumentation Laboratories, MA) and compared to the tissue readings. The rate of change was calculated for the tissue pH and tissue temperature. The relative pCO_2 and pO_2 values were analyzed.
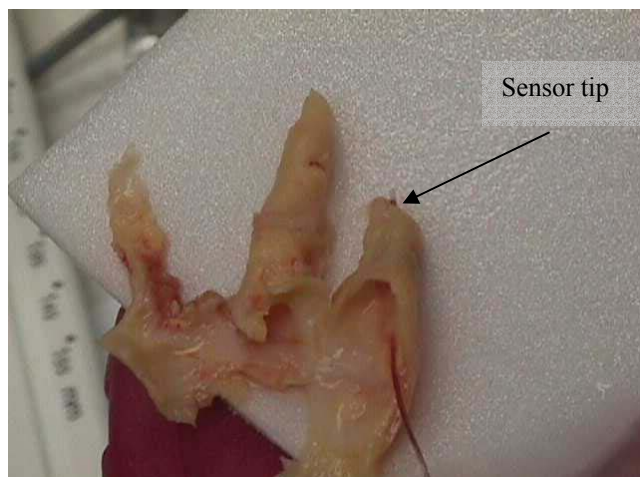
Figure 6.1.2: Photograph of control plaque with Diametrics multi-parameter sensor in place. Sensor measures tissue pH, pCO_2, and pO_2 values continuously in the nine plaques in the validation study.

6.2. Optical Spectra Collection

Optical spectra of 30 different plaque specimens (K1-30) were collected using a 3 mm outer diameter optical probe (as described in Chapter 5 Optical Design, Final Probe) placed in the tissue bath (Laboratory Setup, Section 6.1). A photograph of the probe and a probe-tissue interface schematic are shown in Figure 6.2.1. The probe contains all multimode, 200-micron diameter core, ultra-low OH fibers bundled in a 1.5 m long bifurcated cable. Seven fibers (shown in orange) were arranged hexagonally as the input fibers in one leg, and twelve (shown in yellow) in the other leg to the receiving spectrometer's detector. The center source fibers were separated from the outer 12 fibers by a 50-micron thin walled plastic tube. A 1 mm quartz window (not shown, refractive index, n=1.44) was mounted on the face of the probe (common end).

The probe was cleaned with an isopropyl alcohol pad before each tissue spectrum and allowed to dry in the incubator. The probe was then placed a micromanipulator stage. A reference spectrum was collected on a 50% Spectralon standard (Labsphere, NH). For tissue spectra, the probe was brought to contact the plaque through the liquid media by carefully adjusting the micromanipulator such that the pressure applied caused a 100-mg deflection of the needle on the balance carrying the tissue bath. For the first 14 plaques, absorbance spectra were collected only on an FT-NIR spectrometer. Due to circumstances beyond control, the instrumentation to collect visible spectra was not available until about halfway into the experimental phase. For the remainder of the experimentation, absorbance spectra were collected on both the FT-NIR spectrometer and a PDA-based dispersive spectrometer. At the end of the experiment, all spectra were reviewed to see if the ceramic plate was inadvertently reflected in the tissue spectrum, by

collecting a spectrum through the media at the same applied pressure (without the plaque) and comparing the reflected signals. The probe was cleaned thoroughly with isopropyl alcohol and stored at the end of the day.
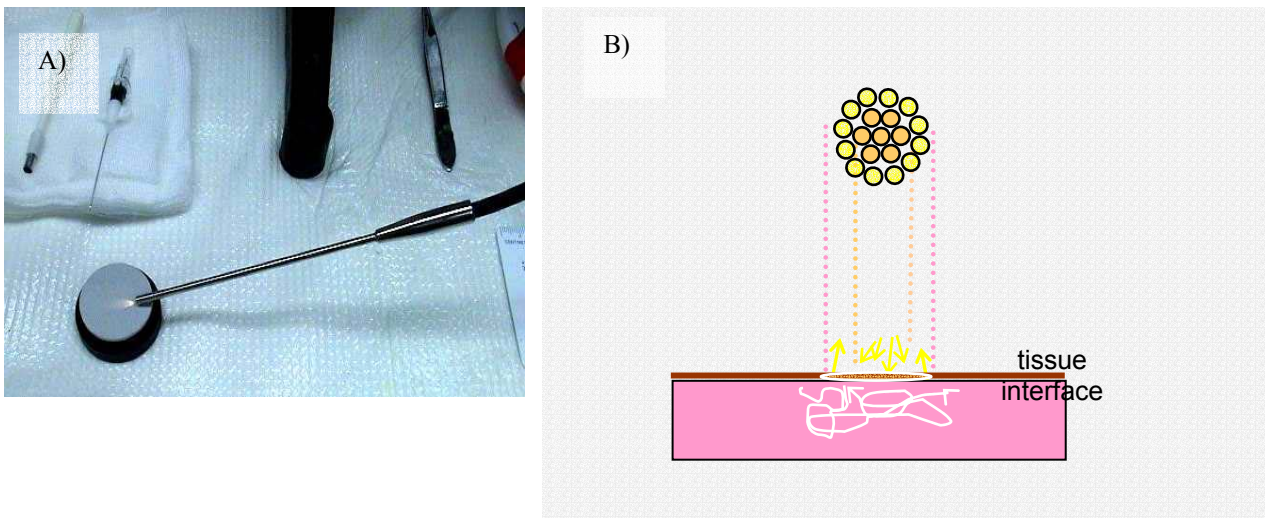
Figure 6.2.1: Optical probe used for all spectra collection. A) Photograph, 3 mm OD probe on reflectance standard. The probe contains all multimode, 200-micron diameter core, ultra-low OH fibers bundled in a 1.5 m total length bifurcated cable. B) Probe-tissue interface schematic. The center, source input fibers (seven shown in orange) are arranged hexagonally at the probe-tissue interface and bundled in one leg attached to the source. The receiving fibers (twelve shown in yellow) are in a ring at the probe-tissue interface, separated from the center seven fibers by a 50-micron thin walled plastic tube, and bundled in another leg attached to the receiving spectrometer's detector interface. A 1 mm quartz window (refractive index, *n*=1.44, not shown) was mounted on the face of the probe. Diffuse light interaction with plaque depicted.

6.2.1.   FT-NIR Spectrometer

Spectra from 28 plaques (plaques K1-14 and K17-30) were collected using a Nicolet Nexus 670 Fourier transform near infrared-based spectrometer (75 Watt tungsten-halogen lamp / quartz beamsplitter) employing a room temperature InGaAs detector and a fiber optic probe module. The spectral range scanned was 667 to 2436 nm (15000-4097 cm^{-1}), and 128 interferogram scans at a spectral resolution of 32 cm^{-1} were averaged. Single-beam spectra were automatically computed with the triangular apodization and Fourier-transformation routines available on the spectrometer software. A reference spectrum was collected using a 50% reflectance standard (Labsphere, NH) prior to each tissue spectrum. The software automatically calculates the absorbance spectrum for each tissue measurement.

The reference detector voltage was checked for stability after the spectrometer was allowed to warm up for ~ 1 hour (±4.6 volts). The signal off of the 50% reflectance standard was set to provide a center burst interferogram voltage of 0.50/-0.45 V. The gain was set to 8 for all spectral measurements. This procedure allowed the signal from the fiber optic probe to have the best possible signal-to-noise ratio given the known fiber optic-to-FT spectrometer losses. The resulting spectral resolution was approximately 2.5 nm and the acquisition time was ~42 seconds. These spectra were used for both lactate and tissue pH optical determinations.

6.2.2.   PDA Spectrometer

Optical reflectance spectra (400 – 1100 nm) from 16 plaques (plaques K15-30) were taken using a Control Development (South Bend, IN) 512 element photo-diode array (PDA) spectrometer with a room temperature Si detector, and converted to absorbance using a dark current-corrected reference single-beam spectrum collected as described below.   The spectral resolution of the spectrometer was 0.5 nm. The source was a separate unmodulated, ~7.5 Watt tungsten-halogen lamp (Ocean Optics, FL). Two plaques (plaque K15 and 16) were used solely for determining the optimal integration time and sample averaging.

After the 50% reflectance standard was measured on the FT spectrometer, the source and receiver fiber optic connectors were removed from the Nicolet FT spectrometer and placed on the Ocean Optics source and Control Development spectrometer respectively. The probe height was maintained and a reference spectrum taken prior to each tissue spectrum. The maximum reference signal at 727 nm was checked (after the spectrometer and source were allowed to warm up for ~1 hr) to be within ±5% of 45,000 A/D counts (minus the dark current signal, measured prior to each reference signal). The integration time was set to be 3.6 seconds, and sample averaging to 15, resulting in an acquisition time of 54 seconds. These settings allowed the tissue spectra to be collected at the maximum signal-to-noise ratio possible with the PDA spectrometer in a reasonable time.

The visible tissue spectra were offset to the peak value at 970 nm on the FT-NIR spectra and spliced together to form spectra for the full range (400–2400 nm). After a preliminary data analysis, the spectrometer's stability was checked by analyzing the reference spectra intensities at 970 and 2250 nm for each day and over multiple days.

6.3.   Reference Measurements

Thirty (K1-30) fresh human carotid endarterectomized plaques were collected over a period of 8 months at the UMass Memorial Healthcare University Campus (IRB approval Docket#10041). Plaques were taken from the operating room and immediately placed in an oxygenated media bath preparation as described in Section 6.1. All standard biological hazard precautions were followed as if handling blood.

First, the plaque was fixed to the ceramic grid in the bath. Plaque features and gross pathology were documented by drawing, descriptive text, and photography (see Figure 6.3.1 for a representative plaque). A random area was chosen for the optical probe to be placed and registered on the drawing by grid mapping. After the optical spectra were collected as described in Section 6.3, the optical probe was adjusted back to zero position (no pressure applied), allowing the area directly under the probe to be visualized. Next, a T-type needle thermistor probe (Omega Engineering, CT) was placed directly under the optical probe and the tissue temperature recorded.   The tissue micro-pH electrode was then inserted in the same area under the probe and as close to the needle thermistor at a depth of ~0.75 to 1 mm and recorded. Lastly, a 4-mm diameter biopsy device was placed close to the optical probe area and allowed to cut into the plaque at the junction.   The

optical probe was pulled away at the same time the tissue biopsy was cutting the area just under the optical probe. Extreme care was taken to make sure the area biopsied was the same as the registered location on the grid, and cut through the entire thickness of the plaque. The thickness of the biopsy was measured. A small sliver was cut and placed in formalin for histology processing. Approximately 9/10 of the biopsy was then finally snap frozen in liquid nitrogen and stored in a cryovial. Each biopsy was labeled with the map location. The apparatus for the specific reference measurements of tissue pH and tissue lactate are summarized below.

The reference measurements, biopsy thickness, and observed gross pathology were entered into a Microsoft Excel spreadsheet. Correlations were drawn for tissue pH versus temperature, pH versus lactate, lactate versus temperature, and pH or lactate versus gross pathology.   The total time the plaque was in the media from start to finish was documented. Experimental notes were maintained and kept in a logbook for future reference. No reference data was collected for K15 and K16 due to needed adjustments in the visible spectrometer data collection.
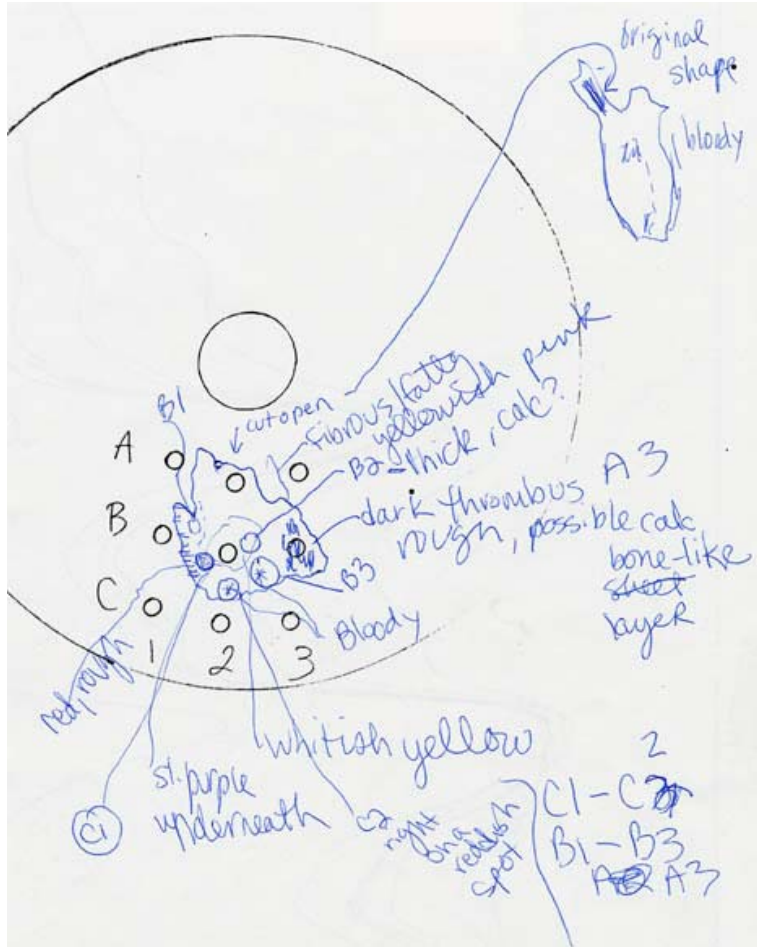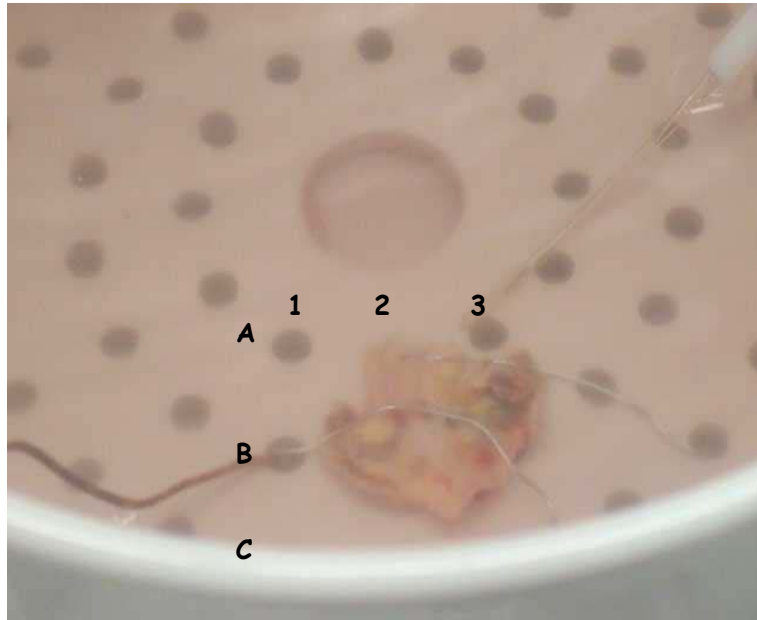
Figure 6.3.1: Top) Photograph, bottom) drawing, and descriptive text of a representative plaque (K13). Ceramic plate grid holes are represented in drawing. Plaque is fixed to grid with stainless steel wires. Co-registration of gross pathology, optical spectra, and reference measurements were collected as described in the text. A thrombotic region can be seen in the upper right side of the tissue (grid position A3).

6.3.3.   Tissue pH

Micro-pH electrodes in a sharp, beveled 21-gauge needle (~750 μm diameter, MI-407 Microelectrodes Inc., NH) were used to make the reference tissue pH measurements. The reference junction electrode was placed in the media bath and both electrodes are connected to a Thermo Orion 720A pH meter. The electrodes were calibrated prior to each experiment using five NIST-traceable buffers (Fisher Scientific, 4.00, 6.00, 7.00, 7.40, and 10.00 at 25°C). The calibration slope was recorded. The pH meter readout was automatically temperature corrected to the *in-vitro* media temperature. The tissue pH measurements were performed and recorded at the same grid location the optical spectra as described in Section 6.2. After each tissue measurement, the electrodes were rinsed in warm Tergazyme solution and distilled water, then checked for drift in a 4.00 buffer at 37°C. This was done to avoid protein buildup and electrode drift from location to location. Two electrodes were calibrated for each experiment such that if one exhibited drift problems, the other could be used until the end of the experiment. These values were used for the optical calibration of tissue pH.

6.3.4.   Tissue Lactate

Biopsy samples were immediately collected after the tissue pH and temperature measurements. A ~4 mm diameter biopsy of the area directly under the optical probe was collected as described in the general procedures. Each biopsy piece was immediately frozen in liquid nitrogen and placed in a cryovial for storage. All samples were stored in liquid nitrogen tanks until ready to extract (no more than 6 weeks).

Tissue weights were obtained prior to assay using a Sartorius analytical balance. A standard Sigma Blood Lactate Kit UV-340A (Sigma Diagnostics, MO) was adapted to tissue extracts and microplate assay. Tissue extracts were prepared by homogenization according to Lowry and Bergmeyer [87, 88] and neutralized to pH 7-8 by addition of $KHCO_3$. For each sample, 25 ul of this neutralized perchloric acid (PCA) extract was combined with 200 ul of assay reagent in a microtiter plate, and incubated for 30 minutes at 25°C. The absorbance at 340 nm was read and recorded on a Dynatech Lab MRX Microplate Reader after incubation. Calibration curves were generated for each batch run by plotting blank-corrected absorbance vs. concentration (mg/ml) of freshly prepared standards. A percent recovery factor (see below) is calculated and multiplied to the dilution-corrected values obtained from the curve. Finally, to obtain a weight basis, the concentration was divided by the weight of each sample to obtain units of micromoles lactate per gram of tissue. These values are used for the optical calibration.

Percent Recovery Procedure (adapted from Bergmeyer et al [88]

In the homogenization and assay process, some tissue is inevitably lost. This loss represents a loss of information that may degrade the optical determination of lactate, due to inaccuracies in the reference measurement. Therefore, for each batch assay, a percent

recovery procedure was performed to make an estimate of precisely how much lactate was lost and correct the data accordingly.

One sample was randomly taken and split in half during homogenization step. A known amount of lactate standard (50 ul of 0.4 mg/ml or 0.02 mg lactate) was added to the second aliquot of the sample. The dilution factors were calculated for both the undoped and doped test tubes. Both test tubes were processed as normal through rest of the procedure. To calculate the percent recovery, first the concentration of both samples was determined from the calibration curve. The percent recovery factor is then calculated by assuming what is in the un-doped homogenate is in the second tube plus the value Y as above. That is, if X represents the concentration of lactate in the original homogenate, then X+Y should be the concentration of the doped sample (volume dilution factors accounted). The ratio of the doped sample concentration from the calibration curve and the expected X+Y concentration is the percent of lactate that can be feasibly recovered. This correction is applied to all other samples. A sample calculation is presented in Figure 6.3.2.

SAMPLE CALCULATION:

Calibration Slope=7.5 Abs. Units/mg/ml lactate   MW of lactate = 90 grams/mole
Calibration Intercept=0.015 Abs. Units
Blank-corrected Absorbance of sample 1 = 0.52

Lactate concentration = (0.52-0.015) ÷ 7.5 = 0.0673 mg/ml lactate or 748 nanomoles/ml

To account for volume added to tissue homogenate in step 1, multiply by supernatant volume correction factor (ex. (200 ul PCA + 20 ul $KHCO_3$)/200 ul PCA). Also account for % Recovery.

To get weight basis, divide concentration by weight of tissue per ml of PCA. For example, if the tissue weighted 15 mg, the above lactate concentration would be reported as:

In this example let % recovery = 85% and amount $KHCO_3$ (neutralization base) added was 20 ul:

748 nanomoles/ml * 1.1 ÷ 0.85 ÷ (15 mg / 0.2 ml)= 12.9 nanomoles/mg tissue or 12.9 umoles /gram tissue.

Figure 6.3.2: Sample Calculation for tissue lactate recovery and final calculations to provide reference lactate concentrations for optical calibration.

6.4. Calibration Model Development

Galactic Grams/32 software (Galactic Industries Corp., NH) was used to visualize and where necessary, compute additional pre-processing of the optical spectra. The PLS/IQ module was used to perform partial least-squares (PLS) multivariate calibrations for both the optical determination of tissue pH and lactate. For the lactate determination, only the near-infrared spectral data was required. The theoretical peaks at ~2250 and 2295 nm should be apparent in a valid PLS model. For the tissue pH determination, no *a priori* information was assumed. Models were created using the full spectral region collected (400-2400 nm) and a wavelength selection approach, based on choosing only those

wavelength regions that are most highly correlated to the reference values. Preliminary data analysis was performed on the first ~20 points to assess data quality. Historically, for optical tissue pH calibrations, twenty points were adequate to generate a reasonable multivariate calibration model.

For the entire calibration data set (lactate 82 points, tissue pH 48 points), additional pre-processing methods were tested. Two standard pre-processing methods available in the software -- Baseline Correction and Multiplicative Signal Correction -- were tested as to their ability to improve the optical determinations over and above standard PLS. An automatic, linear baseline correction was applied to test if spectral drift could be removed by simply calculating a least-squares regression line in the selected spectral range and then subtracting the line from all the spectra [89, 90]. Multiplicative Signal Correction (MSC) was applied to test if the variance in the spectral data could be removed by correcting for light scattering. MSC assumes that the wavelength dependency of scattering is different and unrelated to that of the reference data [89, 91]. The mean spectrum is used as the "ideal" spectrum and a linear regression for all the spectra is calculated. The generated slope is subtracted and the offset is ratioed on each spectrum to give MSC corrected spectra.

In addition to these standard pre-processing methods, cluster analysis and orthogonal signal correction (OSC) were used to evaluate sources of error in either the spectral measurement or reference measurements. Cluster analysis techniques were used to investigate whether if, by finding groups of spectra that are closer together or homogeneous (and therefore have reduced variability compared to the entire spectral data set), improvement in the PLS modeling could be made in an unsupervised fashion (i.e., without information from the reference measurements). Groups of spectra identified by cluster analysis were reviewed to see if other patterns--such as groupings corresponding to gross pathology, experimental conditions, or time--could be deduced for each cluster. The OSC method was used to investigate whether there exists a spectral correction made by removing components orthogonal to the reference measurements, that could allow the reference variation to be modeled independently and thereby improve the PLS models. Cluster analysis and orthogonal signal correction were applied to the spectral data separately and PLS models were repeated using the either newly formed cluster matrices or OSC-corrected spectral matrix.

6.4.1. *Partial least-squares*

Partial least-squares (PLS) calibration is an empirical, factor analysis based multivariate method that decomposes the measured absorbance matrix into two smaller components called loading vectors and scores. Both spectral and the reference values are used in the decomposition. Loading vectors represent linear combinations of the original calibration spectra that explain most of the variance in the set. The score is the weight of each loading vector component needed to reconstruct a calibration spectrum. The first loading vector and score matrix usually contains most of the variance and successive factors are calculated from the residual matrices. The variance in the data should be related to the desired reference measurement for a good calibration fit; however, other chemical

compositions, and experimental conditions may contribute to the model. Spurious correlations, if any, must be identified and removed.

Mean centering was used for pre-processing in all model development. The average spectrum is calculated from all the calibration spectra and then subtracted from all the calibration spectra. Mean centering tends to reduce the model complexity [71]. Loading vectors and scores were calculated for the maximum number of factors and a leave-one-point-out cross validation algorithm was used to assess the model for each factor. Cross-validation predicts the *nth* reference value from the *nth* spectrum, based on an *n-1* PLS model. This was performed successively for each spectrum until all spectra were predicted based on a PLS model of the *n-1* points for all factors. The optimal number of factors for each calibration was determined from the Predicted Residual Sum of Squares (PRESS) for each factor, and using a F-test (alpha level of 0.25) to identify the smallest number of factors required for the model [71]. If there is no minimum PRESS after one factor, no model can be created with the data. Outlier detection was performed according to Haaland (spectra or reference values that have an F-ratio value $\geq$ 3) [71]. Outliers were further investigated for any adverse experimental conditions as well as their histological classification in relation to the calibration method employed.

Correlation plots of the measured reference variable versus the optically determined value were evaluated. The coefficient of multiple determination (or R^2) and the estimated accuracy (standard error of cross-validation (SECV)) were calculated for standard PLS only (preliminary data sets) and for two standard pre-processing methods -- Baseline Correction and Multiplicative Scatter Correction (MSC) -- in analysis of the entire data set.

Where no models could be generated because no minimum in PRESS could be achieved (Model? =N), factor 1 R^2 and SECV were calculated but reported in italicized parentheses for comparison. Where there is a minimum PRESS for a factor greater than 1, but is not statistically significant from factor 1 based on an F-test (Model? =N†), the minimum factor results are reported and additional outlier detection was performed. Where there is a minimum PRESS for a factor greater than 1 and it is statistically significant from factor 1 result (Model? =Y) that factor was reported and additional outlier detection was performed.

6.4.2. *Cluster Analysis*

Cluster analysis is one of several unsupervised pattern recognition techniques. It can be used to study the homogeneity of a large set of complex data. It has been used in several research fields as a pre-processing step to other multivariate statistical methods, based on the assumption of homogeneity. [92]

In order to investigate independently and mathematically whether the entire data set of optical spectra were divisible by pathology, time, or a parameter other than the desired reference tissue pH or lactate values, the spectra were evaluated with general hierarchical clustering techniques available in Matlab (Version 6.1.0.450 Release 12.1, Mathworks,

MA). The Euclidean and Minkowski distance metrics were each tested to find similarities (or dissimilarity) between every combination of pairs of spectra (for *n* spectra there are *n-1* pairs or objects) in the data set. The objects were then clustered by the shortest, average, or centroid proximity metrics. The best clustering solution was evaluated by using the cophenetic correlation coefficient routine available in the software. The closer the cophenetic correlation coefficient is to 1, the better the clustering solution. It indicates that the clustering of groups of objects is strongly correlated with the distances between the objects. Only the clustering algorithms that gave the highest cophenetic correlation coefficient for the data set was further analyzed. Natural groupings in the hierarchical tree were assessed by both comparing the length of each link in a cluster tree with the lengths of neighboring links below it in the tree and by cutting off the hierarchical tree at arbitrary points to create a desired number of clusters. The groupings were further investigated for relationships to the plaque experiments. Cross-validated PLS models were developed for each of the groupings. The efficacy of the cluster analysis subsequent groupings was determined by the resulting PLS models R^2 and SECV.

6.4.3.   Orthogonal Signal Correction

An important pre-processing method that is increasingly used is orthogonal signal correction (OSC) [93, 94]. While other pre-processing methods such as baseline correction, derivatives, multiplicative signal correction, and other mathematical filters may inadvertently remove information from the spectra regarding the measured reference variable, OSC attempts to define a spectral variance matrix that is approximately orthogonal (set of parameters or variables that can be treated independently) to the reference values. OSC was used only for the entire data set for the lactate determination (82 points) because 1) a defined wavelength region could be described that needed correction and 2) no additional convolution regarding data from two different spectrometers (as in the tissue pH calibration) needed to be described.

The algorithm described by Wold [95] was coded into Matlab. The original spectral matrix was corrected by subtracting the orthogonal matrix generated, and PLS models were run by using *n-1* OSC pre-processed spectra for calibration, applying the *n-1* OSC correction factor to the *nth* unprocessed spectrum, and then predicting the reference value using the *n-1* PLS model from the *nth* processed spectrum. One component and two-component orthogonal matrices subtraction were tested. If models could be created, standard PLS outlier detection was followed. The efficacy of the orthogonal signal correction was determined by the resulting PLS models R^2 and SECV.

7. RESULTS

In this section, the results of all the experiments are described. First, the validation of the living status of the freshly excised tissue is presented (Section 7.1). Next, all the spectral and reference data from the large scale *in-vitro* study on ~30 plaques are shown (Sections 7.2 and 7.3). Out of the 126 data points that were collected, only 82 points could be used for the lactate determination, because of adverse experimental conditions as described in Section 7.3 (see tabulation of Reference Measurements Data in Table 7.3.1). Due to circumstances beyond control, full spectral data from 400-2400 nm could only be collected for 57 out of the 126 points. Experimental conditions also ruled out several points for the tissue pH determination; 48 out of the 57 full-spectra data were used in the end. Lastly, the calibration model development results are presented in Section 7.4. Preliminary PLS calibration model results are shown for the first ~20 points for each optical calibration. Additional points that were added to the initial calibration model data were modeled in the aggregate and compared to the preliminary results.

7.1. Laboratory Setup and Validation

The average and standard deviation of each parameter in the nine validation plaques (2 controls, 7 media test plaques) is shown in Table 7.1.1. The tissue pH and pCO_2 for the test plaques are within the physiological range of respiring tissues; the control plaques tissue pH and pCO_2 are lower and may not represent viable tissue. Tissue temperatures of the control plaques are also lower. Tissue pO_2 is higher in the test plaques, indicating oxygen is being delivered and utilized (evidenced by slightly rising pCO_2 values). However, the thickness of the plaque affected the readings. Figure 7.1.2 shows the changes in measured parameters (top: pH and pCO_2, center: pH and temperature, bottom: pH and pO_2) over a three and half hour time period for a representative plaque placed in the media. The sensor itself takes ~ 30 minutes to equilibrate in the tissue (time of sensor placement shown in top plot). The top plot shows the media pH and pCO_2 values as discrete points measured by the blood-gas analyzer (m pH and m pCO_2). Media pH was always higher than tissue pH (~7.45 versus ~7.15 in data shown). Media pCO_2 values were also consistently lower than tissue pCO_2 values. Physiological changes in tissue pCO_2 (slight rise over time) were observed in all plaques. The media pO_2 values were consistently around 400 ± 40 mmHg, while the plaque tissue pO_2 depended more on the thickness of the tissue from experiment to experiment. After the sensor stabilization period, the tissue pH and temperature measurements (center plot) remain stable for the entire time the plaques are in the media. The bottom plot shows the media pH and pO_2 values as discrete points (m pH and m pO_2). Figure 7.1.3 shows box-whisker plots for the pH and temperature changes over time for the plaques in media versus the controls (i.e. Δ, or delta, pH or Δ temperature per hour, indicative of the stability over time for that particular parameter). The change in pH and temperature per hour is significantly greater in the plaques placed only in the warmed, humidified air (mean, controls 0.25 pH units/hr and 1.5°C/hr, *n*=2) than the plaques place in media (mean, test plaques, 0.03 pH units/hr and 0.4°C/hr, *n*=7).

Table 7.1.1: Average and standard deviation of all continuous measurements in validation of the laboratory setup.

Parameters	Control (no media)	Media
pH	6.75±0.15 6.77±0.16	6.93±0.03 7.16±0.01 7.05±0.02 7.04±0.01 7.04±0.02 7.01±0.05 (thick plaque) 7.29±0.01
Temperature (°C)	32.2 ±0.9 32.7±0.6	33.6±0.5 35.4±0.3 33.7±0.5 35.8±0.4 35.2±0.3 36.8±0.4 (thick plaque) 36.9±0.3
PO2 (mmHg)	108±15 39±15	313±17 438±18 228±40 129±62 248±156 6±13 (thick plaque) 266±160
PCO2 (mmHg)	8±4 12±6	50±2 47±6 77±4 81±11 83±4 70±10 (thick plaque) 66±4
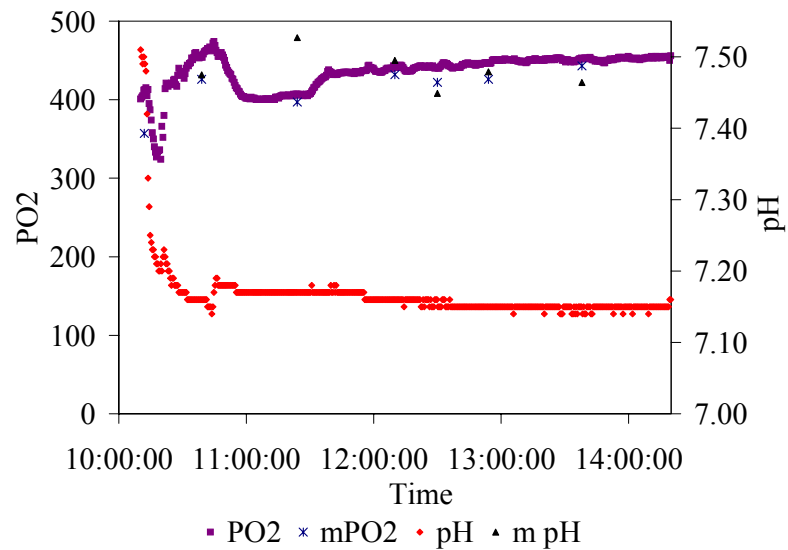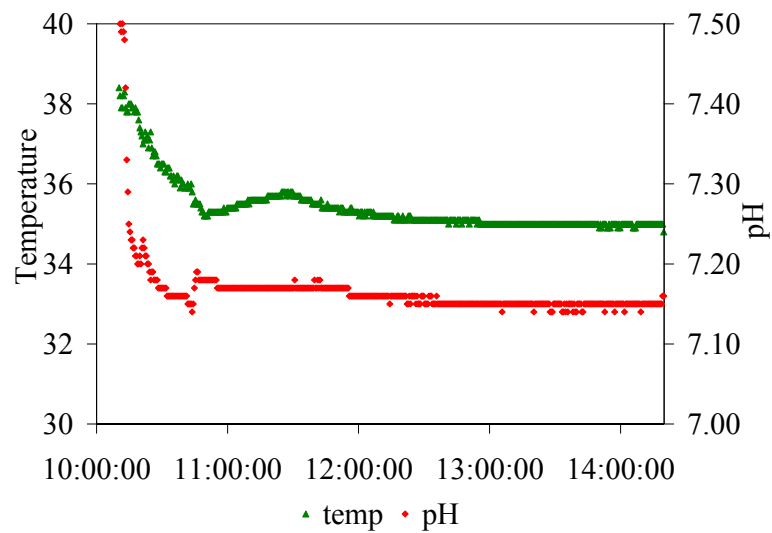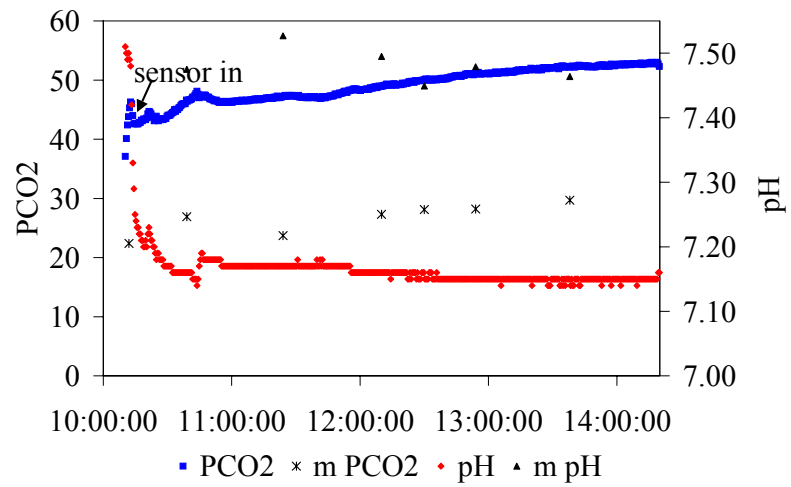
Figure 7.1.2: Changes in parameters over ~3.5 hrs of a representative plaque. (m = media values). Red line = tissue pH, right axis; Blue line = tissue PCO₂; Green line = tissue temperature; Purple line =tissue PO₂.
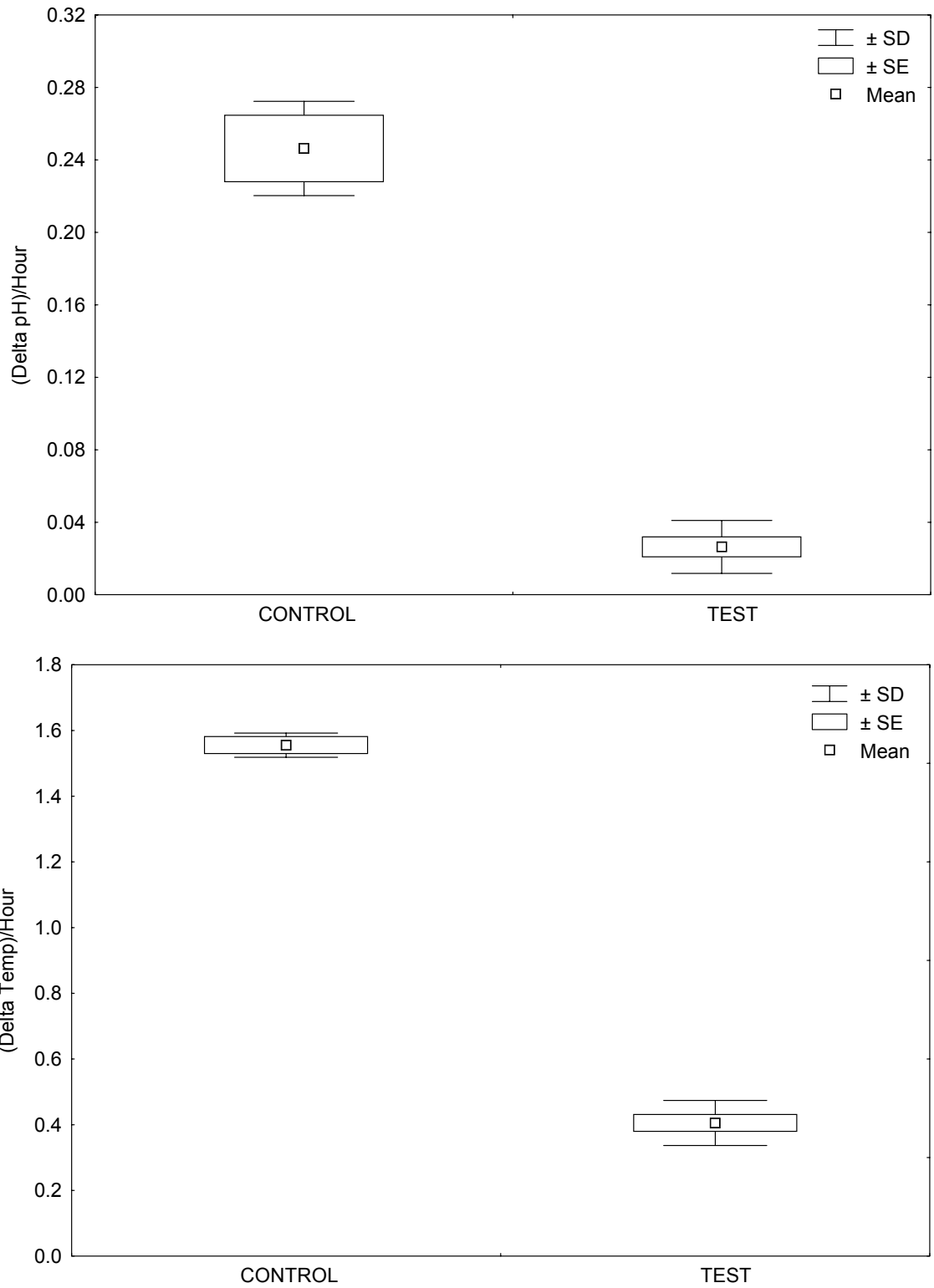
Figure 7.1.3: Box-whisker plots for ∆pH / hour and ∆temperature / hour (respectively) for the control (*n=2*) and test plaques placed in media bath (*n=7*). The change in pH and temperature over time is greater in the controls than the test plaques.

7.2.   Spectra Collection

7.2.1.   Lactate Spectra

Spectra collected for the optical determination of lactate are shown in Figure 7.2.0. The mean spectrum is shown in Figure 7.2.1 for clarity. Peak assignments are listed in Table 7.2.1.
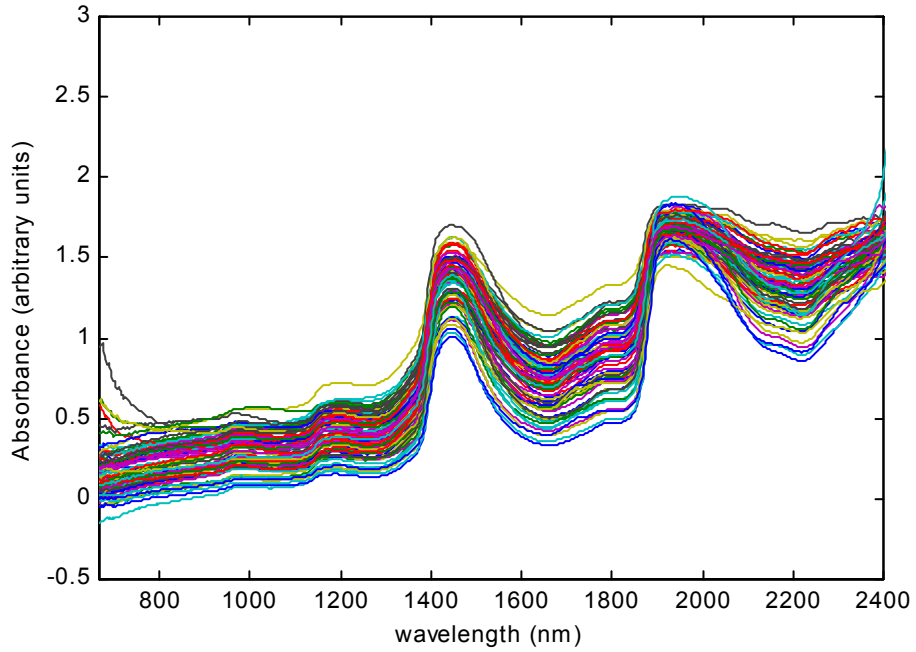
Figure 7.2.1: Optical spectra for lactate determination. 667-2400 nm. 82 pts.
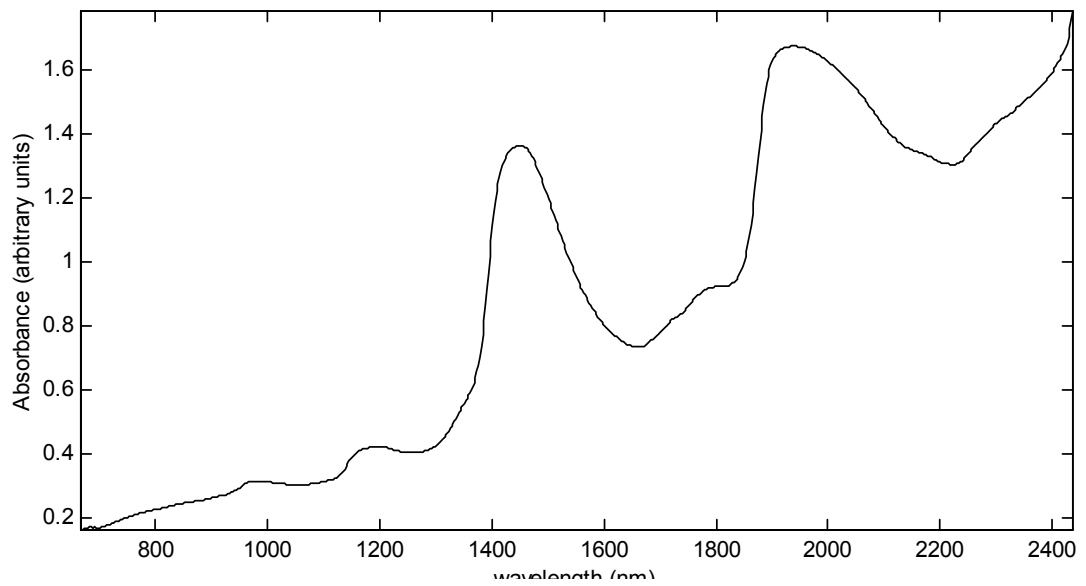
Figure 7.2.1: Mean of spectra shown in Figure 7.2.0. 667-2400 nm. Water bands at ~1450 and ~1940 nm dominate the spectral features. Peak assignments are given in Table 7.2.1.

Table 7.2.1: Peak assignments for mean spectrum shown in Figure 7.2.1. 667-2400 nm.

Peak Wavelength (nm)	Chemical Species	References
982	Water	[96], [97]
1196	Water	[98], [97]
1449	Water	[99]
1730 (weak, broad)	Cholesterol, lipids, alkyl CH groups, proteins	[99], [34]
1780 (weak, broad)	Cholesterol, lipids, alkyl CH groups, proteins	[99], [34], [35]
1943	Water, (lipids)	[97] ([34])
2168 (weak)	Non-specific proteins	[99]
2250, 2295	*Lactic acid*	*[72]*
2318 (weak, broad, shoulder)	C-H combinations from lipids	[35], [34]

7.2.2.   Tissue pH spectra

Spectra collected for the optical determination of tissue pH are shown in Figure 7.2.2. The mean spectrum is shown in Figure 7.2.3. for clarity. Peak assignments are listed in Table 7.2.2.

Between 500-600 nm, the spectral features are varied. Not all the spectra exhibit hemoglobin bands, and in some spectra, the signal is fairly flat and featureless. There is an anomaly observed at 633 nm in all spectra. This was investigated and found to be unrelated to the tissue characteristics. The top most spectrum was taken from an area of plaque that contained a large amount of blood. Below ~515 nm of this spectrum, strong hemoglobin absorption occurs (~10x or an order of magnitude higher than the amount at
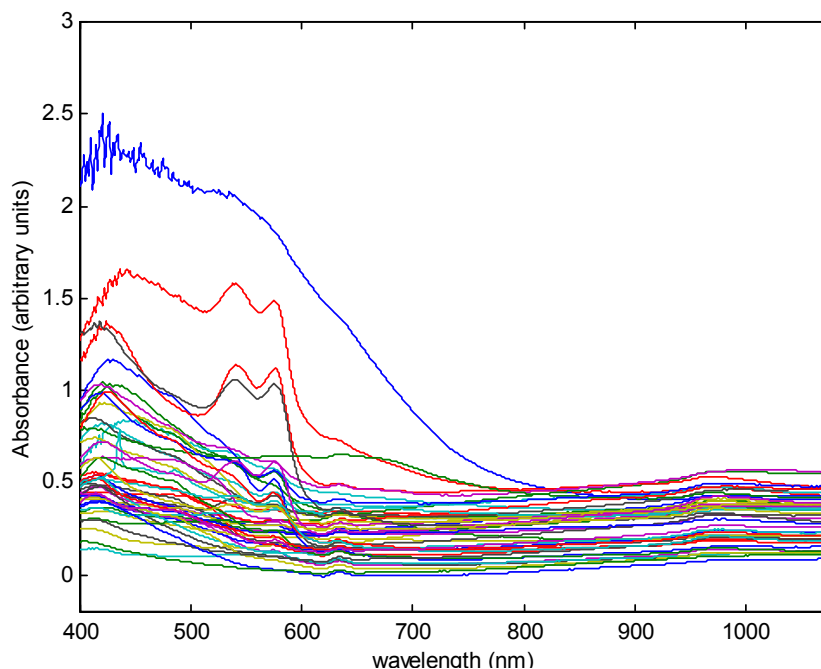
Figure 7.2.2: Optical spectra for tissue pH determination. 400-1075 nm. 48 points. Hemoglobin bands dominate between 500 - 600 nm. However, a few spectra are featureless in this region. Peak assignments are listed in Table 7.2.2.

575 nm). Very little light, if any, is reflected back to the probe interface. The detector noise is apparent at extremely high hemoglobin or blood content.
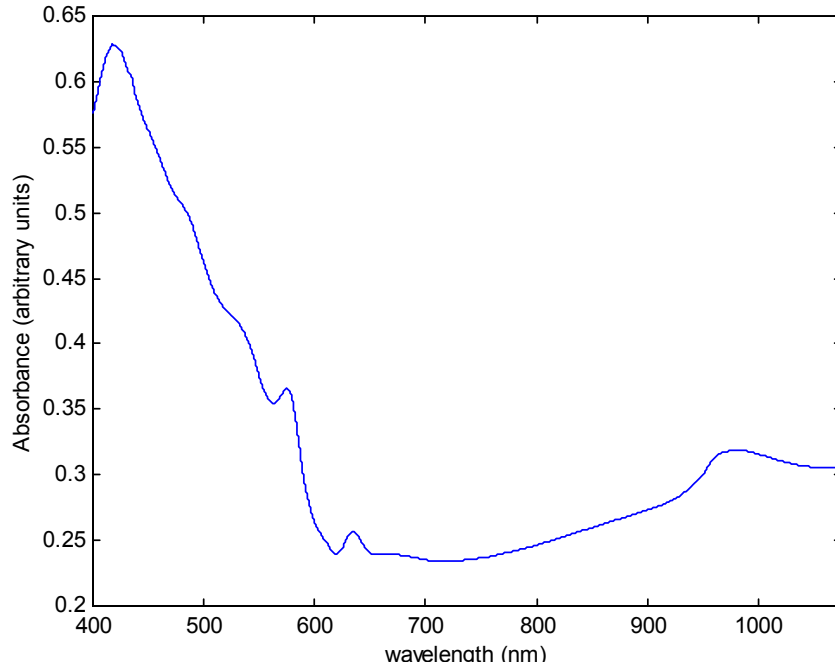
Figure 7.2.3: Mean of spectra shown in Figure 7.2.2. Peak assignments are listed in Table 7.2.2.

Table 7.2.2: Peak assignments for visible spectra shown in Figure 7.2.2.

Peak Wavelength (nm)	Chemical Species	References
417	OxyHb	[100]
540	OxyHb,OxyMb	[100, 101]
574	OxyHb	[100]
633	Optical Anomaly	Removed before models built
970	Water	[96]

Twelve spectra for lactate and six spectra for pH out of 126 points collected (see Reference Measurements Section 7.3) were not used either because they were spectrally flat between 2000-2400 nm, or showed evidence of reflectance off of the ceramic plate underneath the plaque, i.e. the plaque was too thin or optically transparent for the entire wavelength region from 667-2400 nm. Other factors unrelated to spectra collection reduced the number of points available for calibration. Eighty-two and forty-eight spectra were used for the optical determination of tissue lactate and tissue pH respectively. Figures 7.2.4 and 7.2.5 show the spectra broken down by the observed gross pathology.
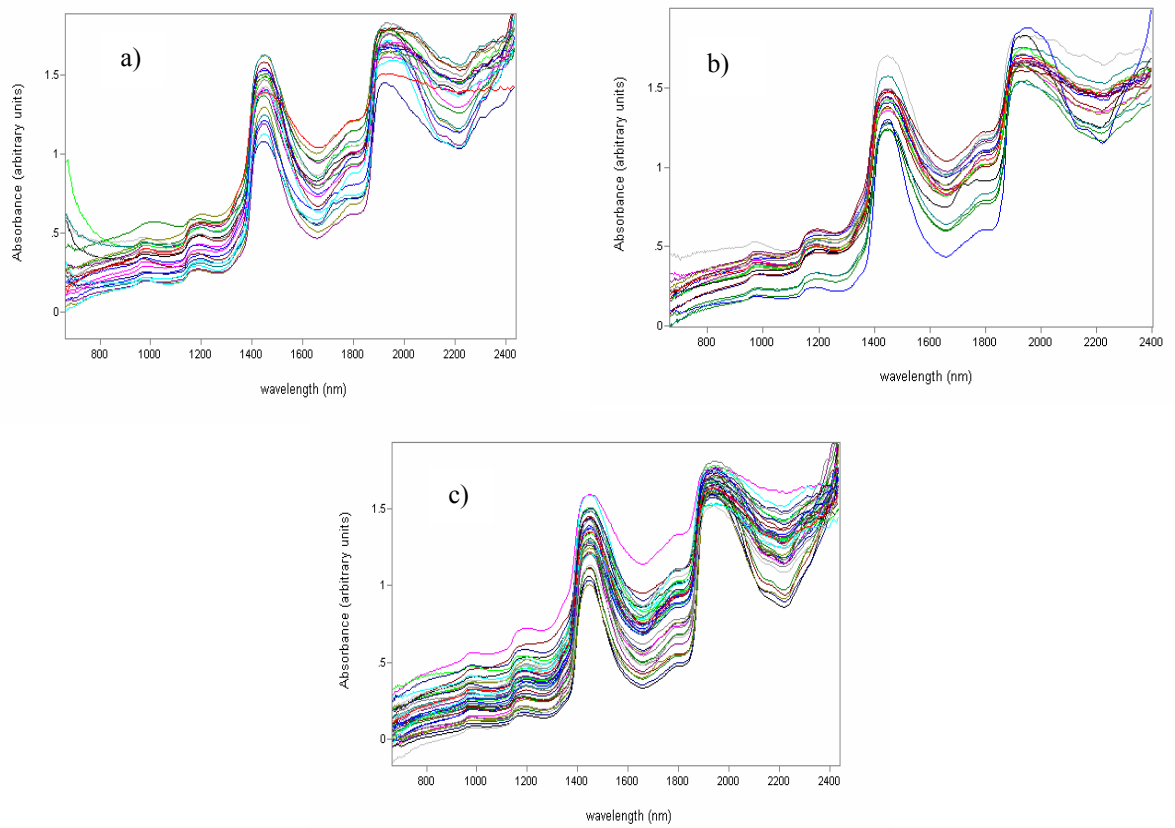
Figure 7.2.4: 82 spectra for lactate determination broken down by gross pathology, a) 22 thrombotic, b) 19 calcified, and: c) 41 yellow/fatty.
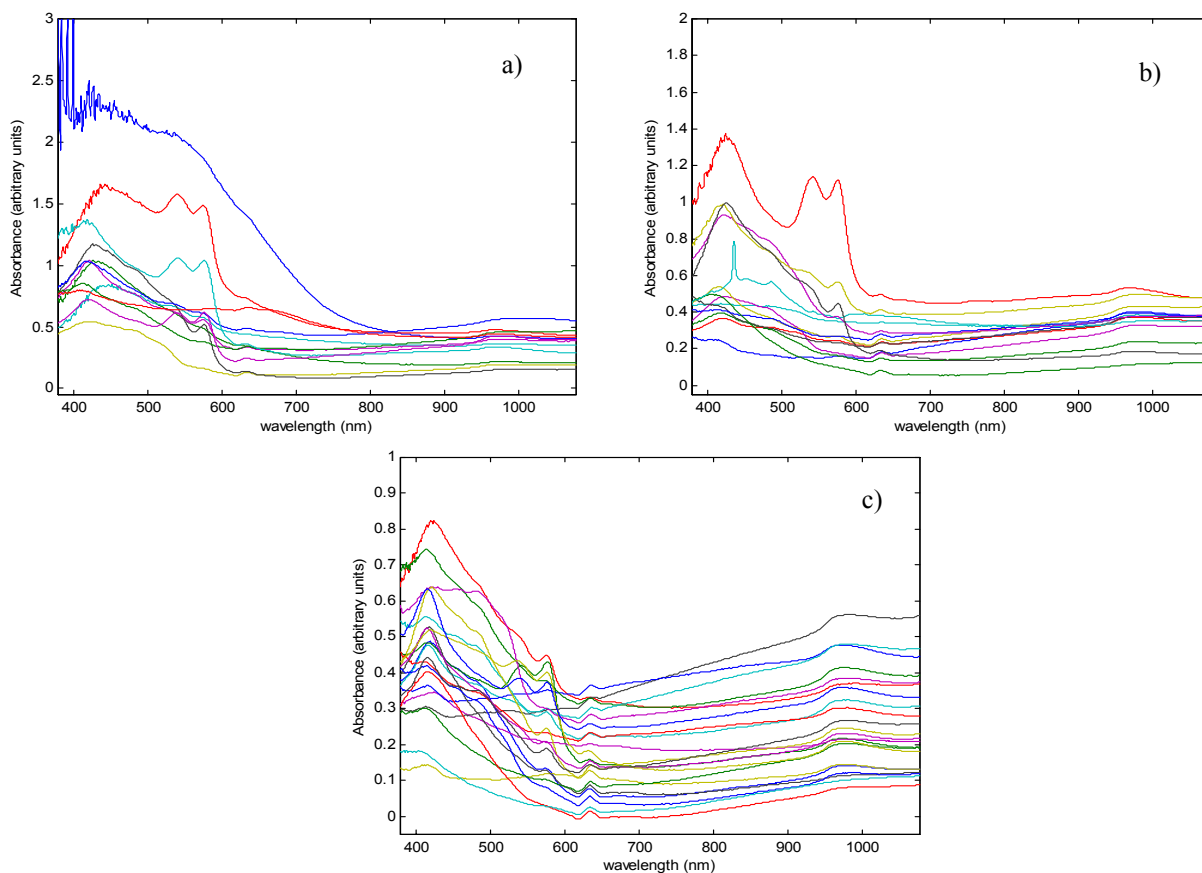
Figure 7.2.5: 48 spectra for pH determination broken down by gross pathology, a) 11 thrombotic, b) 14 calcified, and c) 23 yellow/fatty

Spectrometer variation was analyzed by tabulating the intensities of the reference spectrum collected each day at 970 nm and 2250 nm. The percent change in the intensity of each day, and the average and standard deviation for several representative experiment days are shown in Table 7.2.3. After the initial preliminary sets of optical data were collected and optical calibrations generated to test data quality, the percent change of the intensity of the reference within each day was less than 3%. The intensities at 970 nm and ~2250 nm stayed stable over time.

Table 7.2.3: Spectrometer stability over time. Representative days over an 8 month period of data collection.

Date	970 nm			2248.7 nm		
	% change each day	Average	STD	% change each day	Average	STD
1/10/2002	2.7%	0.13321	0.00151	2.5%	0.21283	0.00204
2/13/2002	2.0%	0.13962	0.00119	1.8%	0.21699	0.00197
4/9/2002	0.5%	0.13416	0.00034	2.1%	0.21279	0.00204
5/8/2002	2.8%	0.13562	0.00128	0.9%	0.21065	0.00077
6/27/2002	0.5%	0.13186	0.00036	1.2%	0.21180	0.00129
7/19/2002	1.3%	0.12763	0.00076	1.9%	0.21319	0.00180

7.3.   Reference Measurements

Table 7.3.1 shows all the reference measurement data, with the points not usable for optical calibration identified. The average experiment time was 2 hours and 54 minutes. The average and standard deviation of all the pH readings (n=86), the lactate readings (n=82), and tissue temperature (n=86) was 7.24 and 0.24 pH units, 3.2 and 2.7 micromoles lactate/gram tissue, and 34.3 and 1.4 °C, respectively. Figure 7.3.1 show histograms of the distribution of the lactate and tissue pH values respectively used for calibration for all points and broken down by observed gross pathology. The actual 82 tissue lactate points used for optical calibration broken down by gross pathology: 19 calcified, 22 thrombotic, and 41 yellow/fatty. The actual 48 tissue pH points (7.33 ± 0.21 *mean ± standard deviation*) used for optical calibration broken down by gross pathology: 14 calcified, 11 thrombotic, and 23 yellow/fatty. It was shown in an earlier section (Laboratory Setup and Validation Results, Section 7.1) that the time of the experiment, if kept under a total of 4 hours (from the OR to last point collection), that the plaque remains viable and values do not change significantly with the continuously oxygenated media preparation. A temperature change of no more than 0.5°C per hour is acceptable, down to the lowest temperature in the validation set of 32°C. Points with tissue temperature greater than or equal to 32°C were used.

Further analysis of the measured variables was made to elucidate spurious correlations before developing calibration models. Table 7.3.2 shows the correlation coefficients calculated between the measured variables used for optical calibration. No correlation was observed. Figure 7.3.2 shows the same reference measurements plotted against each other and temperature (A) Tissue lactate vs. temperature B) Tissue pH vs. temperature, C) Tissue pH vs. lactate).
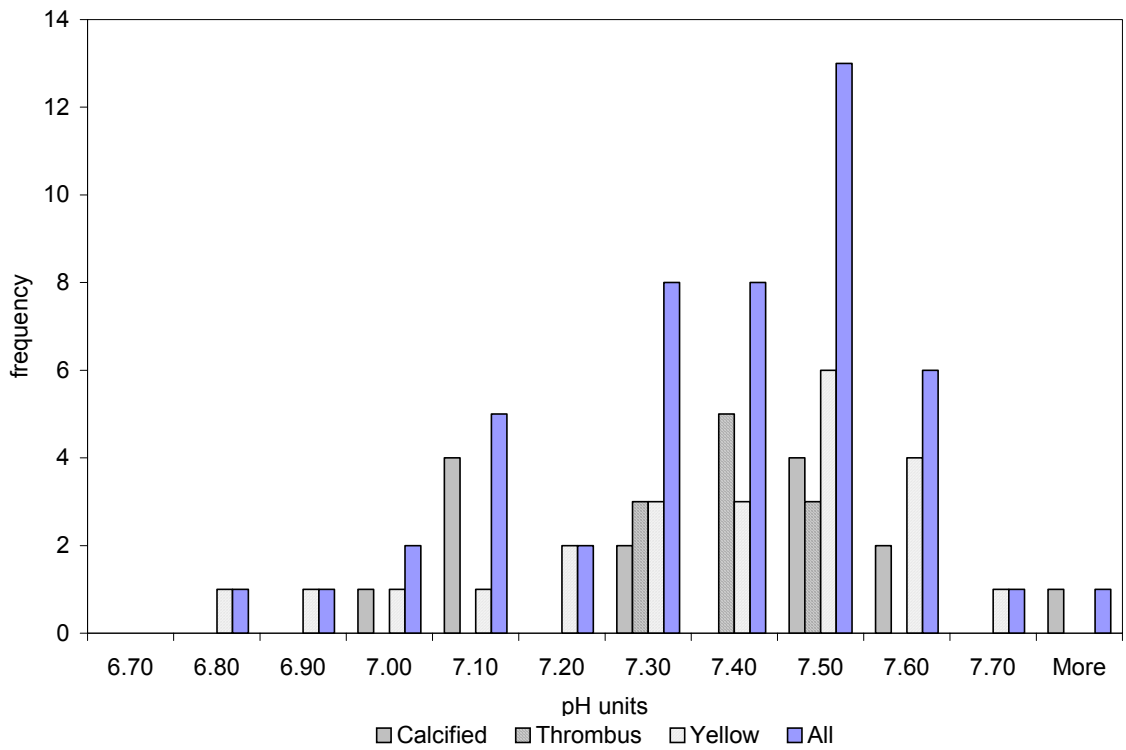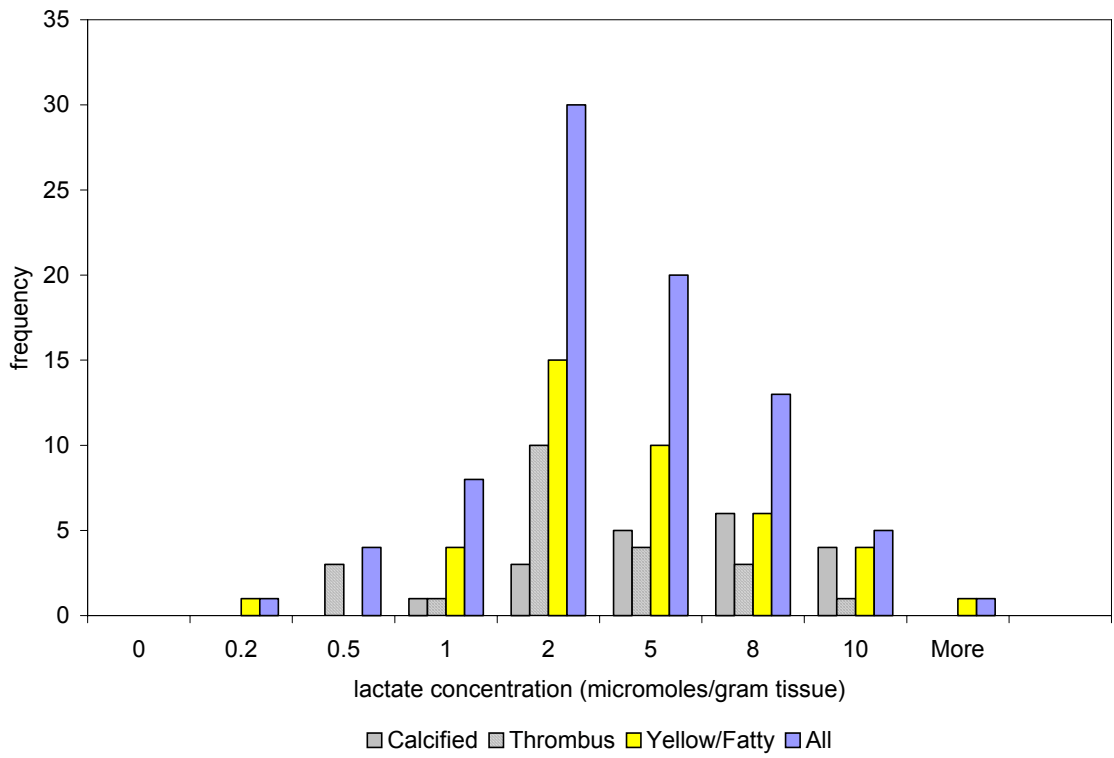
Figure 7.3.1: Histogram for reference lactate (top, total n=82) and tissue pH (bottom, total n=48) measurements broken down by gross pathology.

Table 7.3.1: Reference Measurements Data. Points not usable for optical calibration were identified.

Table Legend: Gross Pathology: c- calcified, y – yellow/fatty, t – thrombus
Used for Model: Y – yes 667-2400 nm for lactate, y – for pH 667-2400 nm only,
Y- both visible and NIR for pH, * - low temperature, # - high off of lactate assay
calibration curve, m – lost sample, or no electrodes for pH, s – spectral
reflection of plate or lactate region flat and featureless

Experiment ID / Total Duration	Point#	pH	Temp	Gross Pathology	LA	Used for Lactate Model?	Used for pH Model?
K1 3 hrs 26 min	1	7.23	33.0	c	5.9	Y	y
	2	7.75	32.9	c	0.9	Y	y
	3	7.87	33.0	c	1.2	Y	y
	4	7.49	32.2	y	1.1	Y	y
	5	7.47	32.6	y	0.6	Y	y
	6	7.28	32.9	t	0.4	Y	y
	7	7.38	33.0	c	0.3	Y	y
	8	7.88	33.0	t	2.3	Y	y
K2 2 hrs 23 min	9	7.37	32.2	y	9.2	Y	y
	10	7.24	31.5	y	10.8	*	*
	11	7.34	31.4	y	4.5	*	*
	12	7.44	31.1	t	1.1	*	*
	13	7.44	31.1	t	2.5	*	*
	14	7.13	31.1	y	2.7	*	*
K3 2 hrs 10 min	15	7.16	30.7	y	1.9	*	*
	16	7.40	31.4	y	2	*	*
	17	7.27	30.7	y	3.7	*	*
	18	7.35	31.2	y	5.7	*	*
K4 2 hrs 13 min	19	7.54	33.3	y	10	Y	y
	20	7.30	32.6	y	10.1	Y	y
	21	7.18	31.8	c	high	#	*
	22	7.12	31.2	y	6.5	*	*
	23	7.27	30.9	t	1.9	*	*
K5 1 hr 53 min	24	7.15	31.5	t	3.9	*	*
	25	7.01	30.9	y	2.4	*	*
	26	7.25	30.6	c	--	m	*
K6 1 hr 25 min	27	7.46	31.2	t	3.9	*	*
	28	7.40	30.2	c	4.8	*	*
	29	7.46	30.0	c	1.4	*	*
	30	7.34	29.2	c	high	#	*
K7 2 hrs 5 min	31	7.36	30.5	y	2.2	*	*
	32	7.37	30.0	y	2.2	*	*
	33	7.44	29.1	y	1.6	*	*
	34	7.37	28.6	y	2.6	*	*
	35	7.21	28.6	c	4.4	*	*
	36	7.24	28.5	c	0.5	*	*
K8 1 hr 46 min	37	6.92	33.4	y	1.5	Y	y
	38	7.16	32.7	t	2.1	Y	y
	39	7.26	32.2	y	1.4	Y	y
	40	7.09	32.0	y	3.4	Y	y

Experiment ID / Total Duration	Point#	pH	Temp	Gross	LA	Used for Lactate Model?	Used for pH Model?
K9 2 hrs 18 min	41	6.89	36.6	y	1.6	Y	y
	42	6.80	36.4	y	4.6	Y	y
	43	6.65	36.0	y	1.9	Y	y
	44	6.64	35.7	y	0.9	Y	y
	45	7.10	35.4	y	1.7	Y	y
K10 1 hr 56 min	46	7.44	34.2	y	2.2	s	s
	47	7.34	33.4	y	2	Y	y
	48	7.49	32.9	c	1	s	s
K11 2 hrs 29 min	49	7.37	36.7	y	1.4	s	s
	50	7.18	35.7	y	1.1	Y	y
	51	7.09	35.5	c	1.9	Y	y
	52	7.08	35.5	t	1.8	Y	y
	53	6.90	37.3	c	2.5	Y	y
K12 1 hr 36 min	54	7.51	37.8	y	high	#	y
	55	7.28	36.7	y	4.7	s	s
	56	7.27	37.5	t	1.2	Y	y
	57	7.40	37.1	c	high	#	y
K13 2 hrs 37 min	58	7.30	33.6	y	3.6	Y	y
	59	7.28	34.2	t	1.9	s	s
	60	7.22	32.9	y	1.9	Y	y
	61	7.10	32.3	c	1.3	s	s
	62	7.30	33.0	t	1.1	Y	y
	63	7.26	33.5	t	0.3	Y	y
K14 2 hrs 32 min	64	7.05	35.2	t	5.3	Y	y
	65	7.13	35.2	y	2.3	Y	y
	66	7.33	34.5	c	high	#	y
	67	7.37	33.6	t	1.2	Y	y
	68	7.14	34.2	c	high	#	y
	69	7.23	33.6	y	7.2	Y	y
K17 2 hrs 11 min	70	7.46	33.3	t	10	Y	**Y**
	71	7.45	33.6	t	6.3	Y	**Y**
	72	7.44	33.4	t	6.3	Y	**Y**
	73	7.27	32.0	t	0.9	Y	**Y**
K18 3 hrs 0 min	74	7.48	35.7	y	7.7	Y	**Y**
	75	7.50	34.3	c	4.9	Y	**Y**
	76	7.55	35.0	y	7.1	Y	**Y**
	77	7.41	33.4	c	2.5	Y	**Y**
K19 4 hrs 0 min	78	7.04	34.1	c	6.3	Y	**Y**
	79	7.08	33.3	c	7.4	Y	**Y**
	80	7.03	34.3	y	4.1	Y	**Y**
	81	6.74	34.2	y	4.0	Y	**Y**
	82	7.39	35.0	y	5.4	Y	**Y**

Experiment ID / Total Duration	Point#	pH	Temp	Gross	LA	Used for Lactate Model?	Used for pH Model?
K20 3 hrs 49 min	83	7.07	36.1	c	1.7	Y	**Y**
	84	6.99	34.6	c	1.5	Y	**Y**
	85	7.32	34.5	t	0.3	Y	**Y**
	86	7.33	34.5	t	3.6	Y	**Y**
	87	7.11	34.5	y	1.4	Y	**Y**
K21 2 hr 52 min	88	7.21	35.1	c	1.5	Y	**Y**
	89	7.30	33.6	c	2.5	Y	**Y**
	90	7.55	33.8	c	10.6	s	**Y**
K22 1 hr 50 min	91	7.38	35.1	t	3.7	s	**Y**
	92	6.97	34.3	y	2.8	Y	**Y**
	93	7.10	33.4	c	4.6	Y	**Y**
	94	7.22	32.7	y	5.4	Y	**Y**
K23 4 hrs 0 min	95	7.22	36.8	t	3.2	Y	**Y**
	96	7.15	35.4	y	2.7	Y	**Y**
	97	7.29	35.5	t	1.2	Y	**Y**
	98	7.40	35.4	y	1.1	Y	**Y**
	99	7.33	35.5	t	1.6	Y	**Y**
	100	7.45	33.9	y	0.1	Y	**Y**
K24 2 hrs 29 min	101	7.48	36.3	c	0.9	Y	**Y**
	102	7.51	34.1	y	0.7	Y	**Y**
	103	7.72	33.6	c	--	m	**Y**
K25 3 hrs 14 min	104	7.32	34.2	t	1.3	Y	**Y**
	105	7.46	33.2	c	4.9	s	**Y**
	106	7.47	32.7	y	--	m	**Y**
	107	7.51	32.5	c	0.6	Y	**Y**
	108	7.34	32.0	y	0.5	s	**Y**
K26 3 hrs 32 min	109	7.26	31.6	t	1.6	*	*
	110	--	32.4	t	1.3	Y	m
K27 3hrs 43 min	111	7.23	32.7	y	8.5	Y	**Y**
	112	--	32.9	c	8.0	Y	m
K28 4 hrs 0 min	113	--	35.2	y	5.9	Y	m
	114	--	34.9	c	3.2	Y	m
	115	--	35.7	y	1.5	Y	m
K29 3 hrs 58 min	116	--	36.5	y	4.6	Y	m
	117	--	35.5	y	1.6	Y	m
	118	--	36.2	t	1.2	Y	m
	119	7.49	35.8	y	1.5	Y	**Y**
	120	7.66	35.1	y	1.5	s	**Y**
	121	7.45	35.5	y	1.9	s	**Y**
K30 3 hrs 59 min	122	7.53	34.4	Y	3.2	Y	**Y**
	123	7.60	34.1	Y	1.4	Y	**Y**
	124	6.89	34.2	Y	9.0	Y	**Y**
	125	7.48	35.8	Y	1.1	Y	**Y**
	126	7.25	34.6	Y	0.9	Y	**Y**

Figure 7.3.2: Correlation plots of the reference measurements from ~24 plaques. A) Tissue lactate vs. temperature B) Tissue pH vs. temperature, C) Tissue pH vs. lactate. Correlations are negligible (Table 7.3.2).
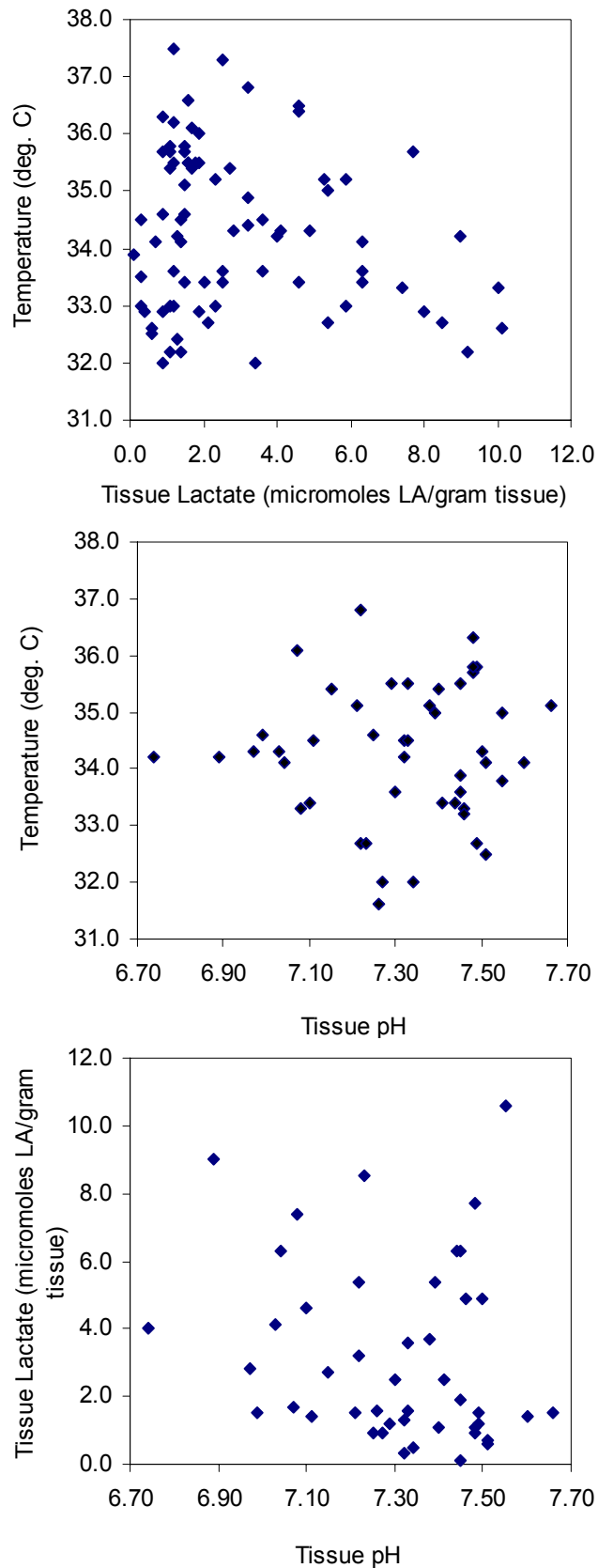
Table 7.3.2: Correlation coefficients between measured (reference) variables. No spurious correlations apparent.

Variables	Correlation Coefficient between data
Tissue Lactate – Tissue Temperature	0.03 (n=82)
Tissue pH – Tissue Temperature	0.00004 (n=48)
Tissue Lactate – Tissue pH	0.0008 (n=48) 0.001 (n=74 inclusive)

7.4.   Calibration Model Development

Preliminary data analysis was carried out on the first 21 points when they were available for both the tissue lactate (Sample #'s 1-9, 19, 20, 37-45, and 47 in Table 7.3.1.) and the first 20 points for tissue pH using full spectral range data, 400-2400 nm (Sample #'s #70-90 in Table 7.3.1). The preliminary analysis was done to provide an initial assessment of data quality. The entire data set (82 points for lactate and 48 points for tissue pH) as tabulated in Table 7.3.1 were analyzed at the end of experimentation and compared to the preliminary data results.

7.4.1.   Lactate Determination

Preliminary data analysis on 21 points from the first six plaques (K1, K2, K4, K8, K9, and K10) showed that a calibration model could be built using the 2030-2330 nm region only. Table 7.4.1 summarizes these results before and after outlier detection was performed. The data description, whether a model could be generated based on PRESS (see Section 6.4), the number of factors required, the correlation to the reference and estimated accuracy (R^2 and standard error of cross-validation or SECV), and the number of points removed are shown. The range of the reference tissue lactate (LA) concentration was 0.1 – 10.1 micromoles LA per gram of tissue.   The raw spectra are shown in Figure 7.4.1.a. The R^2 of the determination was 0.83 and the standard error of cross-validation (SECV) was 1.4 micromoles LA per gram of tissue (correlation plot, Figure 7.4.1.b.). The number of factors used was six, with the percent variance captured by each factor summarized in Table 7.4.2. Figure 7.4.2 show the corresponding loading vectors for a) factors 1-3, and b) factors 4-6. The fourth and sixth loading vectors contain positive correlation peaks at ~2250 and 2295 nm. This preliminary calibration model has acceptable accuracy using 17 points.

Table 7.4.1: Preliminary model results for lactate determination, 2030-2330 nm.

Data / Pre-Processing	Model?	Factors	R^2	SECV	% removed *n=21*
First 6 plaques, mean-centered	Y	6	0.45	2.4	0
First 6 plaques, mean-centered, after statistical outlier detection	Y	6	0.83	1.4	21%
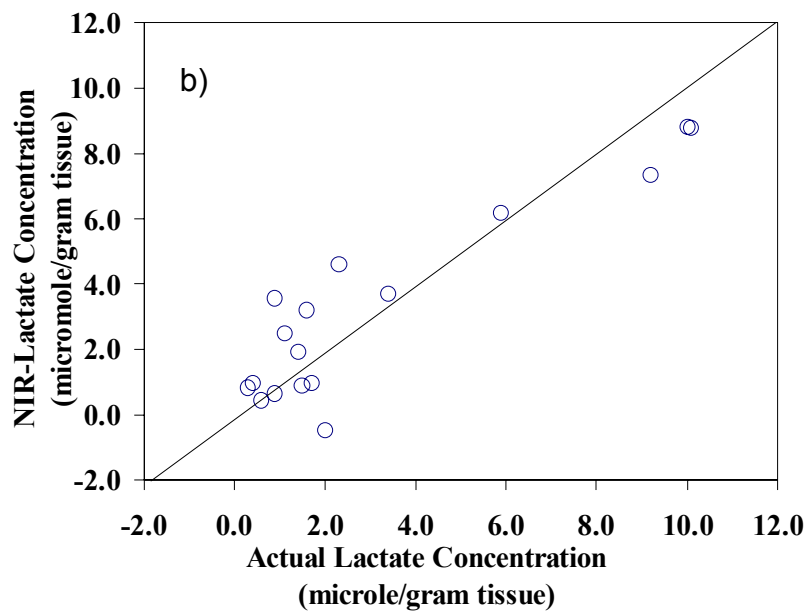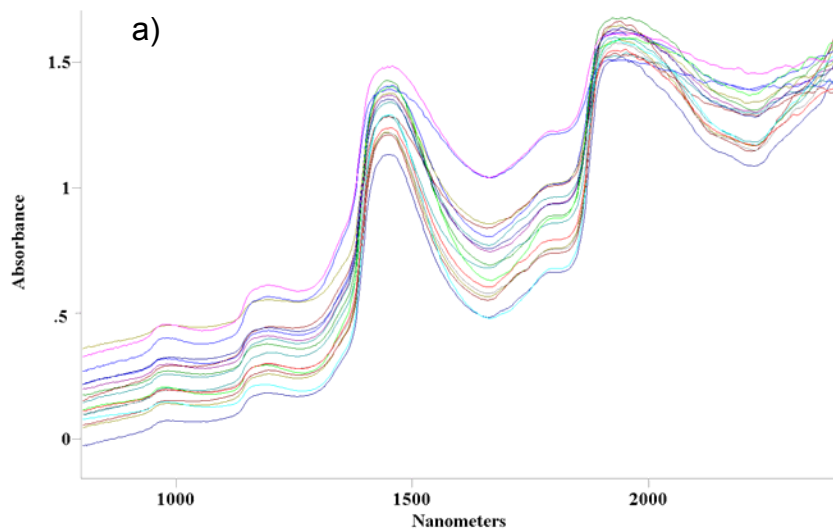
Figure 7.4.1: Preliminary model results: spectra and correlation plot. a) Seventeen spectra from the first six plaques collected. b) Actual versus predicted lactate values. Solid line is unity line. $R^2=0.75$, SECV=1.4 micromoles/gram tissue, 6-factor model.

Table 7.4.2: Preliminary data analysis: percent variance explained by six factor model.

Factor #	Spectral Variance		Reference Lactate Variance	
	% variance captured	Total %	% variance captured	Total %
1	99.7	99.7	43.1	43.1
2	0.036	99.997	19.8	62.9
3	0.001965	99.999	6.0	68.9
4	0.0004	100	12.8	81.8
5	0.00015	100	12.6	94.4
6	7.37×10^{-5}	100	4.4	98.8
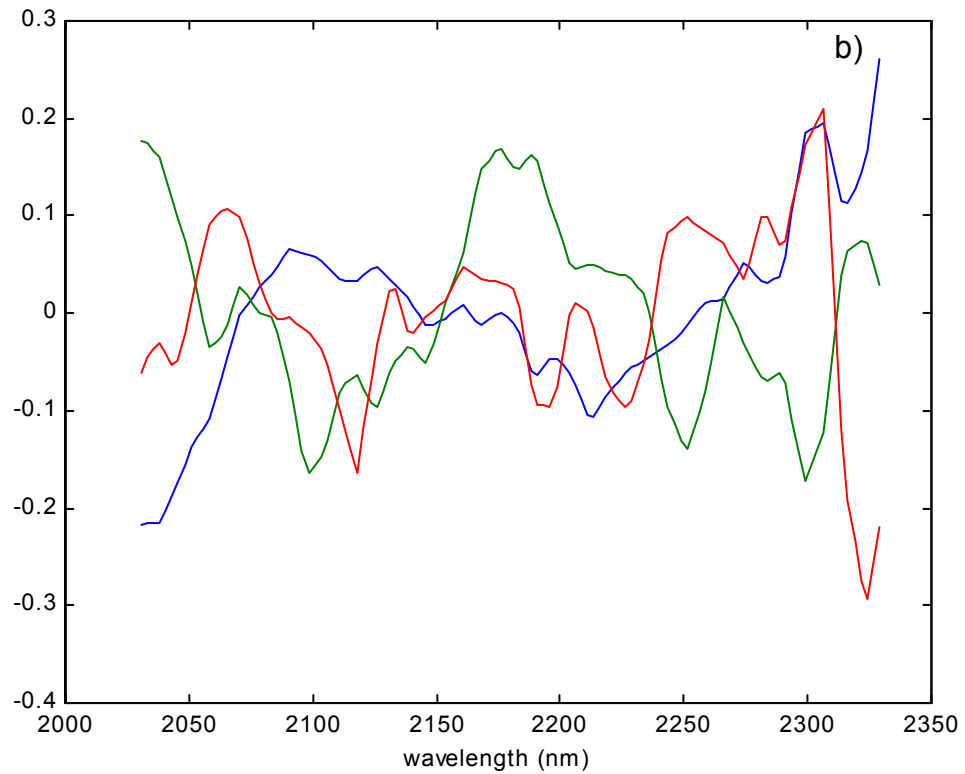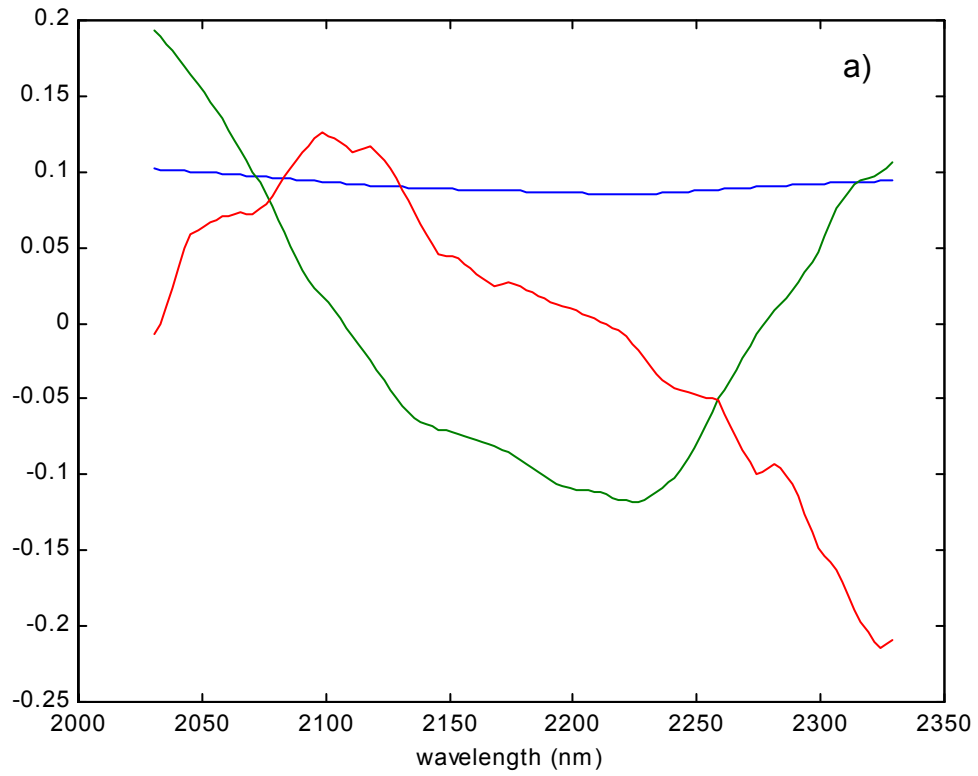
Figure 7.4.2: Preliminary model results: loadings. Six factors. Top: a) Loadings for factors 1-3, blue factor 1, green factor 2, red factor 3. Bottom b) Factors 4-6. Blue factor 4, green factor 5, red factor 6. Note peaks at ~2250 and 2295 nm.

Table 7.4.2 summarizes the calibration model results for the entire 82 data point set for lactate determination. Tests were separated into four groups based on wavelength region and pre-processing methods. For each test, the description, wavelength region, whether a model could be generated based on PRESS, number of factors required, the correlation to the reference and estimated accuracy (R^2 and standard error of cross-validation or SECV), and the number of points removed (from the entire set, *n=82*) are shown. Where no models could be generated because no minimum in PRESS could be achieved (Model? =N, see Methods, Section 6.4), results from the factor 1 model are reported in italicized parentheses only for comparison. Where there is a minimum PRESS for a factor greater than 1, but the results are not statistically different, based on an F-test (Model? =N†), the results from the minimum PRESS factor are reported as well as any results after additional outlier removal. Where there is a minimum PRESS for a factor greater than 1 and it is statistically different (Model? =Y), the results for the minimum PRESS factor are reported as well as the results after additional outlier removal.

Table 7.4.3: Summary of Calibration Model Development Results for 82 lactate points. Preliminary data calibration models shown as test 2d and e for comparison.

Test Group	Data / Pre-Processing	Region	Model?	Factors	R^2	SECV	% removed *n=82*
1a	All 82 points, mean-centered	1100-2400	N†	5	0.10	2.4	0
1b	All 82 points, mean-centered (outliers removed from 1a)	1100-2400	N†	2	0.004	1.8	18%
1c	Baseline Correction	1100-2400	N				
1d	Multiplicative Signal Correction	1100-2400	N				
2a	All 82 points, mean-centered	2030-2330	N	(1)	(0.008)	(1.9)	0
2b	Baseline Correction	2030-2330	N				0
2c	Multiplicative Signal Correction	2030-2330	N				0
2d	First 6 plaques, mean-centered	2030-2330	Y	6	0.45	2.4	75%
2e	First 6 plaques, mean-centered (outliers removed from 2d)	2030-2330	Y	6	0.83	1.4	79%
3	Cluster Analysis	2030-2330					
3a	Group A – 45 points		Y	3	0.21	2.9	45%
3b	Group B – 31 points		N	(1)	(0.13)	(3.9)	62%
3c	Group C – 6 points		Y	2	0.12	2.3	93%
4a	OSC – one components removed	2030-2330	N	(1)	(0.03)	(2.8)	0
4b	OSC – two components removed	2030-2330	N	(1)	(0.02)	(6.3)	0

Group 1 showed using the full spectral range 1100-2400 nm, that no models could be adequately generated that included all the 82 data points (test 1a). Even after statistical outlier removal, no improvement in model could be made (test 1b). Baseline correction (test 1c), Multiplicative Signal Correction (test 1d), and second-derivative (test 1e) standard preprocessing methods did not help.

Group 2 showed using the 2030-2330 nm range, that no models could be adequately generated using all 82 data points (test 2a). Because there was no minimum PRESS in test 2a (Model? =N), meaningful outlier detection is not possible. Baseline correction (test 2b) and Multiplicative Signal Correction (test 2c) standard pre-processing methods did not help. Significant model degradation using the entire data set occurred compared to the preliminary model results using 21 points (results from Table 7.4.1 are shown in Table 7.4.2 as tests 2d and 2e for comparison to entire data set).

Group 3 showed using the 2030-2330 nm range and Cluster Analysis, variation in the spectral data affected the calibration. From the eighty-two spectra, three clusters were determined using Minkowski's distance metric with $p=3$ for *n-1* objects and the centroid proximity metric to find groupings. The clustering solution (or dendrogram) produced is shown in Figure 7.4.3 with the spectra in each cluster plotted on the left. Forty-five spectra were in Group A, thirty-one in Group B, and six in Group C. Spectra from the first six plaques (twenty one points) were all in cluster A. A 3-factor PLS model could be generated with the Group A cluster; however, the accuracy is degraded compared to tests 2d and 2e.

Group 4 showed using the 2030-2330 nm and Orthogonal Signal Correction, variation in the reference data affected the calibration. No models could be created with the entire eighty-two points after either one or two orthogonal components (spectral components whose variation can be treated mathematically independent from the reference data) were removed.
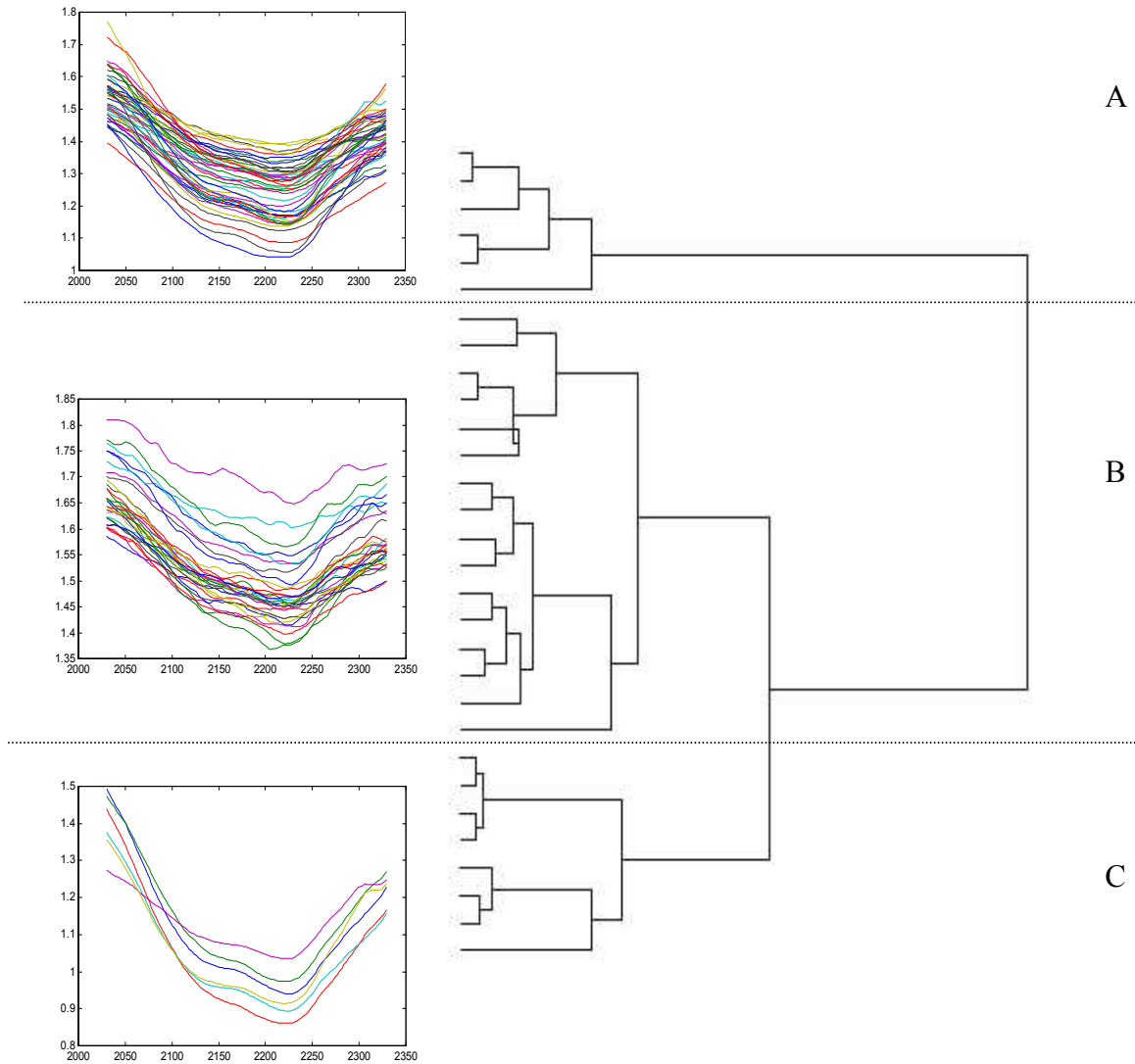
Figure 7.4.3: Clustering solution for 82 spectra for the optical determination of lactate. Cluster A – 45 spectra, B – 31 spectra, and C – 6 spectra. Cluster A contained the first 21 calibration spectra collected, i.e., chronologically those calibration points used from plaques K1, K2, K4, K8, K9 and K10 found in Table 7.3.1 were all in Cluster A.

7.4.2. Tissue pH Determination

Preliminary data analysis on 20 points from the first five plaques (K17 to K21 inclusive) showed that a calibration model could be built using a wavelength selection approach for tissue pH. The three regions that were identified were: Region 1: 400-615 nm, Region 2: 924-1889 nm, and Region 3: 2043-2341 nm. Table 7.4.4 summarizes these results before and after outlier detection was performed. The data description, whether a model could be generated based on PRESS (see Section 6.4), the number of factors required, the correlation to the reference and estimated accuracy (R^2 and standard error of cross-validation or SECV), and the number of points removed are shown. The range of the reference tissue pH was 6.99 to 7.55. Wavelength selection and additional statistical outlier removal produced a 3-factor model with R^2=0.75, SECV=0.09. Figure 7.4.4 shows the a) spectra, and b) correlation plot. The percent variance captured by each factor is summarized in Table 7.4.5. Figure 7.4.5 shows the three loading vectors in each wavelength region. Region 3 only marginally improved the model performance (NS). This preliminary calibration model has acceptable accuracy using 17 points.

Table 7.4.4: Preliminary model results for tissue pH determination. Three regions: R1=400-615 nm, R2=924-1889 nm, and R3=2043-2341 nm.

Data / Pre-Processing	Model?	Factors	R^2	SECV	% removed *n=20*
First 5 plaques, mean-centered	Y	3	0.27	0.18	0
First 5 plaques, mean-centered, after statistical outlier detection	Y	3	0.75	0.09	15%

Table 7.4.5: Percent variance captured by PLS tissue pH model shown in Figure 7.4.4.

Factor #	Spectral Variance		Reference Tissue pH Variance	
	% variance captured	Total %	% variance captured	Total %
1	48.9	48.9%	57.8	57.8
2	45.1	94%	7.3	65.1
3	4.0	98%	19.2	84.3
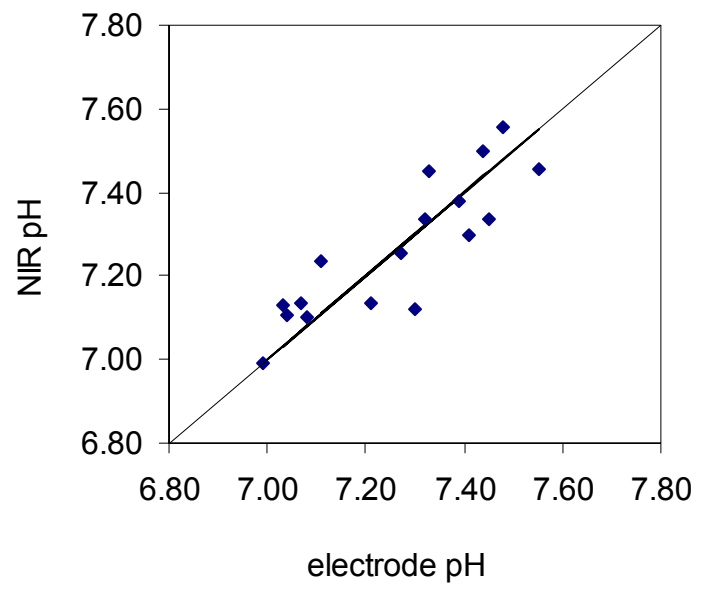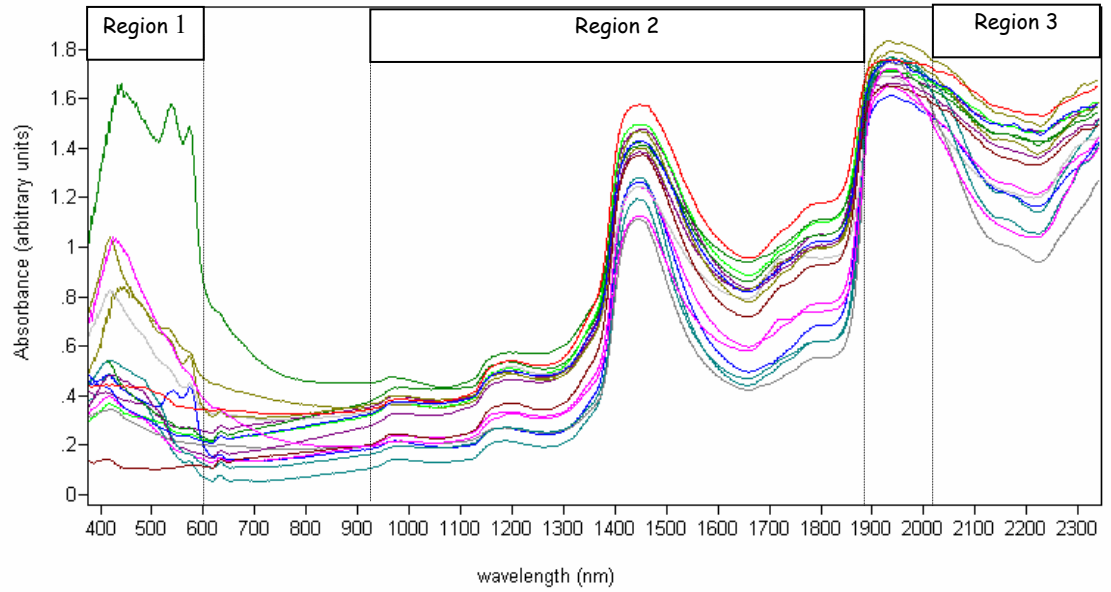
Figure 7.4.4: Preliminary model results from tissue pH calibration, spectra and correlation plot. Top: 17 spectra and the 3 spectral regions used for model. Bottom: Actual electrode pH versus NIR predicted pH. Solid line is unity line. R^2=0.75 and SECV=0.09 pH units.
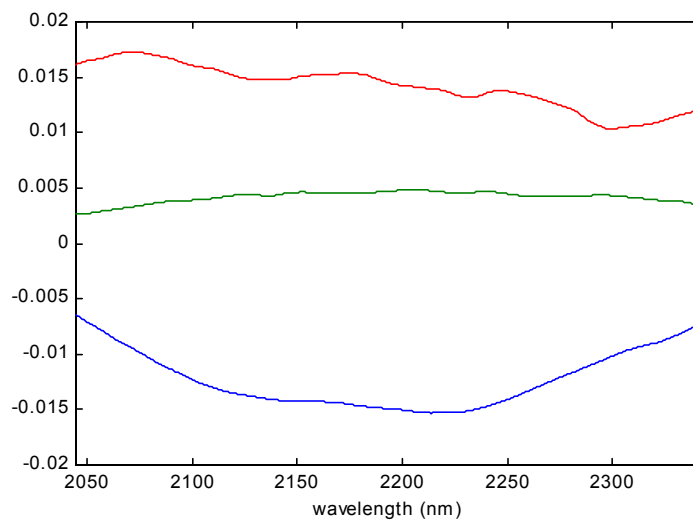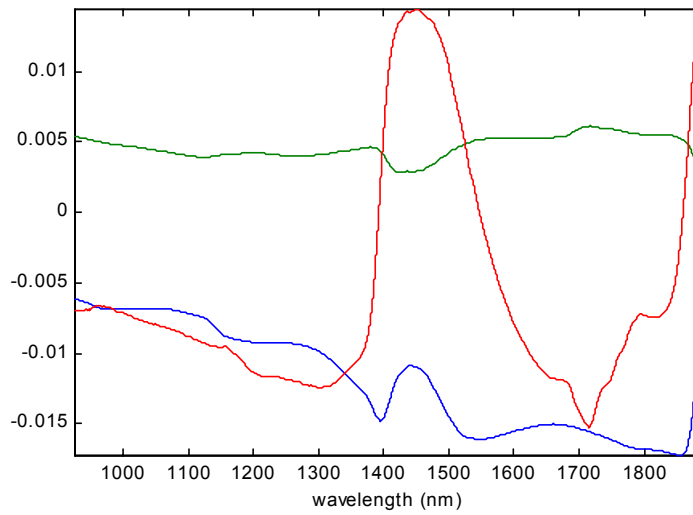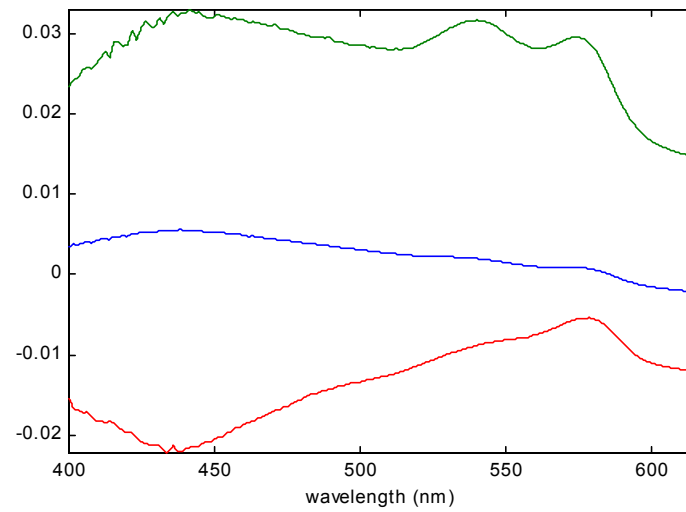
Figure 7.4.5: Preliminary model results: tissue pH loading vectors. Blue Factor 1, Green Factor 2, Red Factor 3. Hemoglobin bands at ~540 ,575 and 1650 nm show up in factor 2 loadings and factor 1 loadings for region 1 and 2 respectively. Region 3 only marginally improves model accuracy and prediction.

89

Table 7.4.6 summarizes the calibration model results for tissue pH determination for three different test groups. For each test, the description, wavelength region, whether model could be generated based on PRESS (see Methods, Section 6.4), number of factors required, the accuracy (R^2), precision (standard error of cross-validation or SECV), and the number of points removed (from the entire set, $n=48$) are shown. Where no models could be generated because no minimum in PRESS could be achieved (Model? =N), factor 1 results are reported in italicized parentheses for comparison. Where there is a minimum PRESS for a factor greater than 1, but is not statistically significant from factor 1 based on an F-test (Model? =N†), the minimum factor results are reported as well as the results after additional outlier removal. Where there is a minimum PRESS for a factor greater than 1 and it is statistically significant from factor 1 result (Model? =Y), that factor is reported as well as the results after additional outlier removal.

Group 1 showed using three regions identified by wavelength selection in the preliminary data analysis, that a weak model could be built (test 1a). The regions identified were 400-615 nm, 924-1889 nm, and 2043-2341 nm. However the accuracy is still not acceptable with 30 points after outlier removal (test 1c) when compared to the preliminary results (shown in Table 7.4.6 as test 1d and 1e).

Group 2 showed using the full wavelength region 400-2400 nm, that a weak model could be built (test 2a). However, no models could be created with greater than one factor, even after significant outlier removal, which is indicative of not being able to properly model tissue pH variance (tests 2b-2d). Multiplicative Signal Correction (test 2e) and Baseline Correction did not help (2f-2i).

Group 3 showed using the 400-1100 nm range and Cluster Analysis, variation in the spectral data affected the calibration. From the forty-eight spectra, two clusters were determined using the Euclidean distance metric for $n-1$ objects and the Shortest Distance proximity metric to find groupings. The dendrogram produced is shown in Figure 7.4.6 with the spectra in each cluster plotted on the left. Thirty-nine spectra were in Group A and nine in Group B. Even after outlier removal, neither cluster A or B provided improved results. The spectra in Group B were identified as arising for plaque measurements having the same gross pathology characteristics, i.e. all were from thrombotic regions of plaque.

Table 7.4.6: Summary of Calibration Model Development Results for tissue pH.

*R1: 400-615 nm, R2: 924-1889 nm, R3: 2043-2341 nm; [#] R1: 431-615; R2: 1354-2029 nm; † minimum PRESS achieved but results from factor 1 not statistically different from the results from the minimum PRESS factor based on F-test

| Test ID	Data / Pre-Processing	Region	Model?	Factors	R^2	SECV	% Removed *n=48*
1a	All points, mean-centered	3 Regions*	N†	1	0.14	0.19	0
1b	All points, mean-centered	3 Regions*	Y	1	0.23	0.16	17%
1c	All points, mean-centered	3 Regions*	Y	2	0.52	0.12	38%
1d	First 5 plaques, mean-centered	3 Regions*	Y	3	0.27	0.18	58%
1e	First 5 plaques, mean-centered (outliers removed from 1d)	3 Regions*	Y	3	0.75	0.09	65%
2a	All points, mean-centered	400-2400	N†	1	0.13	0.19	0
2b	All points, mean-centered	"	Y	1	0.20	0.15	11%
2c	All points, mean-centered	"	Y	1	0.34	0.13	25%
2d	All points, mean-centered	"	Y	1	0.44	0.11	42%
2e	Multiplicative Signal Correction	400-2400	N				
2f	Baseline Correction	2 Regions[#]	N†	1	0.13	0.19	0
2g	Baseline Correction	"	Y	1	0.22	0.15	19%
2h	Baseline Correction	"	Y	1	0.22	0.14	25%
2i	Baseline Correction	"	Y	1	0.36	0.13	33%
4	Cluster Analysis	400-1100					
5a	Group A – 39 points		N†	1	0.14	.21	19%
5b	Group A – 7 outliers removed		Y	1	0.29	0.16	33%
5c	Group A – more outliers removed		Y	1	0.42	0.14	58%
5d	Group B, 9 points		N	1	0.25	0.13	81%
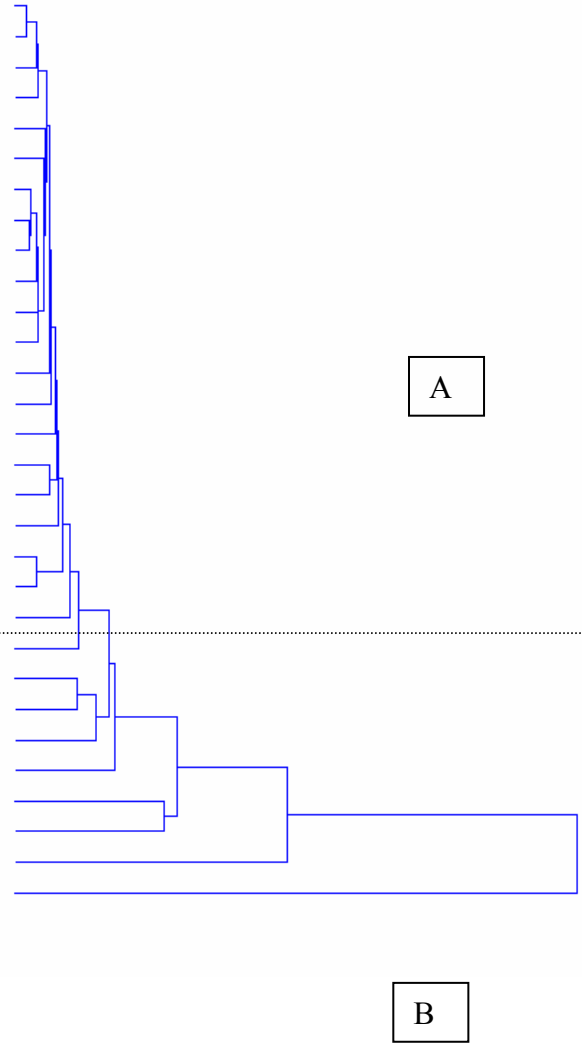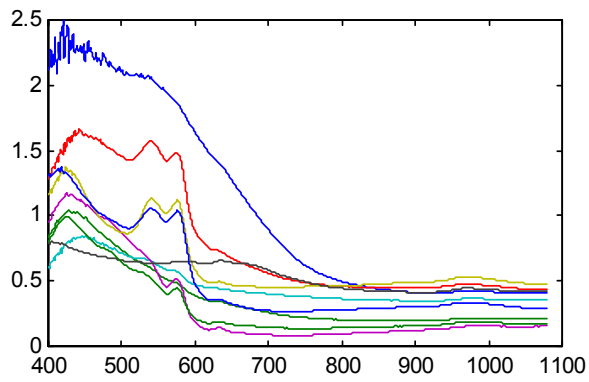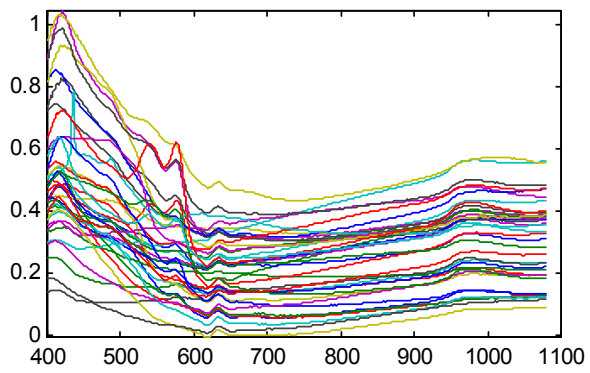
Figure 7.4.6: Clustering solution for optical determination of tissue pH. Two clusters: A contains 39 spectra, B contains 9 spectra. The underlying pathology in cluster B was identified as all thrombotic points.

8. DISCUSSION

In this section, a discussion of the results and interpretation is presented. First, the validation of the living status of the freshly excised tissue is discussed and similar studies reviewed to demonstrate importance of maintenance of metabolic status (Section 8.1). Next, the spectral data collection is discussed to highlight the pathological variability and challenges. The reference data collection is reviewed along with prior studies to demonstrate the challenges of matching reference tissue volume to optical volume and how it might affect the accuracy. Lastly, the calibration model development results are presented in Section 7.4. Preliminary PLS calibration model results showed that for the first ~17 points for each optical calibration, adequate models could be generated. However, when additional points were added, the initial calibration model results were degraded. The sources of variability that were investigated that might contribute to model degradation are reviewed.

8.1.   Laboratory Setup and Validation

The physiological monitoring of plaques in a controlled environment using oxygenated, physiological media demonstrated that over time, the plaque tissue could be maintained at relatively constant metabolism over 4 hours. The oxygenated media environment allowed the plaques to remain in near *in-vivo* status for the duration of the data collection. The liquid media pH, pCO_2, and pO_2 values, were stable and different from the plaque tissue measurements. The measured plaque metabolic parameters were not significantly dependent on the media values. The placement of the sensor may have played a role in the starting value of the tissue pH, pCO_2 or pO_2 reading. The thickest plaque (~3 mm) where the sensor was placed had a pO_2 value of 6 mmHg, although its pH, pO_2 and temperature were within the range of the other test plaques. This may indicate that thicker plaques will not have enough oxygen delivered deep into the tissue and may have less stability over 4 hours. The other six test plaques and two control plaques were closer in thickness (~1.5 mm).

Prior studies [36] of tissue pH in atherosclerotic plaques studied different buffering systems on preserving plaques *ex-vivo*. No significant difference was seen between the coefficients of variation of pH between treating the plaques after surgical removal with Dulbecco's Modified Eagles' Medium (DMEM), normal saline or phosphate buffer after 30 minutes. However, no continuous oxygenation to the plaque tissue was made and no separate determination of oxygenation or tissue viability was provided. The measurement of physiological parameters with the Diametrics sensor described here is the first study that demonstrates that plaques produce CO_2, and enough oxygen is delivered to the inner layers of the plaque to preserve the living cells.

pH heterogeneity in human carotid plaques has been reported using fluorescence ratio imaging microscopy (dual emission, pH sensitive BCECF dye) and pH sensitive SNARF fluorescence microscopy (single emission) and microelectrodes [36] with pH ranging from 6.8 to 8.3 pH units (microelectrodes, mean ± SD 7.55 ± 0.32). In the validation

study reported here, the lower average pH for the controls (6.75 ± 0.15 and 6.77±0.16) and the rate of change in tissue pH (0.25 pH units/hr in the controls) demonstrated that physiological tissue pH can not be maintained for more than ~30 minutes without adequate nutrient supplement. The average pH in the control plaques is similar to other reports of low tissue pH in atherosclerotic plaques. The average pH of the seven plaques placed in the media was consistently higher and more stable than the control plaques. Due to the Diametric sensor's fragility, no measurements could be made in a calcified region of plaque over time. Areas of highly calcified plaques were reported in the literature with significantly higher pH values, up to 8.3 pH units. In addition, the plaques placed in the media had a smaller range in pH (mean, 6.93 to 7.29) and less heterogeneity was observed. The magnitude of pH heterogeneity, reported in the fluorescence microscopy studies that included both calcified and non-calcified areas, was not observed.

Based on the stability of the physiological parameters, the oxygenated media bath preparation established a method to keep the plaque tissue viable for up to four hours. Areas of plaques that were heavily calcified or too thin to place the fragile sensor were not included in the validation. While the stability of calcified areas was not measured directly and could be a limitation it is assumed that these calcified areas will have the same metabolic properties as other areas of the plaque, if the thickness is not too great (>1.5 mm).

8.2. Spectra Collection

Eighty-two spectra for lactate determination and forty-eight spectra for tissue pH determination were collected. Several spectra had to be eliminated out of the 126 total points collected based on adverse reflection of the ceramic grid under the plaque, or featureless (flat) signal between 2000-2500 nm. Although these flat spectra were typically highly calcified plaque, the low signal-to-noise from the known detector response cannot be ruled out.

Figures 7.2.4 and 7.2.5 showed the optical spectra collected (lactate and tissue pH spectra, respectively) broken down by the observed gross pathology. These figures are demonstrative of how gross pathology is a subjective and highly imperfect caterogorization scheme. For several points, a mix of calcified and thrombotic, or thrombotic and yellow, regions was apparent. Heterogeneity in a 3 mm diameter area is typical, and exacerbates the ability to discern the type of plaque with the naked eye. Microscopic heterogeneity as evidenced by histology may be a better indicator of what "type" of plaque the point was and to which category its spectra belong.

The optical spectra of the atherosclerotic plaques were collected in a near-physiological environment. These optical spectra will represent metabolically active tissue, in contrast to static morphological measurements reported elsewhere on plaques frozen then thawed prior to spectroscopic measurements [62, 102].

8.3. Reference Measurements

The reference lactate values measured in the carotid plaques were not uniformly distributed across the physiologically relevant concentration range (2-20 micromoles/gram tissue); the average and median was skewed to the low concentrations (average 3.2, median 1.9 micromoles LA/gram tissue). The micro-enzymatic assay was sensitive to ±0.1 micromoles LA/gram tissue based on the intercept of the calibration curve. The calibrated measurement range was from 0 to 11 micromoles/gram tissue. However, the intra-serial precision was 0.5 micromoles LA/gram tissue, based on three replicate measurements on the same microtiter plate. This error limits the accuracy that can be achieved with the optical determination of lactate.

Other researchers [103] using tissue lactate as an indicator of anaerobic metabolism demonstrated that in cancer tissue, lactate values were predictive of increased risk of metastases, with a median tumor lactate concentration of 7.1 micromoles/gram tissue. Tumors that subsequently metastasized were 12.9 micromoles/gram tissue versus 4.8 micromoles/gram for patients disease-free after two years. Tissue lactate measured in normal and atherosclerotic rabbit aortas [77] were shown to be 2.9 and 5.5 micromoles/gram tissue, respectively. The highest lactate concentrations were seen deep in the plaque (>500 microns). The lactate values measured in this study are within the lower range of the reported literature values. The skewed median of the micro-enzymatic measurements may represent either 1) a lesser degree of anaerobic metabolism in this media preparation than tumors and atherosclerotic rabbit aortas incubated with oxygenated media in approximately a similar manner as described here, or 2) a dilution effect due to the large amount of tissue the biopsy covered. The bioluminescence method used in the other tissue lactate studies provided depth resolution of the lactate concentration per gram of tissue. It may be a better reference method to use for the optical calibration in the future.

The reference pH values were consistent with the values observed during method validation. The electrodes have a reported measurement error of 0.03 pH units. The range of all the tissue pH reference measurements used for the optical calibration was from 6.74 to 7.72. An acceptable error in pH units based on significant digits would be ± 0.05 pH units, given the range of values that are reported for prior plaque tissue measurements (see Section 8.1 discussion). The combined error of ±0.08 pH units was used as an acceptance criterion for the estimated error (or SECV) for the optical determination of tissue pH. However, the volume of tissue measured optically may be too big compared to the electrode measurement (2 mm working optical diameter versus a ~750 micron working diameter of electrode). This difference in volume may affect the calibration accuracy and prediction.

Correlation analysis demonstrated that the measured tissue temperature is uncorrelated to lactate or pH reference measurements This is an important finding because the partial least-squares method employed here could inadvertently model some other variable if it is related to the desired calibration variable of either tissue pH or lactate. Spurious correlation to temperature can be ruled out in assessing the calibration models

interpretability. The fact that optical calibration models could be created with real temperature variation is another indicator that the spectra collected in this *in-vitro* setting is impervious to the temperature. In addition, it was demonstrated that tissue pH and lactate reference measurements were not correlated. The sampling volume difference between the tissue lactate biopsy and the micro-electrode pH measurement alone could cause the lack of correlation between these known, physiologically-related measurements.

8.4.   Calibration Model Development

8.4.1.   Lactate Determination

The calibration model development for lactate determination showed that an acceptable model could be made with only a subset of points (17 out of 82 or 20% of the data in 6 plaques, i.e., plaques K1, K2, K4, K8, K9, K10). This model had loading vectors that demonstrated real chemical species were contributing to the determination. The cumulative percent variation captured in the lactate model demonstrated that by the fourth and sixth loading vector, variation in the spectra could be in part due to the theoretical lactate peaks at ~2250 and ~2295 nm. However, the contribution of the lactate peaks is weak.   Figure 7.4.2, shows that the first three loading vectors for lactate determination are demonstrative of over 99% of the spectral variance. These large changes could be due to dominating effects of water (loading vector 2) or protein concentrations (loading vector 3).   In contrast, by loading vector 3, only ~69% of the variability in the reference lactate concentration was captured. There is still considerable variance in the reference data left to be explained, even though the spectral variation is well captured. This variability could account for the limited accuracy of the preliminary data model.

In the entire data set, this knowledge that the water and protein variability may affect model accuracy was implemented using additional pre-processing techniques to reduce the variability. Since large non-specific proteins may contribute to scattering in the near infrared (1100-2400 nm), it was hoped that Multiplicative Signal Correction (MSC) could provide some reduction in the contribution of scattering components in the full 82-point spectral data set and also reduce model complexity (number of factors required). MSC corrects for scattering by associating the mean spectrum as the "ideal spectrum" and correcting all spectra with linear regression (slope and offset from the ideal). However, no models could be created when MSC was applied either on the full wavelength region or on the 2030-2330 nm data. Automatic baseline correction, intended to remove spectral drift and/or the baseline water shifts, did not help the lactate determination using the full 82-point calibration data in either wavelength region selected.

Other pre-processing techniques that could help elucidate the lack of decent calibration models using the entire data set were used. Cluster analysis methods were employed to assess the spectral (in)homogeneity and find any correlation to other measured experimental variation(s), as the full data set is split up but conserved. Orthogonal signal

correction was used to assess the independence of the variability in the reference measurement.

The clustering algorithm produced three clusters with the 82 spectra in an unsupervised fashion. Cluster A, containing 45 spectra (or 55% of the data), showed that the order the spectra were collected was important and could attribute to deterioration in the model for the full set of data over time. All the points that produced the acceptable lactate model (test 2e in Table 7.4.1) were in cluster A. If there was no chronological dependence, then it should have been possible to generate an acceptable model with any other six plaques or seventeen points randomly chosen. This was performed on 3 different sets of 17 randomly chosen points. However, no models could be created in this manner. The Cluster A PLS results were deteriorated (test 3a) compared to the first twenty-one points model (test 2d), indicating that even within a relatively homogeneous cluster of spectra, significant variability still exists. Clusters B and C were not adequate to produce any PLS models. No correlation to other experimental variation was observed in this clustering solution.

It is important to note that the cophenetic coefficient, a metric that can be used to determine the validity of the clustering solution (the closer to 1 the better), was 0.76, the highest among all the other possible combinations of distance metrics for this data set. A low cophenetic coefficient is indicative of inconsistency among objects and groupings. It can be inferred that the variability in spectral data is high, as inconsistency in the cluster formation was observed. Natural groupings could not be determined based solely on the length of each link in the cluster tree with the lengths of neighboring links below it in the tree. Instead, three clusters were determined by cutting off the hierarchical tree at an arbitrary point. A better clustering algorithm could possibly provide a clustering solution that would group the spectra differently and in such a way that new PLS models could be generated.

Orthogonal Signal Correction demonstrated that variability in the lactate reference measurement could be important. OSC assumes that the reference data is accurate and noise-free. By removing spectral components that are orthogonal to the reference values, it is assumed that no information correlated to the reference values should be lost. However, the OSC results showed no significant model improvement compared to the original 82 point PLS model. The lack of precision in the reference measurement at low concentrations may contribute to the poor accuracy in the optical determination and the inability of OSC to improve the model results using the full 82 point calibration data.

Further investigation of why only the first six plaques (plaques K1, 2, 4, 8, 9, and 10) could create an acceptable model was made. First, chronological logs on the spectrometer were reviewed to see if data was corrupted after experiment K10. Nothing was found. Any equipment changes in the laboratory setup were reviewed. It was noted that a new incubator and heating pad was used starting with experiment K9. Although many points were removed because of low temperatures in K3, and in K5 to K7, the temperatures from the points used in the acceptable model versus the rest (i.e. the points from K11-K30 marked Y in column "Used for Lactate Model?" in Table 7.3.1) were not

significantly different. In addition, the temperature ranges were within the validated range for living plaques (Section 7.1). Any difference in the *in-vitro* temperature was ruled out.

Secondly, the time to collect optical spectra for each point was reviewed. Spectrometer variation between collecting the backgrounds can potentially occur during the 10-15 minutes it takes to make a full set of measurements for one location in the plaque. The time between spectrometer reference/background and tissue spectra collection on the FT-NIR spectrometer and the experiment durations were longer after K14 because additional optical data was being collected with the visible spectrometer. If the time between spectrometer reference collection and tissue spectra collection was significantly different, then adding the points from plaques K11-K14 only to the acceptable model should not lead to model degradation. This was not the case. By adding the K11-K14 points to the first six plaques calibration data, no models could be created. The experiment durations were all within the validated range for living plaques and therefore the differences in the experiment durations was ruled out. Spectrometer reference variability as shown in Table 7.2.3 may contribute to the variability seen in the spectra. An average 1.7% change at 1150 nm was seen over the experiment collection period after the preliminary data set was collected.

Next, calibration curves for lactate assay processing, and the reference lactate measurements % recovery studies were investigated. The slope and intercept values for the calibration curves for each assay batch processed were comparable and therefore should not significantly impact the reported lactate value. There was, however, considerable variability in the percent recovery values determined between the batches of lactate assays. Plaques K1 and K2 were in one batch, K4 was in its own batch, and plaques K8-K10 were in yet another batch. For the rest of the plaques, K11-14, K17-22, and K23-30 were separate batched lactate assays. If the batch a plaque point belonged to was significant, then it is should be that only plaques with similar percent recovery values model. To test this, each batch group was rotated in and out of the calibration set. The large individual batches did not model. Groups of batches with similar percent recovery did not model. However, with all the other variations apparent, the significance of the batch grouping cannot be ruled out. The reported assay error and the range of lactate values (see discussion in Section 8.3) also make this assessment problematic.

Approximately 5 or 6 points per factor are required to demonstrate the model is not overfit [26]. The seventeen points that created an acceptable lactate calibration model based on R^2 and SECV was an overfit model. The many sources of variation within each plaque, between plaques, and variation in spectrometer over time may have confounded the ability to make a model as more points were added to the preliminary model results. The narrow range of lactate values in the entire data set and spreading of the data at low concentrations also limits the accuracy. Increasing the number of calibration samples over a wider lactate concentration range should create a more evenly distributed range of lactate values and may be able to account for plaque-to-plaque variation. Better reference methods such as HPLC or bioluminescence [104] could help discriminate the low concentrations and improve the predictions. Spectrometer variation might be reduced

with a cooled detecting element or by modeling this variability separately. The significant added variability in the data was not adequately modeled and resulted in serious degradation from the preliminary model results.

8.4.2. *Tissue pH Determination*

The preliminary model results showed that tissue pH determination is feasible. This model had loading vectors that resembled hemoglobin and water absorption. The cumulative percent variation captured by the three loading vectors in the tissue pH model, in each wavelength region contributing to the model, showed positive correlation peaks at the wavelengths where oxyhemoglobin absorb in both the visible (Figure 7.4.5 top plot, factors 2 and 3) and near-infrared (Figure 7.4.5. center plot factor 1). Alam *et al* [105] demonstrated in whole blood experiments, that the 1650 nm peak is a pH-inducible shift in the histidine residue of hemoglobin molecule, further corroborating the validity of the tissue pH model in atherosclerotic plaques. The other dominant feature in the loading vectors is water at 1450 nm (Figure 7.4.5. center plot, factor 3). This may be related to hydrogen bonding effects from pH-induced changes in water. A three-factor model is acceptable for the seventeen points used for the tissue pH determination. Most of the spectral variation is captured by the third factor (98%), however, only 84% of the variation in the reference tissue pH was explained. This unmodeled variability could account for the limited accuracy of the model. Additional factors could be used, however, this both increases model complexity and unwanted noise-correlation.

No models could be created using Multiplicative Signal Correction or automatic baseline correction after outlier removal using the full 48 points and additional wavelength selection. It was hoped that MSC could provide a reduction in the contribution of scattering components that was apparent in observing all the spectra together. However, no models could be created. The automatic baseline correction, also intended to remove this shift, did not help. These methods may have reduced model complexity (only models with one factor were generated), but the correlation due to noise overshadows any possibility of modeling the tissue pH.

Cluster analysis methods were then employed for the full 48 tissue pH calibration data to assess the spectral (in)homogeneity and find any correlation to other measured experimental variation(s). Again, the full data set is split up but conserved. The clustering algorithm produced two clusters in an unsupervised fashion. Cluster A, containing 39 points, still contained considerable spectral variability and could not produce models with more than one factor, even after outlier removal. Cluster B, containing 9 points, demonstrated that pathology was the major source of spectral variability. Spectra collected from points that were identified as grossly thrombotic during the experiments were in a unique cluster (Group B, Figure 7.4.6). However, the acceptable model used points in both clusters. The clustering solution was not able to separate based on any time dependence, unlike in the lactate spectra clustering. The variability due to pathology was overwhelming.

The cophenetic coefficient for this solution was 0.9025, the highest among all other combinations of distance metrics. Two clusters were determined by detecting natural groupings based on the length of each link in the cluster tree with the lengths of neighboring links below it in the tree. The solution is better than the lactate spectra clustering in terms of inconsistency (i.e. the clusters formed in the tissue pH clustering solution were more appropriate). Additional pre-processing on Cluster A may reduce spectral variability. Only nine points were available in Group B, so a good model could not be developed. More points that exhibit thrombus pathological characteristics would be required if the model is to be improved. The apparent mismatch in the size of the optical probe tissue volume and the tissue pH reference measurement may be a more important factor in the entire data set, as variability in pathology under the fiber optic probe is seen. This might be resolved by creating a smaller fiber optic probe that is closer to ~1 mm in diameter as the micro-electrodes used.

Further investigation was made on why only the first five plaques measured for the optical determination of tissue pH (i.e. plaques K17 to 21 inclusive) could create an acceptable model. Unlike in the lactate investigation, the time between reference and tissue spectra collection did not change after K21. No adverse chronological logs were found. No changes in the laboratory setup were made at this stage. Spectrometer reference variability as shown in Table 7.2.3 may contribute to the variability seen in the spectra. An average 1.6% change at 970 nm on the FT-NIR spectrometer (affecting spectral Region 2) was seen over the experiment collection period after the preliminary data set was collected.

In a previous work describing optical tissue pH calibration and real tissue pH heterogeneity *in-vivo* in the myocardium [28], similar challenges of matching the optical volume and reference measurement volume were outlined. However, when ischemic changes occur in the intact myocardium, the direction of pH change is homogenous and may be more optically predictable compared to the atherosclerotic plaque. Improvement of the optical depth resolution that was required in the myocardium was on the order of 3-5 mm. The spatial distribution of tissue pH in the atherosclerotic plaque is more heterogeneous, on the order of microns. In addition, due to the histological variability of necrotic and living tissue on the order of microns, the direction of pH change due to ischemic, hypoxic, or anaerobic conditions in the *in-vitro* situation may not be as optically predictable. The averaging effect of the optical probe volume in this research may be a large contribution to the limited accuracy of the optical calibration.

8.5. Medical Interpretation and Significance of Results

While no actual method of detecting vulnerable plaque was undertaken during this research, it has been shown that the two metabolic parameters, namely tissue pH and lactate concentration, can be feasibly determined with optical spectroscopy in the atherosclerotic plaque within the stated limitations. Due to the lack of agreement as to what is the definition of vulnerable plaque, the possibility of using plaque tissue pH and/or lactate measurements (or even other metabolic indicators, optical or otherwise) would be up to the clinician's discretion. Future Receiver-Operator-Curves for tissue pH

and lactate could be defined, with the addition of other independent patient information and diagnostic tests (PET, SPECT, calcium score, etc.) such that the clinician can determine a vulnerability score.

Of the two metabolic parameters proposed to be optically determined, the tissue lactate may be considered more feasible in the long run. The spectral data range for lactate is shorter than the ranges needed for tissue pH determinations. Tissue lactate is more homogenous [77], and high concentrations would provide a signal of anaerobic metabolism or dead tissue, while differences in the spatial distribution of tissue pH is more heterogeneous, and may not be as accurately predicted if a large optical probe is used.

The ultimate optical probe for the determination of the atherosclerotic plaque's metabolic status would embody a catheter that 1) can be inserted safely into the coronary arteries and 2) make measurements anywhere on the vessel wall, whether by 360° or 180° turning of the optical catheter. It has been noted in this study that the optical volume and reference measurements were not adequately matched. Separate optical probes or source-receiver separations may need to be incorporated into one probe and a more complex fiber-optic catheter based optical spectroscopy system would be envisioned to detect metabolic status or vulnerability in atherosclerotic plaque. A realistic coronary artery measurement *in-vivo* may require saline flush or temporary or intermittent stoppage of the blood due to the strong absorbance of hemoglobin and water, and the additional red blood cells that act as scattering components. Brezinski *et al* [106] have shown through optical matching that the OCT measurements of the vessel wall can be made without contacting the wall directly and through the matched blood. Zuluaga *et al* have devised a near-infrared spectroscopic method and correction to determine whether a particular optical configuration can measure a wavelength calibration standard under varying depths of blood [107]. With proper signal conditioning, a system could be developed to take optical spectra through a blood flow field to make metabolic determinations of atherosclerotic plaque.

The significance of the results presented is that optical determinations of the metabolic status of living atherosclerotic plaques are feasible. However, several limitations apply. For tissue pH, the underlying pathology and mismatched volume of measurements were identified as the major limiting factors. Highly calcified plaques could not be validated over time and obtaining accurate reference pH measurements were difficult. Plaques exhibiting both grossly thrombotic areas and mildly yellow fatty plaques with thrombosis were used to create an acceptable model. More calibration data would needed to definitively determine from where unmodeled sources of variation arise. In addition, the optical probe size was much larger than the reference pH electrode size, which could lead to an averaged or an erroneous optical measurement. For lactate, the reference measurement precision and unmodeled tissue characteristics apparent in the loading vectors in the calibration were the major limiting factors. In both determinations, sources of variation that were rejected were the tissue temperature and the duration of one day's plaque experiment (max. 4 hours). However, plaque-to-plaque variability and spectral variation could not be ruled out or deconvoluted in either optical determination.

9. CONCLUSION

The overall goal of this research was to show the feasibility of using optical spectroscopy to accurately determine metabolic derangements (namely, tissue pH and lactate concentration) in living human atherosclerotic lesions. This goal was accomplished in light of several limitations discovered in the process. Methodology was established for using an optical, spectroscopic probe *in-vitro* and maintaining atherosclerotic plaque in the living state for an extended period of time. Preliminary data demonstrated that optical determinations for tissue pH and lactate could be made. By comparing the material presented in Chapters 5-8 of this dissertation with the specific aims of this research listed in Chapter 2, the following conclusions can be made:

1) A reflectance-based optical fiber probe that uses visible to near-infrared light optimally to interrogate a small volume of tissue was developed for *in-vitro* use. The probe design was aided by the generation of diffuse reflectance profiles using Monte Carlo simulations of light propagation and literature values of normal and atherosclerotic wall optical properties. Probes with different optical configurations and source-receiver separations were characterized by signal-to-noise ratio and analyzed over several wavelength regions. It was determined from the simulations that with a 50 micron source-receiver separation, the target volume of 1 mm^3 tissue could be met. The final optimized probe was built to optimally collect visible to near-infrared light using a 50 micron source-receiver separation and an optical window on both FT-NIR and dispersive spectrometers.

2) Using the optimized optical probe the depth penetration was estimated using thin tissue slices. The depth penetration at key wavelengths was estimated by successively stacking thin sections of non-diseased tissue on to the end of optical probe and collecting the reflectance spectra. The results compared well with the theoretical simulations and provided depth penetration data on wavelength regions specific to lactate peak locations. The requirement that the optical probe interrogates 1 mm^3 tissue was met based on the depth penetration tests. The optical probe fully satisfies the specifications set out in Specific Aim 1 and 2.

3) Major interferents to the optical spectra and reference measurements were identified. It was shown that by maintaining the plaque in an oxygenated, nutrient environment, tissue pH and temperature was stable up to 4 hours. By establishing this methodology, it can be concluded that the plaque is living and measured optical spectra will represent metabolically active tissue, in contrast to static morphological measurements reported elsewhere. *In-vitro* tissue temperature was shown not to adversely affect the optical determinations. Pathological variation was identified as a confounder and shown to be detrimental in creating acceptable calibration models using all the data for tissue pH. The duration of one day's (max. 4 hr) experiment was determined not to adversely affect the optical determinations.

4) Using optimized fiber optic probe matched to system instrumentation, ~50-100 data points were collected while maintaining the plaque's physiological state *in-vitro,* and analyzed as a large calibration set of human carotid endarterectomy specimens. Multivariate calibration techniques were used with additional pre-processing methods in attempt to augment the calibration set's ability to optically determine tissue pH and tissue lactate. The optically-predicted values from the empirical model to the reference measurements were compared using calibration metrics of correlation coefficient (R^2), standard error of cross-validation (SECV) and the minimum number of factors needed for model accuracy. Preliminary data with the first 5-6 plaques in both the lactate and tissue pH calibrations (approximately the first 20-21 points in each set, not the same samples) showed that adequate results could be obtained with additional outlier removal. The initial seventeen point, six-factor lactate calibration results met the correlation (coefficient of multiple determination) specification of $R^2 \geq 0.75$. The estimated accuracy did not meet the specification for an SECV of 1.0 micromoles lactate/gram tissue. Further improvement in the SECV could not be achieved. In addition, the lactate model result was an overfit of the data. Adding more points degraded the model R^2 and SECV. Unmodeled spectral variability, inadequate reference measurement spatial resolution and precision, and remaining mismatch between optical volume versus biopsy volume contributed to the model degradation. The initial seventeen point, three-factor tissue pH calibration also met the correlation (coefficient of multiple determination) specification of $R^2 \geq 0.75$ but not the estimated accuracy at 0.08 pH units. Adding more points degraded the model R^2 and SECV. The number of factors indicated a good fit of the data. A smaller optical probe may be required for the tissue pH determination, as well as more points that identify as thrombotic in gross pathology.

The general specification requirements (Table 2.2.1.) is reproduced here with the added information of acceptability of the data clearly marked:

Specification	Tissue pH	Tissue Lactate Concentration [Micromoles lactate/gram tissue]	*in-vitro* Temperature (°C)
in-vitro Experimental Stability Met?	< 0.03 change/hr **YES**	-	<0.4°C change/hr **YES**
Optical Calibration Range Met?	6.80 – 7.60 **PROVISIONALLY, 6.99 – 7.55**	2 – 20 **PROVISIONALLY [0.1 – 10.1]**	32.0 – 38.0 **YES**
Optical Calibration Met? Coefficient of Multiple Determination (R^2) / Estimated Accuracy (SECV)	≥ 0.75 **YES, provisionally** 0.08 pH units **NO**	≥ 0.75 **YES, provisionally** 1.0 μmoles/ gram tissue **NO**	-
Maximum # of Factors in Optical Calibration Model [26]	5 to 6 independent samples per factor **YES**	5 to 6 independent samples per factor **NO, overfit**	-

In Chapter 3, Hypotheses and Research Methods, three hypotheses were outlined that described the focus of this work. Scientific methods were used in the course of the

research and hypothesis testing: statistical analysis of data, mathematical modeling, experimentation, induction and deduction. The validity of these hypotheses are evaluated here based on the scientific method:

1) A small fiber optic prototype (< 3 mm optical working diameter) will make optical measurements *in-vitro* for the assessment of metabolically active plaque in a defined region of tissue (< 1mm^3 volume). Both theoretical and practical considerations are allowed for in the design and implementation.

    This hypothesis is accepted. The fiber optic probe design process achieved its target of being <3 mm optical working diameter and maximum tissue volume interrogation of 1 mm^3.

2) The *in-vitro* experimental factors, identified *a priori* as the tissue temperature, experiment time, and the gross constituent information of the plaque (i.e. gross pathology), can be assessed to their importance in affecting the optical calibration. It is hypothesized that the acceptance criteria for *in-vitro* experimental stability as defined in Section 2.2 can be met.

    This hypothesis is accepted. The *in-vitro* temperature, experiment time, and the gross plaque constituent information, were measured. The effect on the optical calibration was deduced to be minimal for temperature and experiment time. The stability of the atherosclerotic tissue and the media preparation was met up to 4 hours. The gross pathology affected the optical calibration of the tissue pH models.

3) Mathematical models can be developed which relate the corresponding optical spectra to the individual metabolic parameters (pH and lactate), measured with accepted reference methods, in the presence of inherent pathological variability. By collecting the optical spectra in a controlled, stable *in-vitro* environment and by using partial least-squares (PLS) multivariate calibration, accurate determinations can be achieved for the individual metabolic parameters of plaque tissue pH and plaque lactate concentration. The correlation coefficient of the determination and standard error of cross-validation will be used to determine calibration performance. The number of factors will be used to determine the appropriateness (e.g., overfit/underfit) of the optical calibration.

    This hypothesis is accepted on the basis of preliminary data that demonstrated limited models could be created. The coefficient of multiple determination (the acceptance criterion was stated in Section 2.2. as $R^2 \geq 0.75$) was achieved for a seventeen point, six-factor model for lactate. However, the estimated accuracy and maximum number of factors requirement were not met. The coefficient of multiple determination was achieved for a seventeen point, three-factor model for tissue pH. However, the estimated accuracy was not met (0.08 pH units specified versus 0.09 pH units achieved). The maximum number of factors requirement was met in the tissue pH calibration. The accuracy of the optical tissue pH

measurement at an R^2 of 0.75 in the seventeen point model and could not be improved by separation of the points by the observed pathological variability. No models could be created with all the 82 data points for lactate or the 48 data points for tissue pH, in the presence of observed pathological variations.

The overall hypothesis that reflectance-mode optical spectroscopy, using visible to near infrared light energy, can be used *in-vitro* to develop calibration equations that provide an optical determination of the atherosclerotic tissue pH and lactate concentration is accepted with limitations. The optical volumes needed for lactate and tissue pH are considerably different. For each optical determination, 1) the probe size and depth penetration, or optical volume, has to be better matched with the reference volume, 2) the area and volume of the reference measurement has to be small enough such that pathology and optical spectra are nearly homogeneous, 3) accurate, spatially resolved reference measurements need to be made that uniformly spans the physiological range, and 4) all sources of spectral variation must be modeled in order for the correlation and estimated accuracy to be improved to levels acceptable for future *in-vivo* development of this technique.

10. FUTURE WORK

The limited feasibility of the lactate and tissue pH optical calibrations shown here in living, atherosclerotic carotid plaques indicates that significant *in-vitro* model development is still required. The clustering algorithms for both lactate and pH tested were simple algorithms in the family of unsupervised techniques and may not have provided the most appropriate solution for the calibration data. Other algorithms within this family may provide better solutions and ultimately better multivariate calibration results. Supervised pattern recognition techniques such as Artificial Neural Networks or fuzzy clustering could be implemented to assess the spectral differences and reference measurement variation together in a non-linear multivariate calibration methodology. Improved accuracy of the lactate reference measurement would help eliminate a large source of controllable error in the optical calibration. More data collection is prescribed, in an *in-vitro* tissue model where the protein and water content variability can be adequately described or reduced. Long-term spectrometer variation also must be reduced or compensated. This may be achieved by either using more expensive stable spectrometers with cooled detectors (preferred), or additional characterization of the spectrometers to model this drift. A bench simulation or *in-vitro* tissue model that has reduced variability in scattering components should be used to address the concern that unmodeled scattering variation due to protein or water content overwhelms the lactate signal in the 2030-2330 nm region. This should be performed as well for the tissue pH in the visible region to address unmodeled spectral variation seen and to definitively determine if pathology is the root cause of the variation.. All of the sources of variability identified here need to be carefully studied in order to even consider the next step in improving the accuracy and prediction of the optical method for *in-vivo* use, described below for future work.

The Watanabe rabbit model has been used by several investigators to study atherosclerosis progression because it is able to develop classic early lesions similar to humans. However, this animal model is unable to produce lesions of higher complexity. The purpose of testing an optical method in the Watanabe rabbit *in-vivo* would be two-fold: 1) to validate whether the mathematical techniques generated on the *in-vitro* tissue model extend to the *in-vivo* rabbit model with acceptable error, and 2) to provide an initial assessment of the efficacy of placement and overall design strategies of the catheter.

To perform the experiment in a live animal, typical catheterization procedures would be used to optically measure the rabbit aorta. The catheter will be advanced using a stepper motor so the exact placement of the catheter where spectra are taken can be made. If needed, the rabbit's chest will be opened at the same time so the surgeon can identify the catheter's location by hand. Alternatively, a radio-opaque marker can be placed on the catheter tip and the animal x-rayed to find the catheter's exact location. Histology and lactate analysis of the aorta could be performed in the marked locations using the procedures previously described. The reference measurements would be compared to the output of the spectroscopic measurements processed in the mathematical modeling.

Rigorous acceptance criteria should be used to accept or reject the feasibility of performing the optical determinations *in-vivo.*

In summary, only after the optical calibrations are improved to meet or exceed the acceptance criteria on the bench or *in-vitro*, testing on animals *in-vivo* should be considered. Calibration transfer methods would be required to account for any changes in catheter design. The final catheter design may have mechanisms such as radio-opaque markers, an inflatable balloon, and saline flush ports so the optical field can be cleared. The efficacy of building an adult sized optical catheter and conducting human clinical trials for vulnerable plaque detection based on metabolic status could conceivably continue from any additional data collected *in-vitro* that can demonstrate significantly improved accuracy than those described here or *in-vivo* in an acceptable animal model calibration.

11. REFERENCES

1.   American Heart Association. 2002 Heart and Stroke Statistical Update. 2001.

2.   Naghavi M, Madjid M, Khan M, Mohammadi R, Willerson JT, Casscells W: New developments in the detection of vulnerable plaque. *Curr Atheroscler Rep* 2001;2:125-135.

3.   Stefanadis C, Diamantopoulos L, Vlachopoulos C, Tsiamis E, Dernellis J, Toutouzas K, Stefanadi E, Toutouzas P: Thermal heterogeneity within human atherosclerotic coronary arteries detected in vivo: a new method of detection by application of a special thermography catheter. *Circulation* 1999;99:1965-1971.

4.   Lederman R, Raylman R, Fisher S, Kison P, San H, Nabel E, Wahl R: Detection of atherosclerosis using a novel positron-sensitive probe and 18-fluorodeoxyglucose (FDG). *Nucl Med Commun.* 2001;22:747-753.

5.   Vallabhajosula S, Fuster V: Atherosclerosis: imaging techniques and the evolving role of nuclear medicine. *J Nucl Med* 1997;38:1788-1796.

6.   Ciavolella M, Tavolaro R, Taurino M, Di Loreto M, Greco C, Sbarigia E, Casini A, Speziale F, Scopinaro F: Immunoscintigraphy of atherosclerotic uncomplicated lesions in vivo with a monoclonal antibody against D-dimers of insoluble fibrin. *Atherosclerosis* 1999;143:171-175.

7.   Krinsky G, Freedberg R, Lee V, Rockman C, Tunick P: Innominate artery atheroma: a lesion seen with gadolinium-enhanced MR angiography and often missed by transesophageal echocardiography. *Clin Imaging* 2001;25:251-257.

8.   Bonk R, Schmiedl U, Yuan C, Nelson J, Black C, Ladd D: Time-of-flight MR angiography with Gd-DTPA hexamethylene diamine co-polymer blood pool contrast agent: comparison of enhanced MRA and conventional angiography for arterial stenosis induced in rabbits. *J Magn Reson Imaging* 2000;11:638-646.

9.   Patwari P, Weissman N, Boppart S, Jesser C, Stamper D, Fujimoto J, Brezinski M: Assessment of coronary plaque with optical coherence tomography and high-frequency ultrasound. *Am J Cardiol.* 2000;85:641-644.

10.   Nissen S: Clinical images from intravascular ultrasound: coronary disease, plaque rupture, and intervention - the inside view. *Am J Cardiol.* 2001;88:16-18.

11.   Takano M, Mizuno K, Okamatsu K, Yokoyama S, Ohba T, Sakai S: Mechanical and structural characteristics of vulnerable plaques: analysis by coronary angioscopy and intravascular ultrasound. *J Am Coll Cardiol* 2001;38:99-104.

12.   Cassis LA, Lodder RA: Near-IR imaging of atheromas in living tissue. *Anal Chem* 1993;65:1247-1256.

13.   de Korte C, Cespedes E, van der Steen A, Pasterkamp G, Bom N: Intravascular ultrasound elastography: assessment and imaging of elastic properties of diseased arteries and vulnerable plaque. *Eur J Ultrasound* 1998;7:219-224.

14.   Jeremias A, Kolz M, Ikonen T, Gummert J, Oshima A, Hayase M, Honda Y, Komiyama N, Berry G, Morris R, Yock P, Fitzgerald PJ: Feasibility of in vivo intravascular ultrasound tissue

characterization in the detection of early vascular transplant rejection. *Circulation* 1999;100:2127-2130.

15. Uchida Y, Nakamura F, Tomaru T, Morita T, Oshima T, Sasaki T, Morizuki S, Hirose J: Prediction of acute coronary syndromes by percutaneous coronary angioscopy in patients with stable angina. *Am Heart J.* 1995;130:195-203.

16. Flacke S, Fischer S, Scott M, Fuhrhop R, Allen J, McLean M, Winter P, Sicard G, Gaffney P, Wickline S, Lanza G: Novel MRI contrast agent for molecular imaging of fibrin: implications for detecting vulnerable plaques. *Circulation* 2001;104:1280-1285.

17. Rumberger J: Tomographic (plaque) imaging: state of the art. *Am J Cardiol.* 2001;88:66E-69E.

18. Achenbach S, Ropers D, Regenfus M, Pohle K, Giesler T, Moshage W, Daniel W: Non-invasive coronary angiography by magnetic resonance imaging, electron-beam computed tomography, and multislice computed tomography. *Am J Cardiol.* 2001;88:70E-73E.

19. Lehmann K, van Suylen R, Stibbe J, Slager C, Oomen J, Maas A, di Mario C, deFeyter P, Serruys P: Composition of human thrombus assessed by quantitative colorimetric angioscopic analysis. *Circulation* 1997;96:3030-3041.

20. Stary, H. C., Chandler, A. B., Dinsmore, R. E., Fuster, V., Glagov, S., Insull, W., Rosenfeld, M., dam, Wagner, W., and Wissler, R. W. A Definition of Advanced Types of Atherosclerotic Lesions and a Histological Classification of Atherosclerosis. American Heart Association. 2000.

21. Fuster V, Cornhill JF, Dinsmore RE, Fallon JT, Insull W, Libby P, Nissen S, Rosenfeld M, Wagner W: *The Vulnerable Atherosclerotic Plaque: Understanding, Identification, and Modification*, New York, Futura Publishing Company, Inc., 1999, pp 1-429.

22. Schoen F, Cotran R: Blood Vessels, in Cotran R, Kumar V, Collins T (eds): *Robbins' Pathologic Basis of Disease*. ed6. Philadelphia, W.B. Saunders Company, 1999, pp 493-541

23. Libby P: Atherosclerosis: the new view. *Scientific American* 2002;47-55.

24. Romer TJ, Brennan JF, Fitzmaurice M, Feldstein ML, Deinum G, Myles JL, Kramer JR, Lees RS, Feld MS: Histopathology of Human Coronary Atherosclerosis by Quantifying Its Chemical Composition with Raman Spectroscopy. *Circulation* 1998;97:878-885.

25. Virmani R, Kolodgie FD, Burke AP, Farb A, Schwartz SM: Lessons From Sudden Coronary Death : A Comprehensive Morphological Classification Scheme for Atherosclerotic Lesions. *Arteriosclerosis, Thrombosis, and Vascular Biology* 2000;20:1262-1275.

26. American Society for Testing and Materials. Standard Practices for Infrared, Multivariate, Quantitative Analysis; Annual Book of ASTM Standards. 3.06(E 1655), 1-24. 1995. Ref Type: Generic

27. Soller BR, Micheels R, Coen J, Parikh B, Chu L, Hsi C: Feasibility of non-invasive measurement of tissue pH using near infrared reflectance spectroscopy. *Journal of Clinical Monitoring* 1996;12:387-395.

28. Zhang S, Soller BR: In-vivo determination of myocardial pH during regional ischemia using near-infrared spectroscopy. *SPIE* 1998;3257:110-117.

29. Zhang S, Soller BR, Micheels R: Partial Least-Squares modeling of near infrared reflectance data for noninvasive in-vivo determination of deep tissue pH. *Applied Spectroscopy* 1998;52:400-406.

30. McShane MJ, Cote GL: Near infrared spectroscopy for determination of glucose, lactate, and ammonia in cell culture media. *Applied Spectroscopy* 1998;52:1073-1078.

31. LaFrance D, Lands LC, Hornby L, Burns DH: Near-infrared spectroscopic measurement of lactate in human plasma. *Applied Spectroscopy* 2000;54:300-303.

32. Moreno, P. R., Lodder, R. A., Purushothaman, I. K., Vyalkov, V., O'Connor, W. N., and Muller, J. E. Characterization of Composition and Vulnerability of Atherosclerotic Plaques by Near-Infrared Spectroscopy. 1999.

33. Hanlon EB, Manoharan R, Koo TW, Shafer KE, Motz JT, Fitzmaurice M, Kramer JR, Itzkan I, Dasari RR, Feld MS: Prospects for in-vivo Raman spectroscopy. *Phys.Med.Biol.* 2000;45:R1-59.

34. Jaross W, Neumeister V, Lattke P, Schuh D: Determination of cholesterol in atherosclerotic plaques using near infrared diffuse reflectance spectroscopy. *Atherosclerosis* 1999;147:327-337.

35. Wang J, Geng YJ, Guo B, Klima T, Lal BN, Willerson JT, Casscells W: Near-infrared spectroscopic characterization of human advanced atherosclerotic plaques. *Journal of the American College of Cardiology* 2002;39:1305-1313.

36. Naghavi M, John R, Nakatani S, Siadaty S, Grasu R, Kurian KC, van Winkle B, Soller BR, Litovsky S, Madjid M, Willerson JT, Casscells W: pH heterogeneity of human and rabbit atherosclerotic plaques; a new insight into detection of vulnerable plaque. *Atherosclerosis* 2002;164:27-35.

37. Berne RM, Levy MN: *Principles of Physiology*, ed2nd, Boston, Mosby, 1996, pp 1-795.

38. Gray H: *Gray's Anatomy*, ed38, Philadelphia, W.B. Saunders Co, 1980, pp -1578.

39. Williams K, Tabas I: The response-to-retention hypothesis of early atherogenesis. *Arterioscler Thromb Vasc Biol* 1995;15:551-561.

40. Schwenke D, Carew T: Initiation of atherosclerotic lesions in cholesterol-fed rabbits. I. Focal increases in arterial LDL concentration precede development of fatty streak lesions. *Atherosclerosis* 1989;9:895-907.

41. Cohen MC, Muller JE: Onset of acute myocardial infarction--circadian variation and triggers. *Cardiovasc Res* 1992;9:831-838.

42. Muller JE, Abela G, Nesto RW, Tofler GH: Triggers, acute risk factors and vulnerable plaques: the lexicon of a new frontier. *J Am Coll Cardiol* 1994;23:809-813.

43. Manoharan R, Baraga JJ, Rava RP, Dasari RR, Fitzmaurice M, Feld MS: Biochemical analysis and mapping of atherosclerotic human artery using FT-IR microspectroscopy. *Atherosclerosis* 1993;103:181-193.

44. Romer TJ, Brennan JF, Puppels GJ, Zwinderman AH, van Duinen SG, van der Laarse A, van der Steen AFW, Bom NA, Bruschke AVG, Adamson AW: Intravascular Ultrasound Combined with Raman Spectroscopy to Localize and Quantify Cholesterol and Calcium Salts in Atherosclerotic Coronary Arteries. *Arterioscler Thromb Vasc Biol* 2000;20:478-483.

45.   Casscells W, Hathorn B, David M, Krabach T, Vaughn WK, McAllister HA, Bearman G, Willerson JT: Thermal detection of cellular infiltrates in living atherosclerotic plaques: possible implications for plaque rupture and thrombosis. *Lancet* 1996;347:1447-1449.

46.   Leake D: Does an acidic pH explain why low density lipoprotein is oxidised in atherosclerotic lesions. *Atherosclerosis* 1997;129:149-157.

47.   Zemplenyi T: Metabolic intermediates, enzymes and lysosomal activity in aortas of spontaneously hypertensive rats. *Atherosclerosis* 1977;28:233-246.

48.   Zemplenyi T, Fronek K: Chemical sympathectomy by 6-hydroxydopamine and arterial enzymes and lactate in the rabbit. *Exp Mol Path* 1981;34:123-130.

49.   Zemplenyi T, Tidwell DF, Fronek K: Aortic enzymes and lactate in high altitude-raised and cholesterol-fed rabbits. *Atherosclerosis* 1984;52:233-242.

50.   Grasu R, Kurian KC, van Winkle B, Snuggs MB, Siadaty S, John R, Naghavi M, Willerson JT, Casscells W: pH heterogeneity of human and rabbit atherosclerotic plaques. *Circulation* 1999;100:I-542-I-542 (Abstract).

51.   Kirk JE: Lactic Dehydrogenase, in Kirk JE (ed): *Enzymes of the Arterial Wall*. New York, Academic Press, 1969, pp 21-29

52.   Voet D, Voet JG: Glycolysis, in Voet D, Voet JG (eds): *Biochemistry*. ed2nd. New York, John Wiley & Sons, 1995, pp 443-483

53.   Rosenson RS, Koenig W: High-sensitivity C-reactive protein and cardiovascular risk in patients with coronary heart disease. *Curr Opin Cardiol* 2002;17:325-331.

54.   Ridker P, Rifai N, Rose L, Buring J, Cook N: Comparison of C-Reactive Protein and Low-Density Lipoprotein Cholesterol Levels in the Prediction of First Cardiovascular Events. *The New England Journal of Medicine* 2002;347:1557-1565.

55.   Romer TJ, Brennan III, Bakker S, Wolthuis R, van den Hoogen RCM, Emeis JJ, van der Laarse A, Bruschke AVG, Puppels GJ: Raman spectroscopy for quantifying cholesterol in intact coronary artery wall. *Atherosclerosis* 1998;141:117-124.

56.   Buschman HP, Deinum G, Motz JT, Fitzmaurice M, Kramer JR, van der Laarse A, Bruschke AV, Feld MS: Raman microspectroscopy of human coronary atherosclerosis: Biochemical assessment of cellular and extracellular morphologic structures in situ. *Cardiovascular Pathology* 2001;10(2):69-82.

57.   Buschman HP, Motz JT, Deinum G, Romer TJ, Fitzmaurice M, Kramer JR, van der Laarse A, Bruschke AV, Feld MS: Diagnosis of human coronary atherosclerosis by morphology-based Raman spectroscopy. *Cardiovascular Pathology* 2001;10(2):59-68.

58.   Bigio IJ, Mourant JR: Ultraviolet and visible spectroscopies for tissue diagnostics: fluorescence spectroscopy and elastic-scattering spectroscopy. *Phys.Med.Biol.* 1997;42 :803-814.

59.   Mourant JR, Johnson TM, Los G, Bigio IJ: Non-invasive measurement of chemotherapy drug concentrations in tissue: preliminary demonstrations of in vivo measurements. *Phys.Med.Biol.* 1999;44:1397-1417.

60. Christov A, Dai E, Drangova M, Liu L, Abela G, Nash P, McFadden G, Maas A: Optical detection of triggered atherosclerotic plaque disruption by fluorescence emission analysis. *Photochem Photobiol* 2000;72:242-252.

61. Spokojny A, Serur J, Skillman J, Spears J: Uptake of hematoporphyrin derivative by atheromatous plaques: studies in human in vitro and rabbit in vivo. *J Am Coll Cardiol* 1986;8:1387-1392.

62. Moreno PR, Lodder RA, Purushothaman KR, Charash WE, O'Connor WN, Muller JE: Detection of lipid pool, thin fibrous cap, and inflammatory cells in human aortic atherosclerotic plaques by near-infrared spectroscopy. *Circulation* 2002;105:923-927.

63. Neumeister V, Scheibe M, Lattke P, Jaross W: Determination of the cholesterol-collagen ratio of arterial atherosclerotic plaques using near infrared spectroscopy as a possible measure of plaque stability. *Atherosclerosis* 2002;165:251-257.

64. Hicks GL, Hill A, DeWeese JA: Monitoring of midmyocardial and subendocardial pH in normal and ischemic ventricles. *J.Thorac.Cardiovasc.Surg* 1976;72:52-56.

65. Warner KG, Khuri SF, Marston W, Sharma S, Butler MD, Assousa SN, Saad AJ, Siouffi SY, Lavin PT: Significance of the transmural diminution in regional hydrogen ion production after repeated coronary artery occlusions. *Circulation Research* 1989;64:616-628.

66. Kumar G, Schmitt JM: Optimal probe geometry for near-infrared spectroscopy of biological tissue. *Applied Optics* 1997;36:2286-2293.

67. Mourant JR, Bigio IJ, Jack DA, Johnson TM, Miller HD: Measuring absorption coefficients in small volumes of highly scattering media: source-detector separations for which path lengths do not depend on scattering properties. *Applied Optics* 1997;36:5655-5661.

68. Khan, T. and Soller, B. R. NIRS measurement of tissue pH: optimizing small, fiber optic probe designs with the aid of Monte Carlo simulations. Tuan Vo-Dinh, Warren S.Grundfest, and David A.Benaron. 3911(Biomedical Diagnostic, Guidance, and Surgical-Assist Systems II), 244-249. 2000. Proc. SPIE.

69. Adams MJ: *Chemometrics in Analytical Spectroscopy*, Cambridge UK, Royal Society of Chemistry, 1995, pp v-216.

70. Martens H, Naes T: *Multivariate Calibration*, New York, John Wiley & Sons, 1989.

71. Haaland DM, Thomas EV: Partial Least-Squares methods for spectral analyses. 1. Relation to other quantitative calibration methods and the extraction of qualitative information. *Analytical Chemistry* 1988;60:1193-1202.

72. Norris K, Williams P: *Near-infrared technology in the agricultural and food industries*, St. Paul, American Association of Cereal Chemists, 1987.

73. Keijzer M, Richards-Kortum R, Jacques SL, Feld MS: Fluorescence spectroscopy of turbid media: autofluorescence of the human aorta. *Applied Optics* 1989;28:4286-4292.

74. Chance B, Liu H, Kitai T, Zhang Y: Effects of solutes on optical properties of biological materials: models, cells, and tissues. *Analytical Biochemistry* 1995;227:351-362.

75. Steinke JM, Shepard AP: Effects of temperature on optical absorbance spectra of oxy-, carboxy-, and deoxyhemoglobin. *Clinical Chemistry* 1992;38:1360-1364.

76.	Arnold MA, Burmeister JJ, Small GW: Phantom Glucose Calibration Models from Simulated Noninvasive Human Near-Infrared Spectra. *Analytical Chemistry* 1998;70:1773-1781.

77.	Levin, M. Energy metabolic failure within the arterial wall in atherosclerosis. 1-67. 2001. Göteborg University, Sweden. Thesis/Dissertation

78.	Wang L, Jacques SL, Zheng L: MCML - Monte Carlo modeling of photon transport in multi-layered tissues. *Computer Methods and Programs in Biomedicine* 1995;47:131-146.

79.	Wang L, Jacques SL, Zheng L: CONV - Convolution for responses to a finite diameter photon beam incident on multi-layered tissues. *Computer Methods and Programs in Biomedicine* 1997;54:141-150.

80.	Jacques, S. L. Tissue Optics. (SC34), 1-106. 1-24-1999. Oregon Medical Laser Center, SPIE. Short Course Notes.

81.	van Staveren HJ, Moes JM, van Marle J, Prahl SA, van Gemert JC: Light scattering in intralipid-10% in the wavelength range of 400-1100 nm. *Applied Optics* 1991;30:4507-4514.

82.	Flock ST, Jacques SL, Wilson BC, Star WM, van Gemert JC: Optical properties of Intralipid: a phantom medium for light propagation studies. *Lasers in Surgery and Medicine* 1992;12:510-519.

83.	These values for the molar extinction coefficient e in [cm-1/(moles/liter)] were compiled by Scott Prahl (prahl@ece.ogi.edu) using data from W. B. Gratzer, Med. Res. Council Labs, Holly Hill, London and N. Kollias, Wellman Laboratories, Harvard Medical School, Boston.. 2000. Internet Communication

84.	Prince MR, Deutsch TF, Mathews-Roth MM, Margolis R, Parrish JA, Oseroff AR: Preferential light absorption in atheromas in vitro. Implications for laser angioplasty. *J Clin Invest* 1986;78:295-302.

85.	van Gemert JC, Verdaasdonk R, Stassen E, Schets G: Optical properties of human blood vessel wall and plaque. *Lasers in Surgery and Medicine* 1985;5:235-237.

86.	van Gemert JC, Welch AJ, Jacques SL, Cheong Q, Star WM: Light distribution, optical properties, and cardiovascular tissues, in Abela G (ed): *Lasers in cardiovascular medicine and surgery: fundamentals and techniques*. Norwell, Kluwer Academic Publishers, 1990,

87.	Lowry OH, Passonneau JV: *Enzymatic analysis : a practical guide*, Totowa, NJ, Humana Press, 1993,

88.	Bergmeyer R: *Methods of Enzymatic Analysis: Metabolites - Carbohydrates*, ed3rd, 1984, pp 587-587.

89.	Galactic Industries Corp. PLSplus/IQ Handbook. 1996.

90.	Fuller M, Ritter G, Draper C: *Applied Spectroscopy* 1988;42:217-227.

91.	Geladi P, MacDougall D, Martens H: *Applied Spectroscopy* 1985;39:491-500.

92.	Massart DL, Kaufman L: *The interpretation of analytical chemical data by the use of cluster analysis*, New York, John Wiley & Sons, 1983, pp 1-237.

93.   Wold S, Antti H, Lindgren F, Ohman J: Orthogonal signal correction of near-infrared spectra. *Chemometrics and Intelligent Laboratory Systems* 1998;44:175-185.

94.   Fearn T: On orthogonal signal correction. *Chemometrics and Intelligent Laboratory Systems* 2000;50:47-52.

95.   Sjoblom J, Svensson O, Josefson M, Kullberg H, Wold S: An evaluation of orthogonal signal correction applied to calibration transfer of near infrared spectra. *Chemometrics and Intelligent Laboratory Systems* 1998;44:229-244.

96.   Palmer KF, Williams D: Optical properties of water in the near infrared. *J.Opt.Soc.Am.* 1974;64:1107-1110.

97.   Hale GM, Querry MR: Optical constants of water in the 200 nm to 200μm wavelength region. *Applied Optics* 1973;12:555-563.

98.   Buijs K, Choppin GR: *J.Chem.Phys.* 1972;39:2035.

99.   Martin K: in vivo measurements of water in skin by near-infrared reflectance. *Applied Spectroscopy* 1998;52:1001-1007.

100.   Di Iorio, E. Methods in Enzymology. 76, 57. 1981.

101.   Rothgeb, T. M. and Gurd, F. R. N. Methods in Enzymology. 52, 473. 1978.

102.   Marshik B, Tan H, Tang J, Zulaga A, Moreno PR, Purushothaman KR, O'Connor WN, Tearney G: Discrimination of lipid-rich plaques in human aorta specimens with NIR spectroscopy through whole blood. *The American Journal of Cardiology* 2002;90:129H (Abstract).

103.   Brizel DM, Schroeder T, Scher R, Walenta S, Clough R, Dewhirst M, Mueller-Klieser W: Elevated tumor lactate concentrations predict for an increased risk of metastases in head-and-neck cancer. *Int J Radiation Oncology Biol Phys* 2001;51:349-353.

104.   Levin M, Bjornheden T, Evaldsson M, Walenta S, Wiklund O: A bioluminescence method for the mapping of local ATP concentrations within the arterial wall with potential to assess the in-vivo situation. *Arterioscler Thromb Vasc Biol* 1999;19:950-958.

105.   Alam KM, Franke JE, Niemczyk TM, Maynard JD, Rohrscheib MR, Robinson MR, Eaton RP: Characterization of pH variation in lysed blood by near-infrared spectroscopy. *Applied Spectroscopy* 1998;52:393-399.

106.   Brezinski M, Saunders K, Jesser C, Li X, Fujimoto J: Index Matching to Improve Optical Coherence Tomography Imaging Through Blood. *Circulation* 2001;103:1999-2003.

107.   Zulaga A, DeJesus ST: Miniaturized probes for intracoronary optical spectroscopy through blood. *The American Journal of Cardiology* 2002;90:128H (Abstract).